AD-A185 624 TURBULENCE IN HYPERSONIC FLOW(U) HOKENSON CO LOS ANGELES CA G J HOKENSON 01 JUL 87 HOKE-THC-02GH87071A AFOSR-TR-87-1034 F49620-87-C-0012 1/1

UNCLASSIFIED F/G 20/4 NL

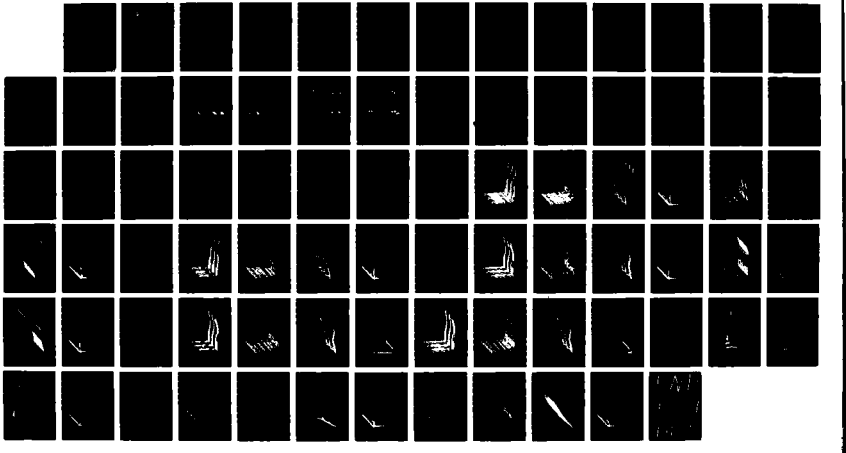

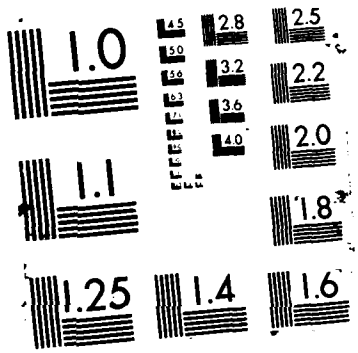
1.0
1.1
1.25
1.4
1.6
1.8
2.0
2.2
2.5
2.8
3.2
3.6
4.0
4.5
5.0
5.6
6.3
7.1
8.0
9.0

UNCLASSIFIED

SECURITY CLASSIFICATION OF THIS PAGE

REPORT DOCUMENTATION PAGE

AD-A185 624

DTIC ELECTE OCT 0 1 1987 S D

DTIC FILE COPY

1a. REPORT SECURITY CLASSIFICATION: (illegible)	1b. RESTRICTIVE MARKINGS: N.A.
2a. SECURITY CLASSIFICATION AUTHORITY: (illegible)	3. DISTRIBUTION/AVAILABILITY OF REPORT: Unlimited
2b. DECLASSIFICATION/DOWNGRADING SCHEDULE: N.A.	
4. PERFORMING ORGANIZATION REPORT NUMBER(S): THC-02GH87071A	5. MONITORING ORGANIZATION REPORT NUMBER(S): AFOSR-TR- 87-1034
6a. NAME OF PERFORMING ORGANIZATION: The Hokenson Company	6b. OFFICE SYMBOL (If applicable):
6c. ADDRESS (City, State, and ZIP Code): 840 S. Tremaine Ave. Los Angeles, CA 90005	7a. NAME OF MONITORING ORGANIZATION: AFOSR/NA
	7b. ADDRESS (City, State, and ZIP Code): same as 7a
8a. NAME OF FUNDING/SPONSORING ORGANIZATION: AFOSR	8b. OFFICE SYMBOL (If applicable): NA
	9. PROCUREMENT INSTRUMENT IDENTIFICATION NUMBER: F49620-87-C-0012
8c. ADDRESS (City, State, and ZIP Code): Bldg. 410 Bolling AFB, DC 20332	10. SOURCE OF FUNDING NUMBERS: PROGRAM ELEMENT NO. 61102F; PROJECT NO 2307; TASK NO A1; WORK UNIT ACCESSION NO.

11. TITLE (Include Security Classification)

Turbulence In Hypersonic Flow

12. PERSONAL AUTHOR(S)

Dr. Gustave J. Hokenson

13a. TYPE OF REPORT	13b. TIME COVERED	14. DATE OF REPORT (Year, Month, Day)	15. PAGE COUNT
Final	FROM 86DEC15 TO 87JUN14	87JUL01	74

16. SUPPLEMENTARY NOTATION

17. COSATI CODES			18. SUBJECT TERMS (Continue on reverse if necessary and identify by block number)
FIELD	GROUP	SUB-GROUP	Turbulence, Hypersonic
1	1	10	
1	1	16	

19. ABSTRACT (Continue on reverse if necessary and identify by block number)

Numerical simulations of hypersonic shear flow, utilizing the full time-dependent compressible flow Navier-Stokes equations, have been carried out to demonstrate the feasibility of exposing, computationally, the essential structure/physics of turbulent fluctuations in high speed flow. The geometry employed is one of interest to the U.S. Air Force in various applications, namely a right circular cylinder whose axis is aligned with the on-coming flow and around which the cylinder could be rotated. By simulating the flow along a cylinder of infinite axial extent, an exceptionally quiet flow was established. Due to limitations of computational time, it was necessary to excite artificially this flowfield with periodic suction and blowing located well upstream of the obervation plane. As a result, fluctuations in the flowfield entropy, vorticity and pressure were observed which revealed a distinct Mach number dependence. At hypersonic Mach numbers, the fluctuating entropy defined a second boundary layer edge, well beyond that of the vorticity but not propagating deep into the inviscid flow, as was observed in both transonic and supersonic regimes.

20. DISTRIBUTION/AVAILABILITY OF ABSTRACT: ☒ UNCLASSIFIED/UNLIMITED ☐ SAME AS RPT ☐ DTIC USERS	21. ABSTRACT SECURITY CLASSIFICATION: UNCLASSIFIED
22a. NAME OF RESPONSIBLE INDIVIDUAL: Dr. James Wilson	22b. TELEPHONE (Include Area Code): (202) 767-4935 / 22c. OFFICE SYMBOL: AFOSR/NA

DD FORM 1473, 84 MAR — 83 APR edition may be used until exhausted. All other editions are obsolete.

SECURITY CLASSIFICATION OF THIS PAGE: UNCLASSIFIED

87 9 24 234

THE HOKENSON COMPANY

FINAL REPORT

Phase I SBIR Contract F49620-87-C-0012

TURBULENCE IN HYPERSONIC FLOW

Prepared for:

Dr. James Wilson
Program Manager
AFOSR/NA
Bldg. 410
Bolling AFB, DC 20332

July 1, 1987

ELIZABETH K HOKENSON • CHIEF EXECUTIVE • 840 S TREMAINE AVE., LOS ANGELES, CA 90005 • TEL (213) 935-3743

Table of Contents

List of Figures

Executive Summary

The subject of the research reported here is the numerical simulation of hypersonic turbulent flow from first principles utilizing the full time-dependent compressible flow Navier-Stokes equations. The objective of this Phase I SBIR project was to demonstrate the feasibility of using such a mathematical formulation to expose the essential physics of turbulence unique to hypersonic flow. Motivation for proposing this project was derived from intense interest by the U.S. Air Force in the TAV and NASP programs, as well as on-going work in hypervelocity projectiles. Research which is currently being carried out by The Hokenson Company in this last area for AFATL/MNG, Eglin AFB has guided the configuration of the flowfield which was simulated during Phase I.

The viscous and heat conducting flow of a perfect gas along right circular cylinder whose axis was aligned with the undisturbed upstream flow was computed over a range of free-stream Mach numbers from 1.4 through 6.3. The cylinder could be rotated about its axis so as to establish a mean velocity field with three components, albeit axisymmetric. Without rotation, the boundary layer mean flow was two-dimensional in the conventional sense. The upstream boundary condition was specified in a unique way so as not to introduce excessive numerical 'noise' into the simulation. The technique developed herein was to allow the (axial and azimuthal) flow to 'transition' from full velocity slip at the wall to zero slip over a finite number of axial grid points. This allowed the boundary layer to develop naturally without generating the huge disturbances that are computed if the upstream uniform flow abruptly encounters a zero slip surface. This tactic also significantly reduced the time and costs associated with solving the entire upstream flow (bow shock, stagnation region, transonic region, etc.) associated with a particular fore-body geometry, which was not the focus of this brief research effort.

In this manner, supersonic and hypersonic flowfields which were exceptionally quiet were computed. For even very large Reynolds numbers, the initial numerical noise level was so low that the spatial-temporal instability growth envelope forced unacceptably long computational times. Therefore, the computed boundary layer flow was excited artificially with an harmonic disturbance on the surface of the cylinder at several grid points well upstream of the observation location. Both (temporally) periodic heating and cooling as well as suction and blowing were studied, the latter being adopted for presentation here over the range of Mach numbers of interest. During Phase II various ambient noise models shall be added to the simulation for more natural excitation.

Numerical simulations of the entire flowfield were carried out for a single value of the wall mass transfer disturbance magnitude (equal to 1% of the freestream mass flux) and various frequencies relative to that associated with the viscous flow length and time scales. The results indicate a distinct Mach number effect when the azimuthal vorticity, entropy and pressure fluctuations are observed. In the supersonic flow regime the viscous and inviscid disturbance flowfields are fully-coupled, with the entropy fluctuations propagating well beyond the location where the vorticity fluctuations terminate. This is reminiscent of the wavelets observed experimentally emanating from TBL structures. At higher Mach numbers, the entropy fluctuations also extend beyond the vorticity fluctuations but do not encompass the entire inviscid flow. Instead, a multiple layer picture appears in which two boundary layer edges may be defined relative to the vorticity and entropy fluctuations.

As a result of this work, the feasibility of using first principle numerical simulations of hypersonic turbulence to expose the unique physics of a boundary layer flow has been demonstrated. In addition, it is likely that the results of such computations could also

be useful for developing more compact engineering representations of the turbulent transport processes. Based on intense Air Force interest in the aforementional projectile and aerospace vehicle projects, it is clear that an extensive computational study carried out in a 6.1 Phase II SBIR effort would produce information and data that could be transitioned rapidly for use in various 6.2 programs and beyond.

Discussion

Introduction

During the past few years the resurgence of research activity in the field of hypersonics has been motivated by U.S. Air Force interest in the TAV and NASP program, as well as various high speed projectile/missile applications. Based on extensive experimental studies, the space shuttle was developed more than a decade ago without a satisfactory comprehensive theoretical formulation for the turbulent transport processes. Instead, a patchwork quilt of semi-empirical analyses were tuned to the available data in order to predict full-scale heat transfer, drag, separation, etc. Unfortunately, in the intervening years between the shuttle R&D and the current hypersonic flow programs, breakthroughs in the understanding of turbulent shear flow structure have so far been focused in the lower speed flow regimes. As a consequence, the accurate prediction of heat transfer rates, for example, in turbulent hypersonic flows is still essentially an art form guided by the available data. Numerical predictions of the time-averaged flow is carried out within the context of modeling principles known to be generally valid only in quite different Mach number regimes. Relative to the knowledge of turbulent structure physics in lower speed flows, where transport models can be relatively successful, our understanding of the detailed processes in hypersonic shear flows is indeed minimal.

For incompressible shear flows, numerical simulations are now being used to predict the detailed vortical dynamics in turbulent structures. This is important not only in and of itself to understand nature and have the ability to predict chaotic flows from first principles, but also in providing a basis for developing representations of various fluctuation correlations in time-averaged flow transport models. In supersonic flow, experimental

data regarding the detailed temporally- and spatially-resolved structure of turbulent vorticity, entropy and pressure fluctuations is orders of magnitude less than that available in incompressible flow. In addition, first principle computation of such phenomena is in its infancy, whereas the prediction of time-averaged flow using various semi-empirical models has been in high gear for decades. The success which such an approach has enjoyed rests on the abundance of time-averaged data with which models can be 'tuned' as well as the apparently simple structure of at least the small amplitude disturbances, as first exposed by Kovasznay and his co-workers:

WEAKLY NON-LINEAR FLUCTUATION MODEL DUE TO KOVASZNAY

$$(\partial\omega/\partial t) - \nu\Gamma^2\omega = \Omega(\omega, P, s)$$

$$\frac{\partial s}{\partial t} - \frac{4\nu}{3}\nabla^2 s = S(\omega, P, s)$$

$$\frac{1}{a^2}\frac{\partial^2 P}{\partial t^2} - \nabla^2 P - \frac{4\gamma\nu}{3a^2}\frac{\partial\Gamma^2 P}{\partial t} = \Pi(\omega, P, s)$$

	Sound source	Vorticity source	Entropy source
Sound–sound	' steepening ' and ' self-scattering ' $\frac{\partial^2(v_{p_i} v_{p_j})}{\partial x_i \partial x_j} + a_0^2 \nabla^2(P_p^2) + \frac{\gamma-1}{2}\frac{\partial}{\partial t^2} P_p^2$	$O(\alpha^2\epsilon)$	$O(\alpha^2\epsilon)$
Vorticity–vorticity	' generation ' $\frac{\partial^2(v_{\Omega_i} v_{\Omega_j})}{\partial x_i \partial x_j}$	' self-convection ' $-v_{\Omega_j}\frac{\partial \Omega_i}{\partial x_j} + \Omega_j \frac{\partial v_{\Omega_i}}{\partial x_j}$	$O(\alpha^2\epsilon)$
Entropy–entropy	$O(\alpha^2\epsilon)$	$O(\alpha^2\epsilon^2)$	$O(\alpha^2\epsilon)$
Sound–vorticity	' scattering ' $2\frac{\partial^2(v_{\Omega_i} v_{p_j})}{\partial x_i \partial x_j}$	' vorticity convection ' $-v_{p_j}\frac{\partial \Omega_i}{\partial x_j} + \Omega_j \frac{\partial v_{p_i}}{\partial x_j} - \Omega_i \frac{\partial v_{p_j}}{\partial x_j}$	$O(\alpha^2\epsilon)$
Sound–entropy	' scattering ' $\frac{\partial^2}{\partial t \partial x_i}(S_p v_{p_i})$	' generation ' $-a_0^2(\nabla S_p) \times (\nabla P_p)$	' heat convection ' $-v_{p_i}\frac{\partial S_p}{\partial x_i}$
Vorticity–entropy	$O(\alpha^2\epsilon)$	$O(\alpha^2\epsilon)$	' heat convection ' $-v_{\Omega_i}\frac{\partial S_p}{\partial x_i}$

Second-order non-linear interaction between modes

The utility of dilitation as a variable, in lieu of entropy, has been exploited by the Principal Investigator in previous research. The enclosed paper indicates that the structure of non-linear fluctuations, such as those encountered in hypersonic flow, may be more readily understood when dilatation is selected.

Dilatation wave/soliton dynamics in variable density flows

Gustave Hokenson
Dynamics Technology, Inc., Torrance, California 90505

(Received 24 July 1981; accepted for publication 5 January 1982)

The dynamics of dilatation has been investigated for variable density flows which exhibit a temporal evolutionary character. In lieu of decomposing the conservation of mass equation (appropriate for strictly nondiffusive/incompressible flows) and utilizing div $\mathbf{u} = 0$ to generate a Poisson pressure equation, the closure relation "small div $\mathbf{u}$" was used. This suggests an approximate decomposition of the div $\mathbf{u}$ governing equation into a steady elliptic pressure equation and a time-dependent equation for nonacoustic waves which governs div $\mathbf{u}$ (herein denoted by $\tilde{\Omega}$): $\partial\tilde{\Omega}/\partial\tilde{t} - [1 - \int\tilde{\Omega}d\tilde{x} - (1/4\,\mathrm{Re})\partial \ln \rho/\partial\tilde{x}](\partial\tilde{\Omega}/\partial\tilde{x}) = \tilde{\Omega}^2 - (1/\mathrm{Re})\partial^2\tilde{\Omega}/\partial\tilde{x}^2$, utilizing the exact equations of continuity and momentum. The solution of this ("vorticity-like") equation provides information on how an initially small div $\mathbf{u}$ field evolves, frequently into a solitary wave. Should the dilatation remain "small," rather than be (nonphysically) forced equal to zero, the full conservation relations may be utilized. However, if div $\mathbf{u}$ grows large, the elliptic pressure equation is inconsistent with the untampered governing equations. The motivation for this approach is to provide a structure within which: (1) small diffusive/compressibility effects may be studied, (2) the significance of div $\mathbf{u}$ physics, in flows which are traditionally treated as approximately dilatation free, may be analyzed, and (3) evolutionary pressure transport formalisms may be developed and evaluated for computational efficiency/accuracy and the inclusion of nonlinear acoustic waves.

PACS numbers: 47.10.+g, 47.30.+s, 47.55.Hd

INTRODUCTION

Fluid flows which are *approximately* incompressible and nondiffusive are often analyzed/computed utilizing a decomposed conservation of mass equation $D\rho/Dt \simeq 0$ and, therefore, $\Omega \simeq 0$ [see Eq. (A1), Appendix]. This allows the governing system of equations to be closed, independent of dealing with the equations of state and thermodynamics.

In this context, incompressible means that the equation of state, e.g., $\rho = \rho(T, S_i)$, is independent of pressure and relates the fluid density, ρ, to the local thermodynamic temperature, T, and various chemical species constituents, S_i. The term nondiffusive indicates that, relative to macroscopic flowfield length scales, the scales characteristic of molecular transport, over typical flow times, are negligible and, therefore, $DT/Dt \simeq 0 \simeq DS_i/Dt$. Clearly, that implies $D\rho/Dt \simeq 0$ and, from Eq. (A1), $\Omega \simeq 0$.

The arguments required to establish $DS_i/Dt \simeq 0$ involve only small transport coefficients and zero species production via chemical reaction. However, $DT/Dt \simeq 0$ only if heat and momentum transport coefficients are small and it is assumed *a priori* that buoyancy and pressure work is negligible ($\Omega \simeq 0$). A consistent $D\rho/Dt \simeq 0 \simeq \Omega$ foundation is thus established.

A complementary way of viewing this traditional equation decomposition, which relates to subsequent discussions, involves differentiating Eq. (A1), resulting in

$$\frac{D\Omega}{Dt} = \Omega^2 - \kappa, \tag{1}$$

where $\rho\kappa \equiv D^2\rho/Dt^2$. According to Eq. (1), if $\kappa = 0$ exactly, by virtue of the aforementioned assumptions, $\Omega = 0$ (initial conditions would be maintained for all time). However, *an arbitrarily small* initial dilatation anomaly (Ω) approaches ∞ as $\Omega_i t \to 1$, in convected coordinates. A strictly incompressible/nondiffusive model would require $\Omega = \Omega_{,i} = 0$ as a requisite auxiliary relationship on the basis of boundedness alone. However, imposing this constraint on slightly diffusive/compressible flows has a significant effect on the mathematical structure and the physics which it reflects, as indicated by Eq. (1).

In the context of $D\rho/Dt \simeq 0$, utilization of the full conservation relations to solve for an evolutionary Ω field is, therefore, apparently a delicate matter which is the focus of this work. The sensitivity of its mathematical structure and Eq. (1) itself are reminiscent of the vorticity transport/stretching equation. In fact, the symbol Ω was chosen to represent div $\mathbf{u}$ precisely to emphasize the t^{-1} character as ω conventionally does for vorticity (curl $\mathbf{u}$). For homogeneous flows, vorticity is typically generated locally, e.g., at solid boundaries, shock wave intersections, etc., and diffuses/convects into adjacent, nearly irrotational regions. Similarly, the div $\mathbf{u}$ field equation serves the variable density flow by representing the generation of dilatation in certain diffusive/compressible "boundary layers" in space/time and its subsequent influence on neighboring, nearly dilatation-free flow. Such "boundary layers" might arise due to the presence of large gradients near sources of heat and chemical species. The associated vorticity production term in nonhomogeneous flows, $\nabla p \times \nabla \rho^{-1}$, is also active in these dilatation boundary layers.

EQUATION DEVELOPMENT

In order to expose the "vorticity-like" role which div $\mathbf{u}$ may play in both the physics and computational treatment of rotational, variable density flows, the following formulation was developed. It is intended, initially, to illuminate the unique features of dilatational dynamics and, subsequently,

 0021-8979/82/053461-08$02.40

to provide a framework within which the accuracy and generality of the analysis may be increased.

Combining the governing equations of motion[1] (A1) and (A2), subsequent differentiation and summing leads to the following exact expression for Ω:

$$\frac{\partial \Omega}{\partial t} + \frac{\partial^2 u_i u_j}{\partial x_i \partial x_j} - \Omega^2 - u_i \frac{\partial \Omega}{\partial x_i} = -\rho^{-1} \frac{\partial^2 p}{\partial x_i \partial x_i} - \rho^{-1} \frac{\partial \ln \rho}{\partial x_i} \frac{\partial p}{\partial x_i} + \frac{4\nu}{3} \frac{\partial^2 \Omega}{\partial x_j \partial x_j} - \nu \frac{\partial \ln \rho}{\partial x_i} \left(\frac{\partial^2 u_j}{\partial x_j \partial x_i} + \frac{1}{3} \frac{\partial \Omega}{\partial x_i} \right). \quad (2)$$

where the summation convention is assumed. The traditional incompressible/nondiffusive model ($\Omega = 0$) of variable density flows reduces Eq. (2) to

$$\frac{\partial^2 p}{\partial x_i \partial x_i} - \left(\frac{\partial \ln \rho}{\partial x_i} \right) \frac{\partial p}{\partial x_i} = -\rho \frac{\partial^2 u_i u_j}{\partial x_i \partial x_j} - \left(\frac{\partial \ln \rho}{\partial x_i} \right) \mu \frac{\partial^2 u_i}{\partial x_j \partial x_j}. \quad (3)$$

Note that setting $\Omega = 0$, in lieu of a small value, has dramatic consequences on the mathematical structure of Eq. (2), converting an evolutionary equation into an elliptic equation in space. This structure is consistent with the physical interpretation of infinite signal propagation speed in dilatation-free flows. In addition, Eq. (3) displays explicit flow nonuniformity effects ($\partial \ln \rho / \partial x_i$) which modify the classical Poisson pressure equation by introducing pressure gradient and viscous terms, "weighted" by the density variation.

In lieu of dealing with a precise, yet inexact, closure relation ($\Omega = 0$) and decomposing conservation of mass into *approximate* equations, it is of interest to investigate an alternate, imprecise, closure technique *in the context of the exact conservation of mass relation*. As will be shown, the effect of a "small Ω" closure is to suggest the decomposition of Eq. (2) instead of (A1). The stability and faithfulness to the "small Ω" assumption of this approach is the subject of this study.

Realizing that $\Omega = 0$ is often a relatively weak assumption in variable density flows, *the sum of all Ω terms in Eq. (2) is estimated to be of order* ϵ, where $\epsilon \ll (u/L)_c^2$ and $(u/L)_c^{-1}$ is a characteristic macroscopic flowfield time scale. The feasibility of retaining Eq. (3), along with the untampered governing conservation equation of mass and momentum is investigated.

Note that the essence of this argument is identical to that previously used to decompose the conservation of mass equation according to $D \ln \rho / Dt = \epsilon$ and $\Omega = -\epsilon$, where $\epsilon = 0$ is implemented after evaluating the smallness of $D \ln \rho / Dt$ from the equations of state, thermodynamics, and species. In the present case, each group of terms, namely those Ω terms in Eq. (2) and the pressure/velocity terms in Eq. (3), is small and subsequently set equal to zero. The consequence of this closure approximation is to establish governing equations [Eqs. (A1), (A2), (3)] which implicitly force Ω to vary according to

$$\frac{\partial \Omega}{\partial t} - \left(u - \frac{\nu}{3} \frac{\partial \ln \rho}{\partial x_i} \right) \frac{\partial \Omega}{\partial x_i} = \Omega^2 + \frac{4\nu}{3} \frac{\partial^2 \Omega}{\partial x_i \partial x_i}. \quad (4)$$

To make this development more precise, various formal expansions of Eq. (2) are possible. However, for the purposes of this work, the following heuristic approach is sufficient. Consider Eq. (2) in the representational form $\partial \Omega / \partial t + f(\Omega) = \epsilon$, where ϵ is the error arising from the fact that Eq. (3) is not satisfied exactly [in Eq. (2)]. It is assumed that ϵ is small and Ω in Eq. (2) is expanded in the form $\Omega = \Omega_1 + \epsilon \Omega_2 + \text{H.O.T.}$ To first order, Eq. (4) is retained which essentially filters out all nonlinear acoustic aspects of dilatation wave propagation.

To reiterate, Eq. (4) is a consequence of solving the untampered conservation of mass and momentum equations in conjunction with an elliptic pressure field relation. In general, Eq. (4) need not be solved since its only function is to serve as an Ω growth monitor. However, the Ω characteristics may be assessed, to a considerable extent independent of specific flowfield details, by analyzing the solutions of Eq. (4).

Due to nonzero initial/boundary conditions, Ω will exhibit some evolutionary behavior. If it maintains a "relatively small" value, the solution of the governing equations will remain faithful to the untampered conservation relations. However, if Ω grows (nonphysically), the formulation for pressure expressed in Eq. (3) is inconsistent with the small Ω closure model, at least in the context of the full conservation relations, and an alternate pressure formulation is required.

ANALYSIS

In order to examine the characteristic behavior of Eq. (4), consider a one spatial dimension case for which $u \to u_0$ as $x \to -\infty$. The ensuing expression may be nondimensionalized according to Eqs. (A3), resulting in

$$\frac{\partial \tilde{\Omega}}{\partial \tau} - \left(1 + \int \tilde{\Omega} d\tilde{x} - \frac{1}{4\,\text{Re}} \frac{\partial \ln \tilde{\rho}}{\partial \tilde{x}} \right) \frac{\partial \tilde{\Omega}}{\partial \tilde{x}} = \tilde{\Omega}^2 + \frac{1}{\text{Re}} \frac{\partial^2 \tilde{\Omega}}{\partial \tilde{x}^2}. \quad (5)$$

Initially, it is of interest to consider the solutions to Eq. (5) for various limiting cases. Note that a uniform $\tilde{\Omega}$ field varies according to

$$\frac{d\tilde{\Omega}}{d\tau} = \tilde{\Omega}^2, \quad (6)$$

and, as with Eq. (1), approaches ∞ as $\tilde{\Omega}_0 \tau \to 1$. Similarly, a nonuniform $\tilde{\Omega}$ field evolves according to Eq. (6) as $\text{Re} \to \infty$ in characteristic coordinates defined by

$$d\tilde{x}/d\tau = -\left(1 + \int \tilde{\Omega} d\tilde{x} - \frac{1}{4\,\text{Re}} \frac{\partial \ln \tilde{\rho}}{\partial \tilde{x}} \right). \quad (7)$$

At least for these limits, the linearized solutions motivated by situations where $\tilde{\Omega}_0 \ll 1$ degenerate into solutions of the form $\tilde{\Omega} = \tilde{\Omega}_0$. Considering the fact that arbitrarily small values of $\tilde{\Omega}_0$ become unbounded for sufficiently large τ, these solutions are of trivial importance in the assessment of the limitations of the "small Ω" closure model proposed here.

For cases with finite Reynolds number, the linearized version of Eq. (5) becomes

$$\frac{\partial \tilde{\Omega}}{\partial \tau} + c \frac{\partial \tilde{\Omega}}{\partial \tilde{x}} = \frac{1}{\text{Re}} \frac{\partial^2 \tilde{\Omega}}{\partial \tilde{x}^2}, \quad (8)$$

where $c \equiv -(1 - \partial \ln \tilde{\rho}/\partial \tilde{x}/4\,\mathrm{Re})$. In this case the $\tilde{\Omega}$ solution takes the form $\tilde{\Omega}_i = \tilde{\Omega}_0 e^{(\mathrm{Re}\,(\cdots)\tau - 2\tilde{x}^2)}$ so that the solution simply diffuses relative to the curve $\tilde{x} - c\tau/2 = 0$. However, sufficiently large Reynolds numbers invalidate the viscous linearization, even for small $\tilde{\Omega}_0$, with the behavior indicated by Eq. (6) taking over in either the intrinsic or characteristic coordinate system. Therefore, simultaneous consideration of both viscous and nonlinear effects is generally required.

As an illustrative example which has some bearing on subsequent computations, consider the case for which the $\tilde{\Omega}^2$ nonlinearity is dominated by $(\int \tilde{\Omega} d\tilde{x})(\partial \tilde{\Omega}/\partial \tilde{x})$. In this situation, Eq. (8) becomes

$$\frac{\partial \tilde{\Omega}}{\partial \tau} + c(\tilde{\Omega}) \frac{\partial \tilde{\Omega}}{\partial \tilde{x}} = \frac{1}{\mathrm{Re}} \frac{\partial^2 \tilde{\Omega}}{\partial \tilde{x}^2}, \tag{9}$$

where $c \equiv -(1 + \int \tilde{\Omega} d\tilde{x} - \partial \ln \tilde{\rho}/\partial \tilde{x}/4\,\mathrm{Re})$.

It is of interest to search for steady solutions[2] in the convected frame of reference defined by $\eta \equiv \tilde{x} \pm U\tau$, where U is a (constant) wave convection speed. In this coordinate system Eq. (9) becomes

$$[c(\tilde{\Omega}) \pm U]\tilde{\Omega}' = \frac{1}{\mathrm{Re}} \tilde{\Omega}'', \tag{10}$$

where the prime denotes differentiation with respect to η. Equation (10) may be integrated to provide

$$C(\tilde{\Omega}) \pm U\tilde{\Omega} + \lambda_0 = \frac{1}{\mathrm{Re}} \tilde{\Omega}', \tag{11}$$

where $C = \int c\, d\tilde{\Omega}$ and λ_0 is an integration constant. Various "jump-type" phenomena may be exposed by seeking exponential solutions (approximately) consistent with the functional dependence: $\int \tilde{\Omega} d\tilde{x} = -(2\lambda_2)\tilde{\Omega}$, where λ_2 is a constant. In this case, C may be written: $(\lambda_1 \tilde{\Omega} + \lambda_2 \tilde{\Omega}^2 + \lambda_3)$, where $\lambda_1 \equiv -1 + \partial \ln \tilde{\rho}/\partial \tilde{x}/4\,\mathrm{Re}$ and Eq. (11) may be integrated in the form

$$\mathrm{Re}\,\eta = \int \frac{d\tilde{\Omega}}{(\lambda_0 + \lambda_3) + (\lambda_1 \pm U)\tilde{\Omega} + \lambda_2 \tilde{\Omega}^2}, \tag{12}$$

to provide the solution

$$\frac{\tilde{\Omega}_i - \tilde{\Omega}}{\tilde{\Omega} - \tilde{\Omega}_i} = \exp\,(\lambda_2\,\mathrm{Re}\,\eta(\tilde{\Omega}_f - \tilde{\Omega}_i)). \tag{13}$$

It is clear from Eq. (13) that, as $\eta \to \pm\infty$, $\tilde{\Omega} \to \tilde{\Omega}_{i,f}$ exponentially. Therefore, the "jump" in $\tilde{\Omega}$ across this solitary wave is $\tilde{\Omega}_f - \tilde{\Omega}_i$ and $\tilde{\Omega}_{i,f}$ are related to the parameters of the problem by $\tilde{\Omega}_i \tilde{\Omega}_f = (\lambda_0 + \lambda_3)/\lambda_2$ and $\tilde{\Omega}_i + \tilde{\Omega}_f = -(\lambda_1 \pm U)/\lambda_2$. Additionally, as $\eta \to \pm\infty$, Eq. (10) may be evaluated to provide $\mp U = [C(\tilde{\Omega}_f) - C(\tilde{\Omega}_i)]/(\tilde{\Omega}_f - \tilde{\Omega}_i)$. Therefore, for certain situations, the presence of "shock" or "jump-type" solitary wave solutions to Eq. (5) should be anticipated.

In order to assess the fully nonlinear/viscous case, consider Eq. (5) with the (generally small) density nonuniformity term temporarily set equal to zero. Once again, hypothesizing similarity solutions of the form $\tilde{\Omega} = \tilde{\Omega}(\eta)$, where $\eta \equiv \tilde{x} \pm U\tau$ and U is a (constant) wave convection speed, Eq. (5) may be written

$$\pm U f'' - f f'' = f'^2 + \frac{1}{\mathrm{Re}} f'''. \tag{14}$$

The dimensionless velocity, $f(\tilde{x})$, is defined such that $\partial f/\partial \tilde{x} = \tilde{\Omega}$ and $f \to 1$ while all its derivatives (as indicated by the primes) approach zero as $\tilde{x}$ and $\tilde{\eta} \to \pm\infty$.

Equation (14) may be integrated twice to provide

$$\frac{f'}{\mathrm{Re}} + \frac{f^2}{2} \mp Uf = \lambda_4 \eta + \lambda_5, \tag{15}$$

where λ_4 and λ_5 are constants of integration. Applying the boundary conditions on f to Eq. (15) results in

$$\frac{f'}{\mathrm{Re}} + \frac{f^2}{2} \mp Uf = \frac{1}{2} \mp U, \tag{16}$$

which may be integrated in the form

$$\int \frac{df}{-f^2/2 \pm Uf + (1/2 \mp U)} = \mathrm{Re} \int d\eta, \tag{17}$$

resulting in

$$f = \pm U - \delta \tanh(-\delta\,\mathrm{Re}\,\eta/2), \tag{18}$$

and

$$\tilde{\Omega} = \delta^2(\mathrm{Re}/2)\mathrm{sech}^2(-\delta\,\mathrm{Re}\,\eta/2), \tag{19}$$

where

$$\delta \equiv (U^2 \mp 2U + 1)^{1/2}. \tag{20}$$

Note that, since sech is symmetric about $\eta = 0$ with a maximum value of 1.0, Eq. (19) provides the relationship

$$\tilde{\Omega}_{\max} = \delta^2\,\mathrm{Re}/2, \tag{21}$$

and, therefore

$$U = 2(\pm 1 \pm (2\tilde{\Omega}_{\max}/\mathrm{Re})^{1/2}), \tag{22}$$

where the first $\pm$ sign corresponds to the one in Eq. (14), whereas the second arises from the two roots to the solution. At this point, either root may be physically reasonable with the "observed" value dependent on the details of the initial conditions and its evolution. However, it is clear that negative-valued initial conditions are incompatible with this solitary wave solution. The $\delta = 0$ solutions admit negative values of $\tilde{\Omega}$ but require $\tilde{\Omega} \to \infty$ as $\eta \to 0$. Note that constant density nonuniformity cases may be accommodated by redefining U to be $U + \partial \ln \tilde{\rho}/\partial \tilde{x}/4\,\mathrm{Re}$.

Therefore, for certain ranges of Re, arbitrarily small $\tilde{\Omega}_0$ values grow nonlinear and form various types of stationary (in the convected reference frame) waves, which remain a permanent part of the solution.

COMPUTATIONS

As discussed in the previous section, given any $\tilde{\Omega}_0$, there exists a Re such that, for sufficiently large τ, the $\tilde{\Omega}$ solution becomes dominantly nonlinear. In lieu of utilizing small values of $\tilde{\Omega}_0$ and computing long evolutionary periods, the approach taken here is to expose the unique features of dilatation dynamics by focusing on larger $\tilde{\Omega}_0$ values with consequently smaller critical Re and nonlinear evolution times. Therefore, Eq. (5) has been integrated[3] for various Reynolds numbers and initial conditions, assuming a Gaussian $\tilde{\Omega}_0$ disturbance at a given spatial location. The functional form used, $\exp(-4\tilde{x}^2)$, reflects a characteristic length which equals the width of the initial conditions at the e-folding amplitude. Analysis indicated that the nonuniformity term $(\partial \ln \tilde{\rho}/\partial \tilde{x}/4\,\mathrm{Re})$ is of secondary importance (relative to the dominant terms, $1 + \int \tilde{\Omega} d\tilde{x}$) and has, therefore,

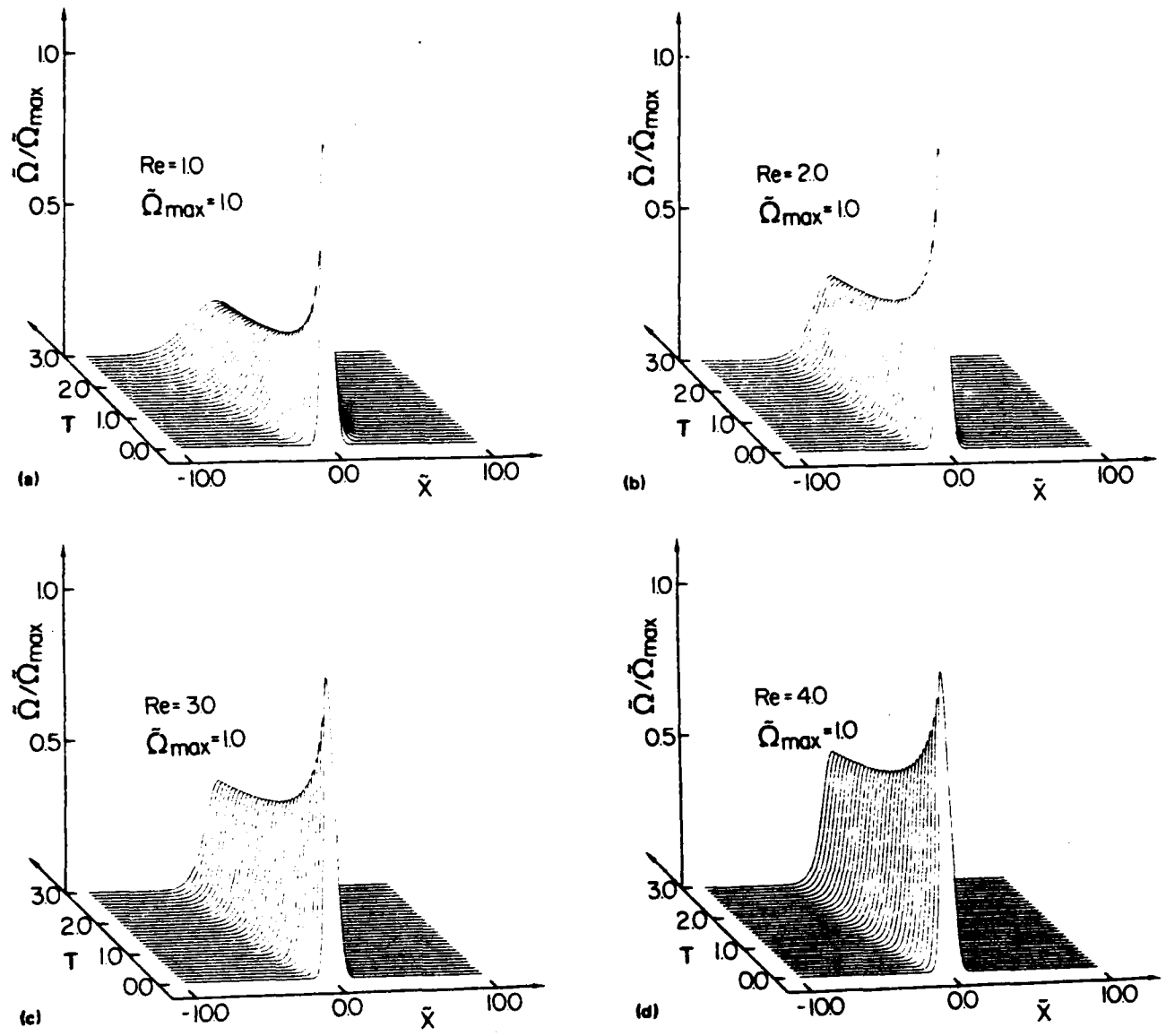

FIG. 1. The evolution of a Gaussian initial $\tilde{\Omega}$ disturbance of magnitude $\tilde{\Omega}_{max} = 1.0$ at a Reynolds number, (a) Re = 1.0, (b) Re = 2.0, (c) Re = 3.0, and (d) Re = 4.0.

been set equal to zero in these calculations. The results of the integrations illustrate that both bounded and unbounded $\tilde{\Omega}$ solutions arise.

The effects of Reynolds number, initial condition amplitude and sign are depicted in Figs. 1–4. For a positive initial $\tilde{\Omega}$ disturbance of amplitude 1.0, the effect of Reynolds number is depicted in Figs. 1(a)–1(d). Note that the dilatation disturbance wave propagates upwind. Therefore, $\tilde{\Omega}$ will distort the field ahead of its origin and eventually contaminate the entire domain. At Reynolds numbers of approximately 10.0 or smaller, the initial amplitude diminishes with time until an approximately steady profile is attained in the convected frame of reference at $\tau \simeq 3.0$, as discussed in the previous section. For Reynolds numbers greater than 10.0, the initial conditions grow with time.

At a Reynolds number of one, the effect of an increasingly positive initial condition was computed and is presented in Figs. 2(a)–2(d). Note that, with increasing amplitude, both nonlinearities in Eq. (5) come into play with increasing strength. This is evident from the increased amplitude (relative to $\tilde{\Omega}_0$) and its upwind "tilt." The solution exhibits a decrease in amplitude with time for initial amplitudes less than ~ 10.0. As the amplitude increases, the convection speed increases and tilts the solution to the left, as the tendency for a "growth-mode" solution is approached at an amplitude of approximately 10.0

When the sign of the initial conditions is changed, the effect of the nonlinearities on the solution is altered. As shown in Figs. 3(a)–3(d) for an amplitude of -1.0, increasing the Reynolds number narrows the spatial extent of the disturbance at large times with a dramatic change in its characteristic shape. Note that the initially rapid damping of the initial conditions, due to the (now negative) $\tilde{\Omega}^2$ terms, decreases and the disturbance eventually relaxes toward zero

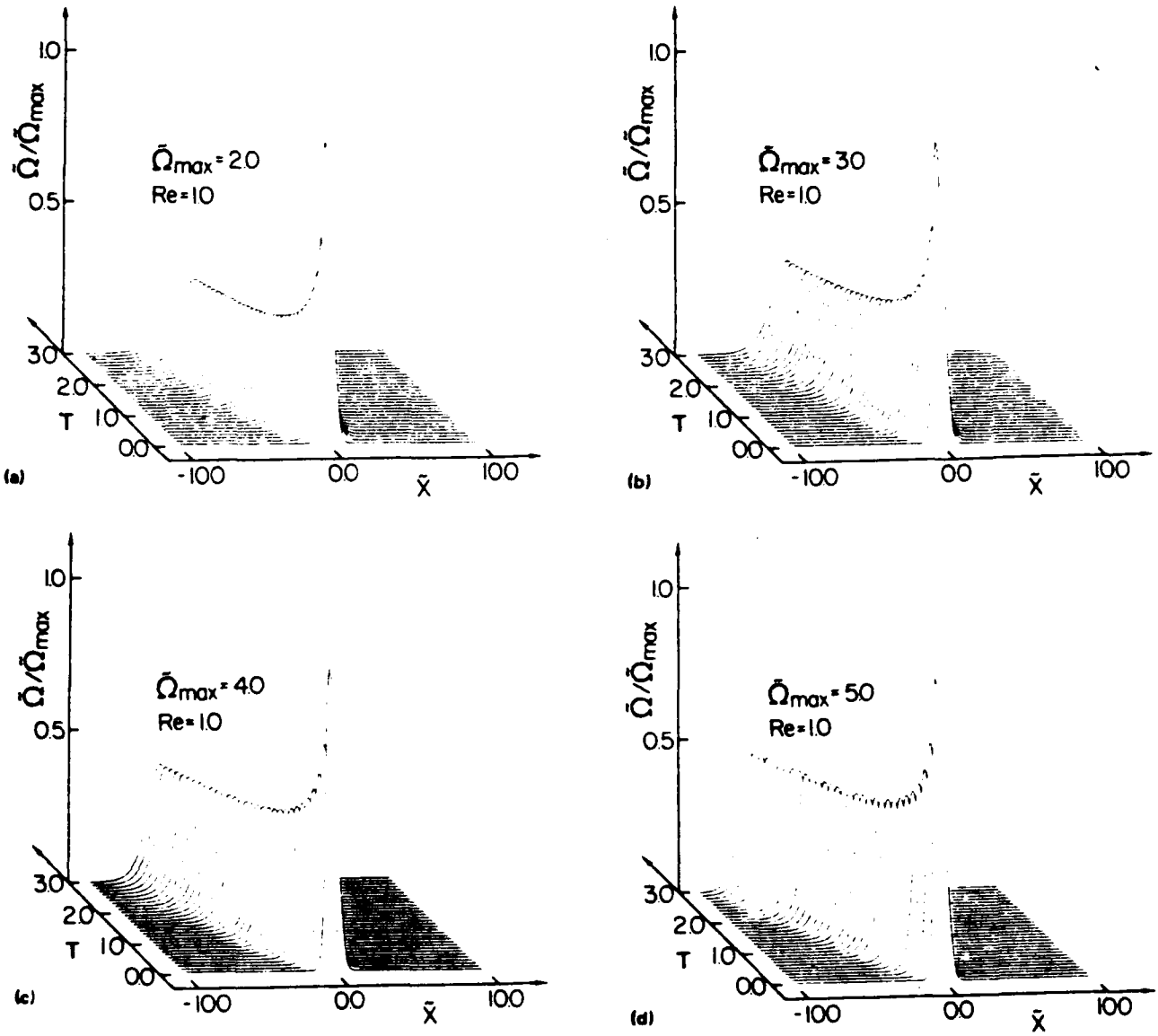

FIG. 2. Evolution of a Gaussian initial $\tilde{\Omega}$ disturbance of: (a) magnitude $\tilde{\Omega}_{max}$ = 2.0 at a Reynolds number, Re = 1.0; (b) magnitude $\tilde{\Omega}_{max}$ = 3.0 at a Reynolds number, Re = 1.0; (c) magnitude $\tilde{\Omega}_{max}$ = 4.0 at a Reynolds number, Re = 1.0; (d) magnitude $\tilde{\Omega}_{max}$ = 5.0 at a Reynolds number, Re = 1.0.

asymptotically. In this case, the effect of a change in the sign of $\int \tilde{\Omega} d\tilde{x}$ is to direct the wave downstream and to eventually dominate the nonlinearities by modifying the shape according to whether $\partial \tilde{\Omega} / \partial \tilde{x}$ is a source or sink term in the overall dynamic balance.

Finally, for a Reynolds number of 10.0 (above which the solution changes only slightly) the effect of increasingly negative initial conditions is presented in Figs. 4(a)–4(d). As the initial conditions become more negative several consequences on the solution are observed. First, although the initial decay of the solution is increasingly effective in damping the disturbance, its spatial extent is enlarged. In addition, the characteristic shape becomes a more nearly flat profile with relatively abrupt transition to the undisturbed freestream at its leading and trailing edge, reminiscent of the "jump-type" solitary wave profile discussed in the previous section. Finally, the abruptness at the leading edge of the wave propagating downstream is significantly different than the relatively smooth trailing edge waveform.

CONCLUSION

It has been shown that, when the untampered conservation equations of mass and momentum are solved in conjunction with a steady elliptic pressure field equation, complicated dilatation dynamics arise which significantly alter the computed flowfield characteristics. Depending on the Reynolds number, sign and amplitude of the initial conditions, both bounded and unbounded solutions exist for the dilatation evolution. For positive initial conditions, an upstream-propagating solitary wave solution exists which may contaminate the entire flowfield. However, its amplitude is a fraction of the disturbance initial condition. For negative

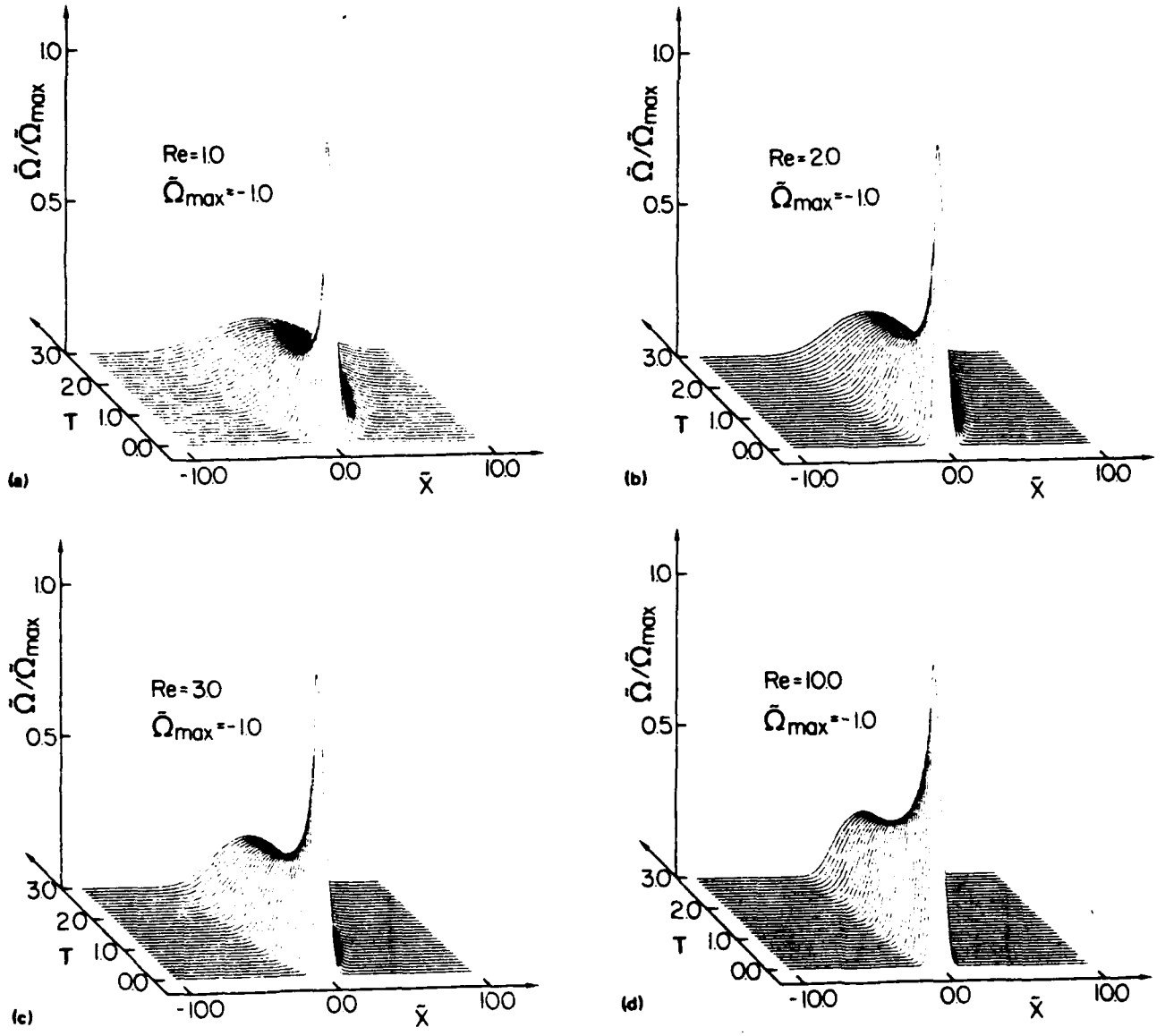

FIG. 3. Evolution of a Gaussian initial $\tilde{\Omega}$ disturbance of magnitude $\tilde{\Omega}_{max} = -1.0$ at a Reynolds number, (a) Re = 1.0, (b) Re = 2.0, (c) Re = 3.0, and (d) Re = 10.0.

initial conditions, the initial disturbance spreads out and forms two "jump-type" transitions connected by a "rooftop" profile. Therefore, the Poisson pressure equation is compatible with the full conservation relations only within a window determined by the parameters which characterize the dilatation disturbance. Outside of this window, a "small $\tilde{\Omega}$" formulation utilizing the untampered conservation equations is inconsistent with Eq. (3), due primarily to the invalidation of the arguments which led to the decomposition of Eq. (2).

On-going work involves alternate forms for an evolutionary pressure (transport) equation which complements Eq. (2). The objective is to alleviate both the steady pressure equation inconsistency and the need for generating a computationally time consuming (yet approximate) elliptic field solution, thus admitting nonlinear acoustic waves. Along with the generation of an elliptic field pressure equation goes the establishment of a set of equations which exceeds the number unknowns, albeit not linearly independent. Therefore, some machinations are required to satisfy all equations simultaneously, typically via an Ω "correction" term to Eq. (3). Inasmuch as the "small Ω" decomposition of Eq. (2) avoids the equation excess problem, it is felt that increasing the accuracy of an Ω-oriented approach may be fruitful in generating a completely evolutionary pressure formalism for nonacoustic as well as acoustic waves. Short of embarking on an exact variable ρ computation, the conservation of mass equation suggests the following form for a pressure transport relation:

$$\frac{Dp}{Dt} + \rho\Omega/\epsilon' = 0, \tag{23}$$

where $\epsilon' \equiv a^{-2}$ for isentropic flow and a is the local speed of sound. For gases, in this case $\rho\Omega/\epsilon' = \gamma p\Omega$, whereas in iso-

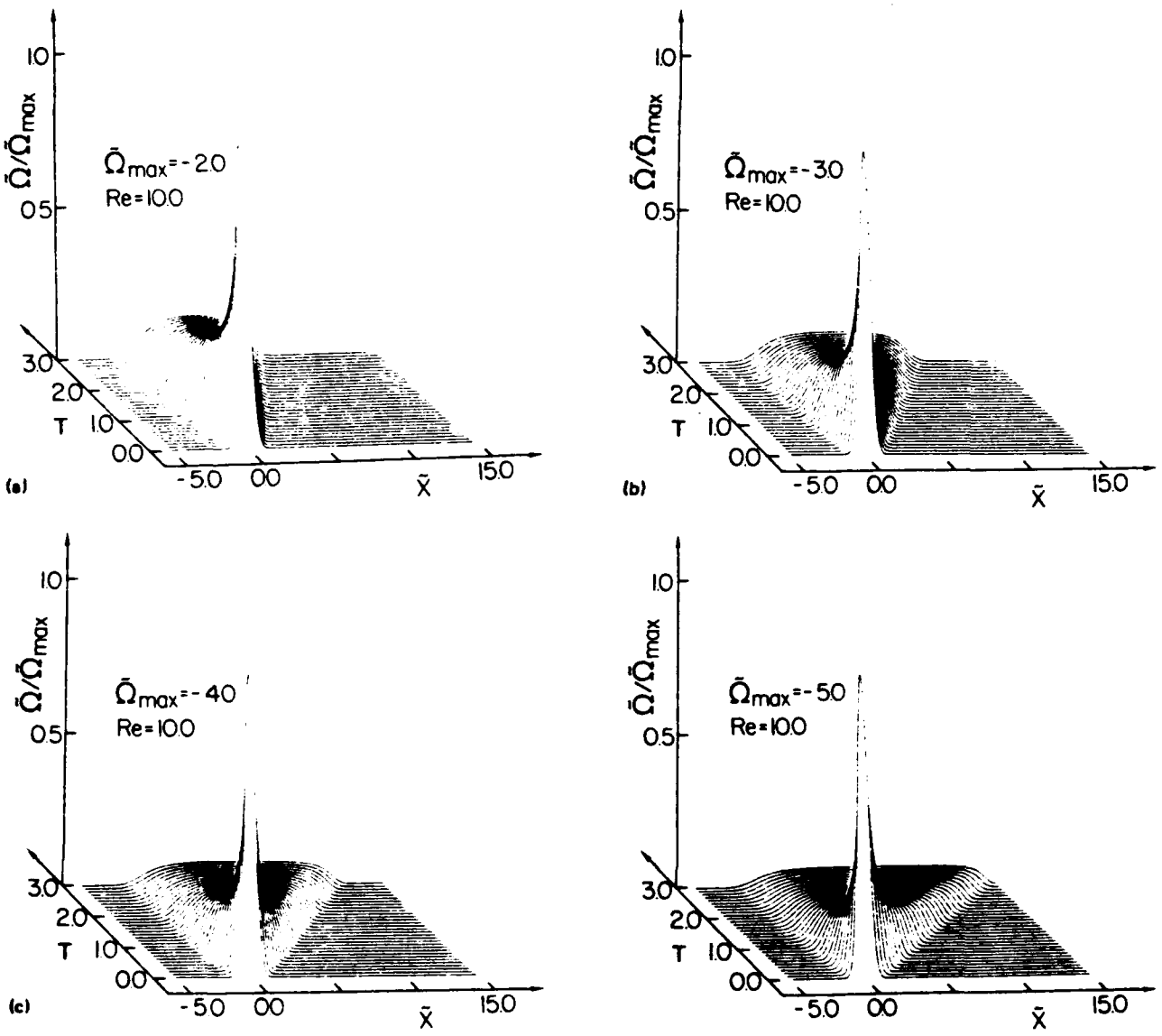

FIG. 4. Evolution of a Gaussian initial $\tilde{\Omega}$ disturbance of: (a) magnitude $\tilde{\Omega}_{max} = -2.0$ at a Reynolds number, Re = 10.0; (b) magnitude $\tilde{\Omega}_{max} = -3.0$ at a Reynolds number, Re = 10.0; (c) magnitude $\tilde{\Omega}_{max} = -4.0$ at a Reynolds number, Re = 10.0; (d) magnitude $\tilde{\Omega}_{max} = -5.0$ at a Reynolds number, Re = 10.0.

thermal (or $DT/Dt \simeq 0$) flow $\rho\Omega/\epsilon' = p\Omega$. For nondiffusive ($T$ and S_i) liquid flows $\epsilon' = (\partial p/\partial\rho)^{-1}_{S,T}$ which, in general, is a function of the local S_i and T, forcing the S_i and T fields to be computed. In some cases, however, $\partial p/\partial\rho$ for a liquid may be approximately a function of ρ alone.

Regardless of the particular ϵ' formulation, the coupling of Eqs. (23) and (2) forms a candidate evolutionary pressure transport system to mimic the predictions of Eq. (3), while admitting nonlinear acoustic waves, and allows the conservation of mass equation to be retained in a computationally effective framework. The unique Ω dynamics indicated in Eq. (2) would be similar to those encountered here in Eq. (5) and, therefore, the present computations serve as a model for the behavior of Eqs. (2) and (23). An appropriate form for ϵ' must be validated. However, for moderate Ω, this structure might allow Eq. (3) to be replaced without ϵ' reflecting the *detailed* compressibility/diffusive physics. In the framework of exact, multiequation solutions for $\tilde{\Omega}$, the effect of coupling through $-(1/4\,\mathrm{Re})\,\partial \ln\tilde{\rho}/\partial\tilde{x}$ is readily examined. However, the structure of the solitary waves is not then analytically accessible, due to the form of $-(1/4\,\mathrm{Re})(\ln\tilde{\rho})'$: $(\tilde{\Omega}/4\,\mathrm{Re})(1 + \int\tilde{\Omega}d\tilde{x} \pm U)$, derived from continuity. At Re of interest this effect is generally small.

In addition, the implications of complex Ω dynamics [not only in Eqs. (4), (5), and (6), but also in Eq. (23) where small Ω is amplified by ϵ] to problems of physical importance, which are traditionally treated within the $\Omega = 0$ framework, is being studied, e.g., in vortex stretching dynamics. Finally, utilization of this technique to approximately quantify the significance of compressibility/diffusive phenomena in weakly nonhomogeneous flows is being investigated. With the inclusion of nonlinear acoustic waves, the effect of bulk viscosity on the dilatation phenomena in liquids and nonmonatomic gases must also be considered. In

these cases the dilatational viscosity does not equal $-2\mu/3$.

APPENDIX

Continuity:

$$\frac{\partial \rho}{\partial t} + \frac{\partial \rho u_i}{\partial x_i} = 0$$

or

$$\frac{D\rho}{Dt} + \rho\Omega = 0 \tag{A1}$$

where

$$\frac{D}{Dt} \equiv \frac{\partial}{\partial t} = u_i \frac{\partial}{\partial x_i}, \quad \Omega \equiv \frac{\partial u_i}{\partial x_i}.$$

Momentum (for a fluid obeying Stokes hypothesis):

$$\frac{\partial \rho u_i}{\partial t} + \frac{\partial \rho u_i u_j}{\partial x_j} = -\frac{\partial p}{\partial x_i} + \rho g_i + \mu \frac{\partial^2 u_i}{\partial x_j \partial x_j} + \frac{\mu}{3} \frac{\partial \Omega}{\partial x_i}. \tag{A2}$$

Nondimensionalization:

$$\left.\begin{aligned} &\tilde{\Omega} \equiv \Omega / \Omega_r; \quad \tau \equiv \Omega_r t \quad ; \quad \Omega_r \equiv u_0 / L \\ &\tilde{x} \equiv x/L \quad ; \quad \mathrm{Re} \equiv 3\Omega_r L^2 / 4\nu; \quad \tilde{\rho} \equiv \rho / \rho_r. \end{aligned}\right\} \tag{A3}$$

[1] G. K. Batchelor, *An Introduction to Fluid Dynamics* (Cambridge University, London, 1967), p. 147.
[2] G. B. Whitham, *Linear and Nonlinear Waves* (Wiley, New York, 1974), p. 33.
[3] R. D. Richtmyer and K. W. Morton, *Difference Methods for Initial-Value Problems* (Interscience, New York, 1967), p. 189.

Note that, for linearized supersonic flow, there are no first-order interactions between the vorticity, entropy and pressure fluctuations. In hypersonic shear flows the available turbulent structural data is essentially nil and it is likely that the intrinsic nature of the vorticity, entropy and pressure fluctuations is more complex than in supersonic flow. Unfortunately, the interest in and need to predict hypersonic turbulent flows is far outpacing our ability to acquire data or develop adequate compact mathematical formulations thereof.

Therefore, in spite of the fact that numerical simulation of turbulent structure in even low supersonic Mach number shear flows is still an evolving art, an attempt to predict hypersonic turbulent vorticity, entropy and pressure fluctuation dynamics is indicated on several bases. First, a general first principle prediction investigation will provide fundamental new information on the essential flowfield structures/physics which are unique to this regime. At the same time, such simulations shall serve to guide forthcoming experiments on hypersonic turbulent transport processes. Equally important, however, is the role which such simulations could play in the formulation of compact mathematical representations of various fluctuation correlations required in time-averaged flow transport models of TAV, NASP and various hypervelocity projectile/missile flowfields. The pressure of U.S. Air Force interest in such programs will not allow hypersonic turbulent flow R&D to await the natural evolutionary acquisition of experimental data, development of first-principle prediction of hypersonic vorticity/entropy/pressure fluctuations, and the eventual construction of compact transport models. Instead, the aforementioned R&D programs, and others, require the timely execution of a high payoff research program which attempts to leap-frog some of the traditional steps of evolution. The Phase I SBIR effort reported upon here was proposed in order to demonstrate the feasibility of using direct numerical simulations of hypersonic shear flows as a vehicle to assist in this leap-frogging and thus achieve the aforementioned goals.

Formulation

The numerical simulations carried out during this Phase I SBIR effort employed the full time-dependent, viscous and compressible flow Navier-Stokes equations written in the following vectorized form:

EQUATIONS OF MOTION

$$\frac{\partial U}{\partial t} + \frac{\partial F}{\partial x} + \frac{\partial G}{\partial y} + \frac{\partial H}{\partial z} = 0$$

$$U = \begin{bmatrix} \rho \\ \rho u \\ \rho v \\ \rho w \\ \rho E \end{bmatrix}$$

$$F = \begin{bmatrix} \rho u \\ \rho uu - \tau_{11} \\ \rho uv - \tau_{12} \\ \rho uw - \tau_{13} \\ \rho Eu - K\frac{\partial T}{\partial x} - (u\tau_{11} + v\tau_{12} + w\tau_{13}) \end{bmatrix} \quad G = \begin{bmatrix} \rho v \\ \rho uv - \tau_{12} \\ \rho vv - \tau_{22} \\ \rho vw - \tau_{32} \\ \rho Ev - K\frac{\partial T}{\partial y} - (u\tau_{12} + v\tau_{22} + w\tau_{32}) \end{bmatrix} \quad H = \begin{bmatrix} \rho w \\ \rho uw - \tau_{13} \\ \rho vw - \tau_{23} \\ \rho ww - \tau_{33} \\ \rho Ew - K\frac{\partial T}{\partial z} - (u\tau_{13} + v\tau_{23} + w\tau_{33}) \end{bmatrix}$$

where

$$\tau_{ij} = \delta_{ij} P - \mu\left(\frac{\partial u_i}{\partial X_j} - \frac{\partial u_j}{\partial X_i} - \frac{2}{3}\delta_{ij}\frac{\partial u_k}{\partial X_k}\right)$$

The gas was assumed to follow the perfect gas law and obey the Newtonian and Fourier formulations for molecular transport of momentum and heat. Due to time constraints, no extensive competition amongst the various available numerical schemes in the existing code was carried out in order to determine the optimum approach for this problem. As a result, MacCormack's explicit scheme was selected and, on the basis of various test solutions, the traditional artificial viscosity terms were deleted. An exponential compression of the grid spacing near the wall allowed the shear flow to be fully resolved.

In the course of evaluating the aforementioned numerics, various geometries were investigated. Due to the problems which were encountered with planar geometries (of both finite and infinite span-wise extent) relative to flowfield 'noise', an axisymmetric configuration shown in Figure 1. was specified. A right circular cylinder, whose axis was aligned with the on-coming flow and around which it could be rotated was chosen, in part, due to its relevance to various U.S. Air Force research initiatives.

Along the control volume surfaces which contained the cylinder, sufficient numerical boundary conditions were specified to obtain a unique solution. At a large radial distance from the cylinder uniform freestream flow was imposed. At the downstream end of the computational domain, outflow boundary conditions were used to simulate a cylinder of at least semi-infinite axial extent. With respect to the leading 'edge', a considerable number of test cases were studied. Initially, various specific forebodies were employed. As a result, the flowfield was dominated by bow shocks and expansion waves, bogging down the numerical analysis on interesting phenomena which were irrelevant to the research. After several weeks of experimentation, it was decided to abandon the approach of employing any forebody at all. It was assumed that the cylinder was, in fact, infinitely long. However, in the region $-\infty < x \leq 0$, the flow was allowed to slip along the

surface whereas the surface temperature equalled the freestream static temperature. In this manner a uniform upstream flow entering the computational domain was established. In the region $0 < x \leq 10\ \Delta x$, the (axial and azimuthal) velocity slip was linearly decreased to zero so as to initiate the growth of the boundary layer without the very strong leading edge disturbances, otherwise computed at high speeds, that previously dominated the downstream flow.

With this set of equations, numerical integration scheme, configuration and boundary conditions, the flowfield was computed over a range of Mach numbers in order to establish the feasibility of utilizing direct numerical simulation for computing the essential turbulent shear flow structures/physics unique to hypersonic flow.

Results

Over a range of Mach numbers from 1.4 to 6.3 the aforementioned flowfield was computed at Reynolds numbers which were known to be unstable and provide significant viscous interaction, with a wall temperature equal to the freestream static temperature. At a Mach number of 6.3 numerical instabilities could not be controlled with a time step of practical size. In addition, for all of the remaining Mach numbers, the low numerical 'noise' resulted in unacceptably long computational times for the small ambient disturbances to follow linear instability growth into the non-linear three dimensional regime. During Phase II various ambient noise models shall be added to the simulation. Therefore, all of the numerical simulations presented here are associated with an artificial excitation described earlier in the form of a temporally harmonic normal wall mass transfer, with periodic suction/blowing and various frequencies relative to the time scales of the mean flow and viscous layer thickness.

The main body of the simulations in Figures 2-6 & 9-11 pertain to a non-rotating cylinder. Two cases including cylinder rotation at a Mach number of 3.0 are presented in Figures 7 & 8 to demonstrate the capability for including three dimensional mean flow effects. Inasmuch as the cylinder rotation results did not qualitatively affect the principal discovery of this study, they shall not be referred to further and are left for the reader to review. With regard to the non-rotating cylnder, the results are presented in groups for each Mach number and excitation frequency combination, beginning with the highest Mach number. Within each set of simulations for a given Mach number, the excitation frequencies include one or both of the cases 10^{-1} and 10^{1} times the frequency computed from the local freestream velocity and boundary layer thickness. These are referred to as low and high frequency, respectively. The cases with an excitation

frequency of 10^{0} times the reference were essentially identical with 10^{-1}. Within each group of results for a given Mach number and excitation frequency, the fluctuating entropy, azimuthal component of vorticity and pressure are presented along with characterizations of the mean flow. Some fifty boundary layer thicknesses downstream of the excitation, the effect of such disturbances on the flow was 'observed' and is presented in the various plots.

Although it is true that the bulk of the research time was consumed with structuring the computations, a significant observation has been made. This is most readily seen by comparing Figures 2a & 2b with 7a & 7b. As the Mach number increases, the entropy fluctuations exhibit a second distinct boundary layer 'edge' well beyond that established by the vorticity. At lower Mach numbers the entropy fluctuations radiate much further into the freestream flow. (As a part of Phase II, the full range of high subsonic and transonic Mach numbers shall also be evaluated to understand the entropy fluctuation field in the regime where entropy and pressure fluctuations are just beginning to be significant.) As a result, Phase I of this SBIR program has not only demonstrated the feasibility of utilizing direct numerical simulations to expose the essential physics of turbulent structure in hypersonic flow, but has also provided an initial direction for future research into the possible multiple layer structure of hypersonic TBL fluctuations.

Conclusions and Recommendations

Numerical simulations of boundary layer flow from the hypersonic down through transonic regimes have been carried out utilizing the full time-dependent, viscous and compressible flow Navier-Stokes equations for a perfect gas. The nominally axial flowfield over a circular cylinder, with and without rotation about its axis, was computed utilizing existing numerical techniques coupled with a unique leading edge flow development formulation. In order to generate a numerically 'quiet' solution, the (axial and azimuthal) zero slip boundary conditions were introduced gradually over the first ten grid points beginning at the leading edge of the cylinder. A linear distribution ranging from full slip at the first node to zero slip at the tenth node was imposed. The wall temperature was set equal to the freestream static temperature. In future simulations with various hot and cold walls the temperature difference shall also be phased in over the first ten nodes. This procedure allows for the computation of a generic boundary layer flow which is essentially noise free, without the complications associated with the specification of a particular forebody.

Due to the low noise level in the flow, growth of natural disturbances into instability waves with subsequent non-linear three-dimensional breakdown required intolerably long computational times. In order to meet the Phase I SBIR cost and time constraints, the boundary layers were, therefore, artificially excited with a temporally harmonic disturbance at the wall several boundary layer diameters upstream of the observation station. Both periodic suction and blowing as well as heating and cooling were evaluated, with the former being selected for this study. The peak magnitude of the mass flux was held constant at 1% of the freestream whereas the time constant was varied over a range of values relative to the viscous flow length and velocity scales.

By utilizing such artificial excitation, the development of disturbances into the nonlinear regime and the beginnings of essential three-dimensionality could be computed over a wide range of Mach numbers. For the sake of economy of time and costs the computations were terminated when any essential characteristic of the disturbance field was observed at that Mach number so that a wide range of Mach numbers, frequencies and mean flow conditions could be reported upon.

As a result of these computations, a unique effect of Mach number on flowfield disturbances has been observed. When viewed in terms of the vorticity, entropy and pressure fluctuations, hypersonic flows appear to exhibit a distinct multiple layer structure in which the vorticity fluctuations are confined to the region established by the mean vorticity whereas the entropy and pressure fluctuations extend further out into the uniform flow yet still terminate relatively near the solid boundary. At lower supersonic Mach numbers the entropy and pressure fluctuations propagate increasingly far away from the body and are reminiscent of shadowgraph pictures of waves emanating from the edge of a turbulent boundary layer.

In accordance with the objectives of a Phase I SBIR, the feasibility of utilizing direct numerical simulations to expose the essential physics of turbulent boundary layer structures at hypersonic speeds has been demonstrated. It is apparent that simulations carried out in this manner could be invaluable in both the complete description of the unique vorticity-entropy-pressure field dynamics as well as providing guidance in the formulation of more compact engineering models.

Based on this established feasibility, an exhaustive computational study is indicated in which longer computational times could be tolerated and natural disturbances followed

into non-linearity and eventually chaos. It would be particularly advantageous, if the Phase II SBIR effort is able to be supported, if the work would be associated with an effort in which experimental data on hypersonic turbulent flow is being obtained. The Hokenson Company is under contract to AFATL/MNG, Eglin AFB, FL to carried out experimental studies on spinning hypersonic projectiles with base bleed flow and optimal forebody shaping. It is our recommendation that the Phase II work on computing turbulent hypersonic flow boundary layer and wake structures be linked to the geometrical configuration being studied therein. In this manner two research programs which are exclusively computational and experimental, respectively, would benefit from the association with one another and the achievements of two Air Force research interests would be significantly enhanced.

Supplemental Information

The professional personnel involved with the work were Dr. Gustave J. Hokenson and Mr. Richard D. Crouse, who holds an MS in Aerospace Engineering from Stanford University.

Contingent upon obtaining Phase II SBIR support, The Hokenson Company intends to present several papers related to this work at the First National Fluid Dynamics Congress with subsequent journal publication.

Results of this effort have also been invaluable in supporting an SBIR program being carried out by The Hokenson Company for AFATL/MNG, Eglin AFB. In that work, drag reduction on 20-mm hypersonic projectiles is being studied experimentally through application of base bleed and optimal forebody shaping. Advances in the understanding of turbulent transport processes derived from the AFOSR Phase I SBIR work reported upon here significantly impacts the design of an effective experimental program. In addition, the experimental data from such a study would significantly enhance the ability to validate the numerical simulations scheduled to be carried out during the AFOSR Phase II SBIR effort.

Bibliography

Beam, R.M. and Warming, R.F. "An Implicit Factored Scheme for the Compressible Navier-Stokes Equations," AIAA Journal, Vol. 16, April 1978, pp. 393-402.

Briley, W.R. and McDonald, H., "Solution of the Multidimensional Compressible Navier-Stokes Equations by the Generalized Implicit Method," Journal of Computational Physics, Vol. 24 Aug. 1977, pp. 372-397.

Jameson, A. and Turkel, E., "Implicit Schemes and LU Decompositions," Mathematics of Computation, Vol. 37, Oct. 1981, pp. 385-397.

Korduila, W. and MacCormack, R.W., "Transonic Flow Computation Using an Explicit-Implicit Method," Proceedings of the Eighth International Conference on Numerical Methods in Fluid Dynamics, Springer-Verlag, New Your 1982, pp. 286-295.

Kumar, A., "Some Observations on a New Numerical Method for Solving the Navier-Stokes Equations," NASA TP-1934, Nov. 1981.

Lin, N.S., Shamroth, S.J., and McDonald, H., "Numerical Solution of the Navier-Stokes Equations for Compressible, Turbulent Two/Three Dimensional Flows in the Terminal Shock Region on an inlet/Diffuser," AIAA Paper 83-1892, July 1983.

MacCormack, R.W., "A Numerical Method for Solving the Equations of Compressible Viscous Flow," AIAA Paper 81-0110, Jan. 1981.

MacCormack, R.W., "The Effect of Viscosity in Hypervelocity Impact Cratering," AIAA Paper 69-354, Jan. 1969.

Stone, H.L., "Iterative Solution of Implicit Approximations of Multidimensional Partial Differential Equations," SIAM Journal of Numerical Analysis, Vol. 5, Sept. 1968, pp. 530-558.

Swanson, R.C., Rubin, S.G., and Khosla, P.K., "Calculation of Afterbody Flows with a Composite velocity Formulation," AIAA Paper 83-1736, July 1983.

Von Lavante, E. and Thompkins, W.T., "An Implicit, Bi-Diagonal Numerical Method for Solving the Navier-Stokes Equations," AIAA Paper 82-0063, Jan. 1982.

Walters, R.W., "LU Methods for the Compressible Navier-Stokes Equations," Ph.D. Thesis, North Carolina State University, Raleigh, April 1984.

Figure 1.

Flowfield Schematic

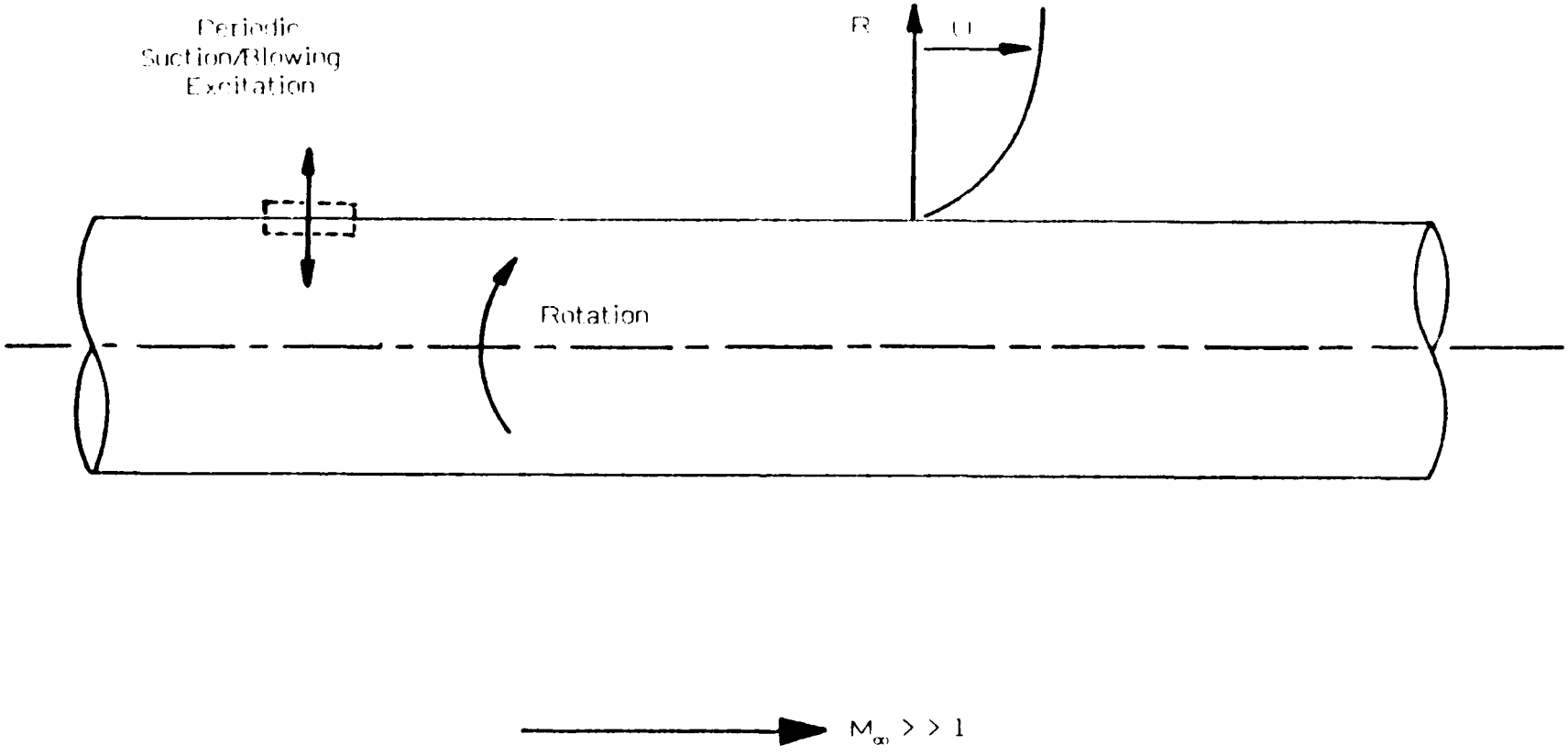

Case I.: M=5.3, Zero Rotation

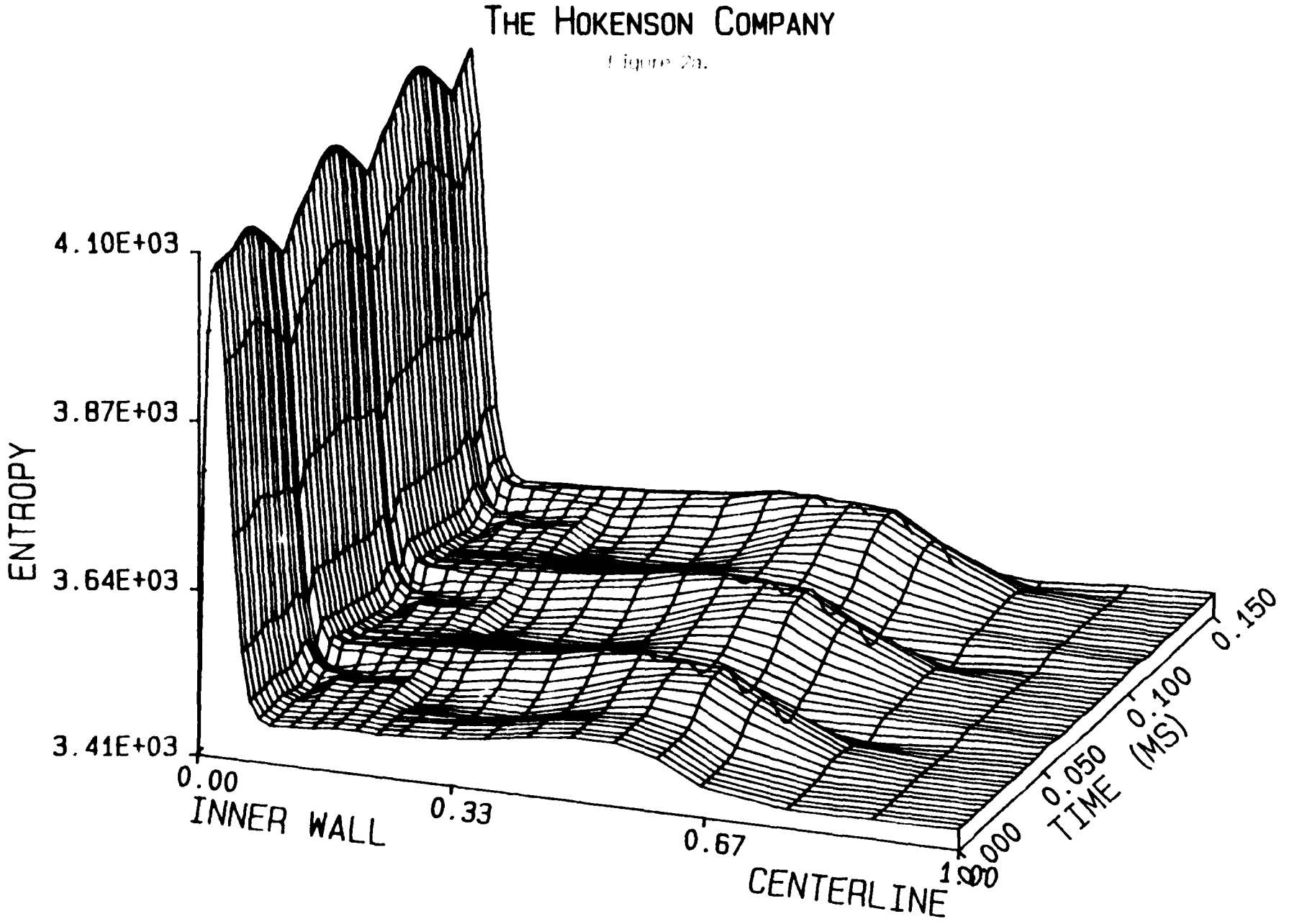
THE HOKENSON COMPANY
4.10E+03
3.87E+03
3.64E+03
3.41E+03
ENTROPY
0.00
INNER WALL
0.33
0.67
1.00
CENTERLINE
0.000
0.050
0.100
0.150
TIME (MS)

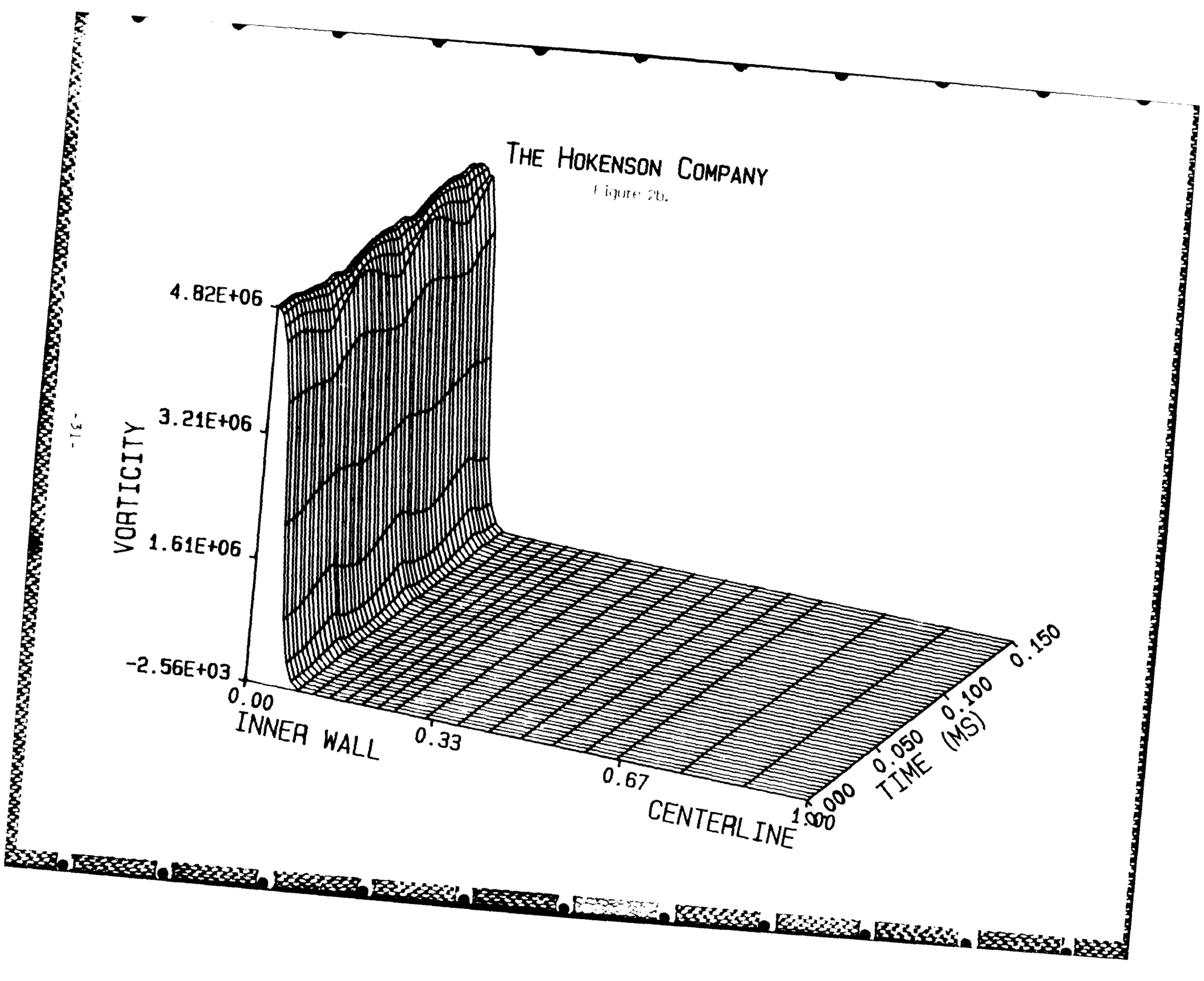
THE HOKENSON COMPANY
4.82E+06
3.21E+06
1.61E+06
-2.56E+03
VORTICITY
0.00
INNER WALL
0.33
0.67
1.00
CENTERLINE
0.000
0.050
0.100
0.150
TIME (MS)

Figure 2b.

THE HOKENSON COMPANY

Figure 2c.

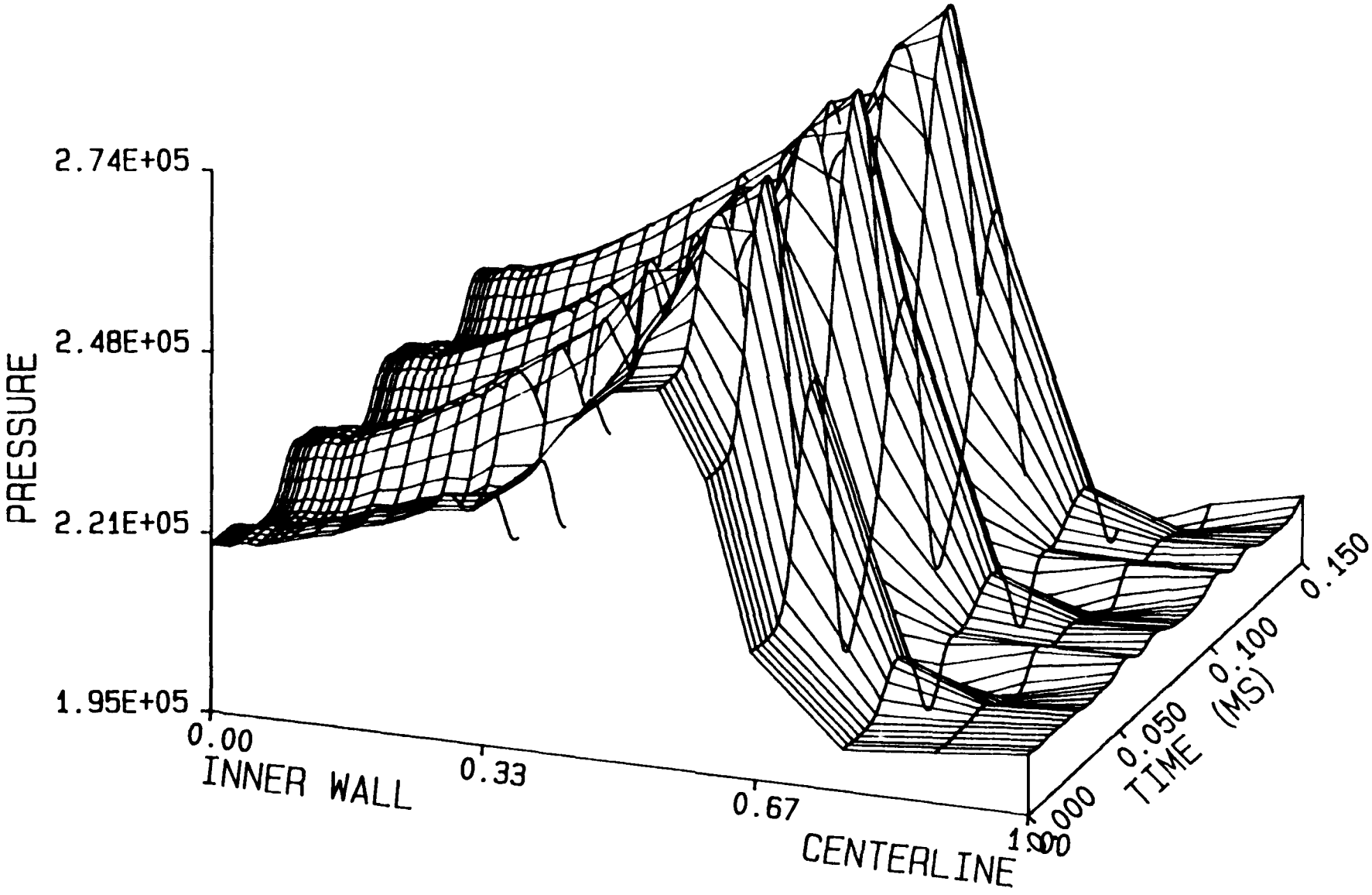

Figure 2d.

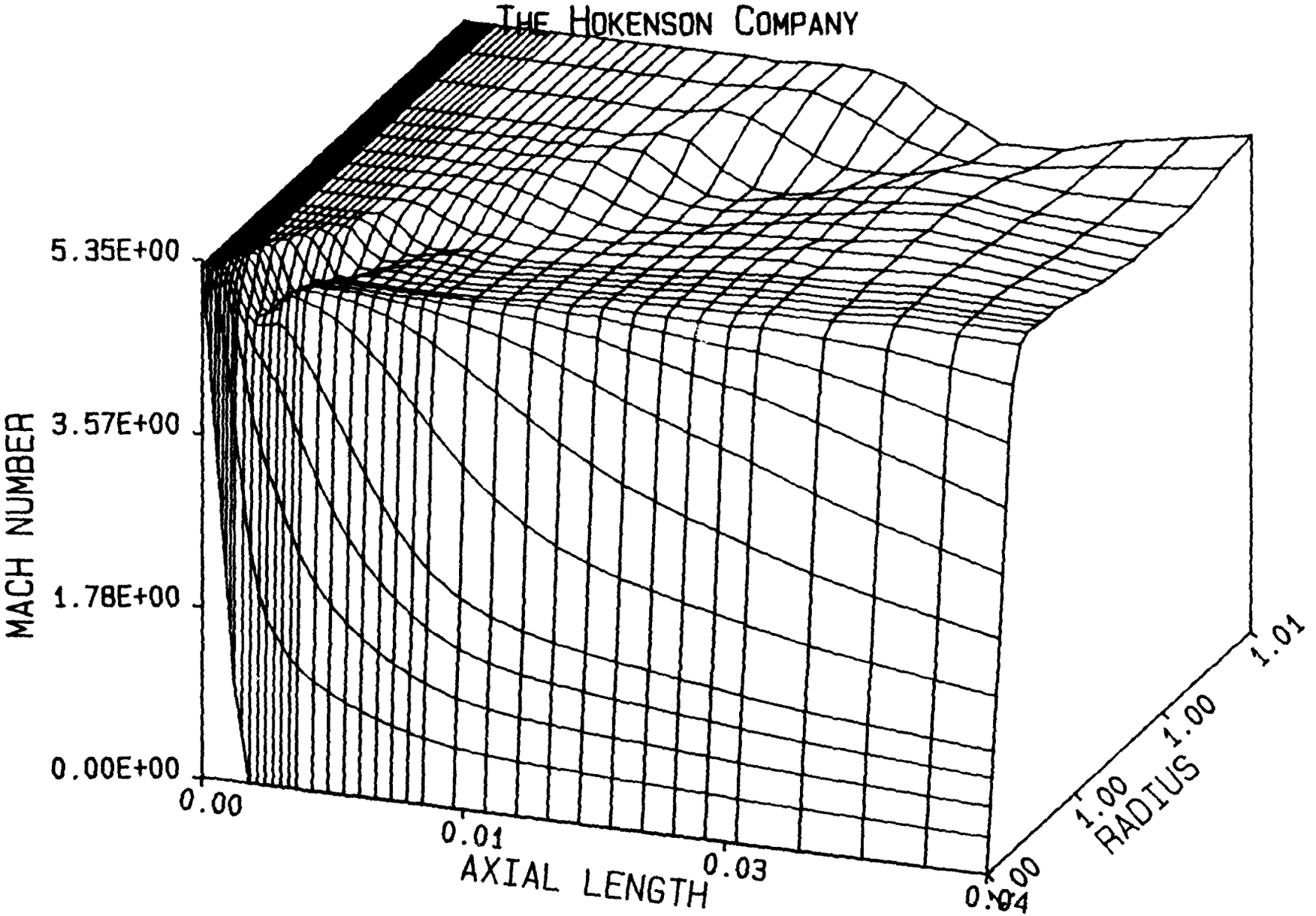
THE HOKENSON COMPANY
5.35E+00
3.57E+00
1.78E+00
0.00E+00
MACH NUMBER
0.00
0.01
0.03
0.04
AXIAL LENGTH
1.00
1.00
1.01
RADIUS

THE HOKENSON COMPANY

Figure 3a.

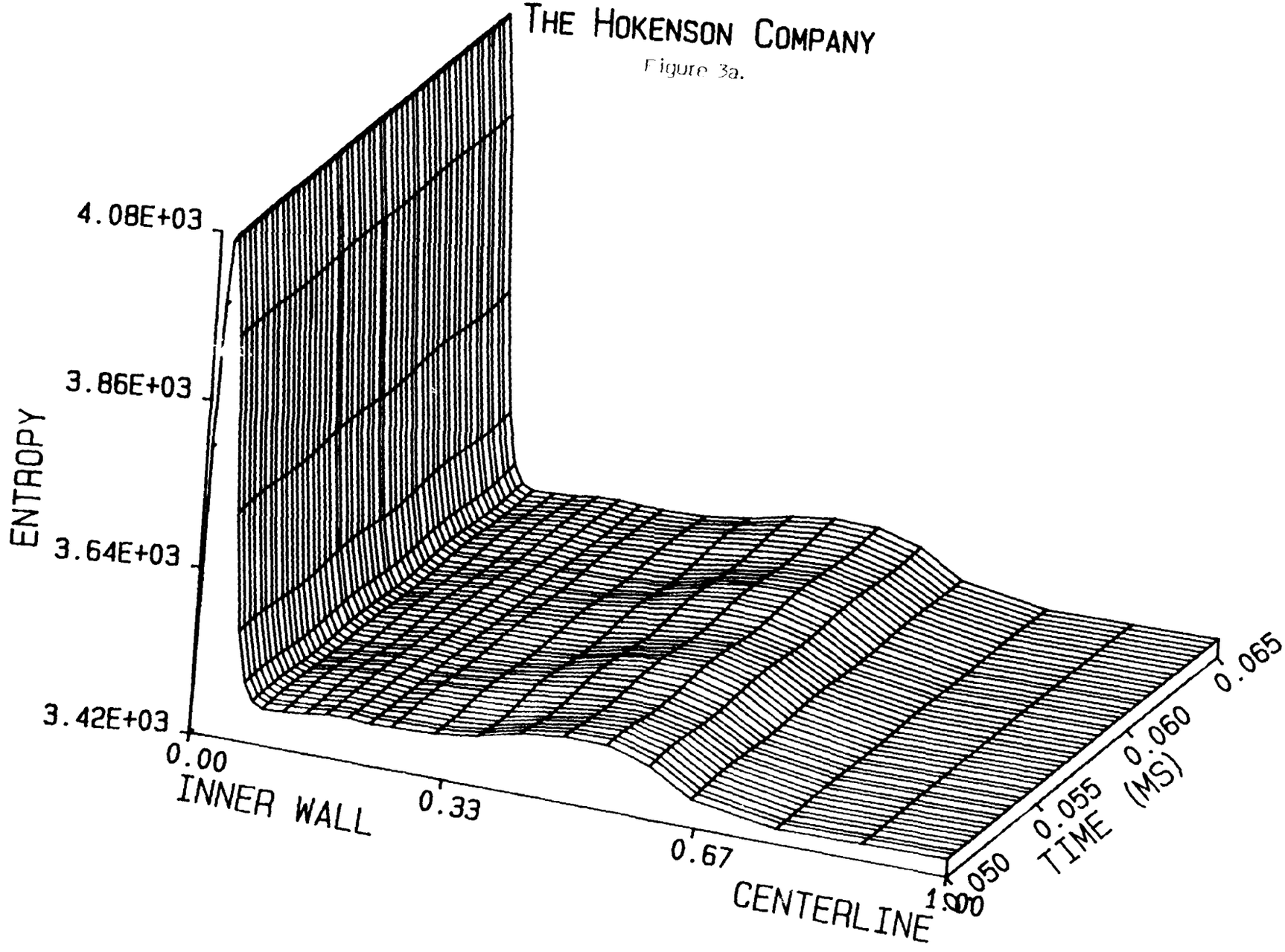

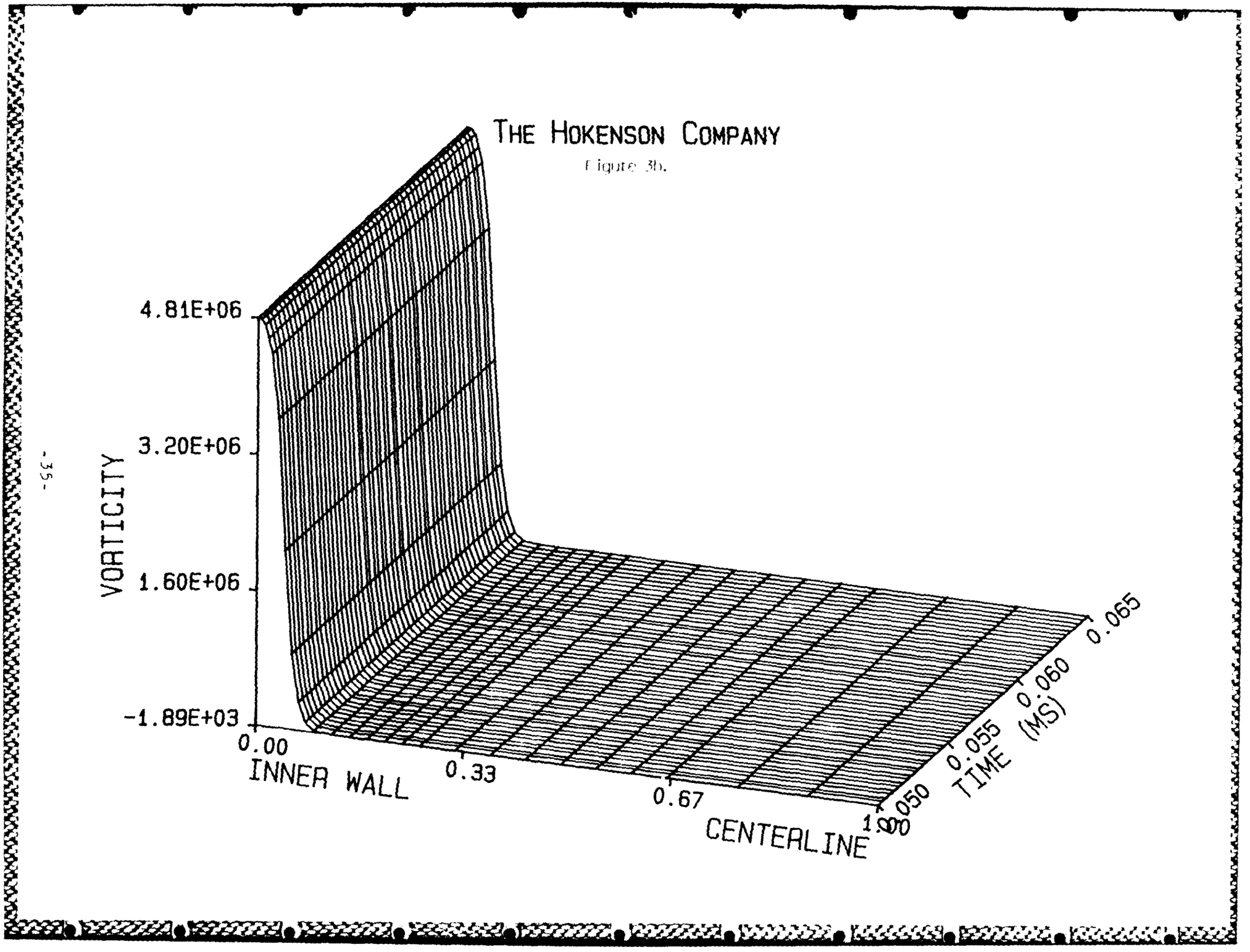
THE HOKENSON COMPANY
4.81E+06
3.20E+06
1.60E+06
-1.89E+03
VORTICITY
0.00
INNER WALL
0.33
0.67
1.00
CENTERLINE
0.050
0.055
0.060
0.065
TIME (MS)

Figure 3b.

THE HOKENSON COMPANY

Figure 3c.

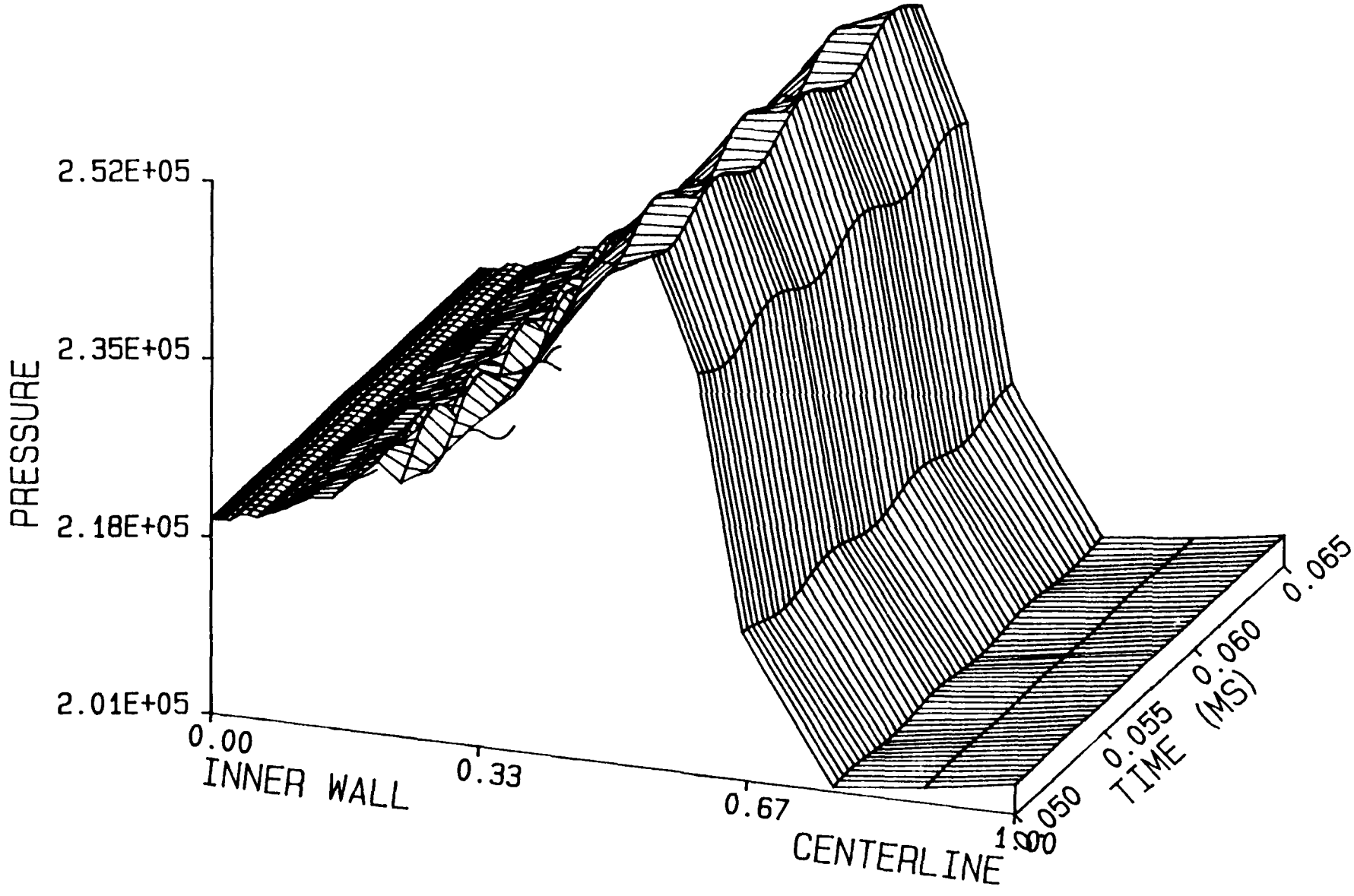

Figure 3d.

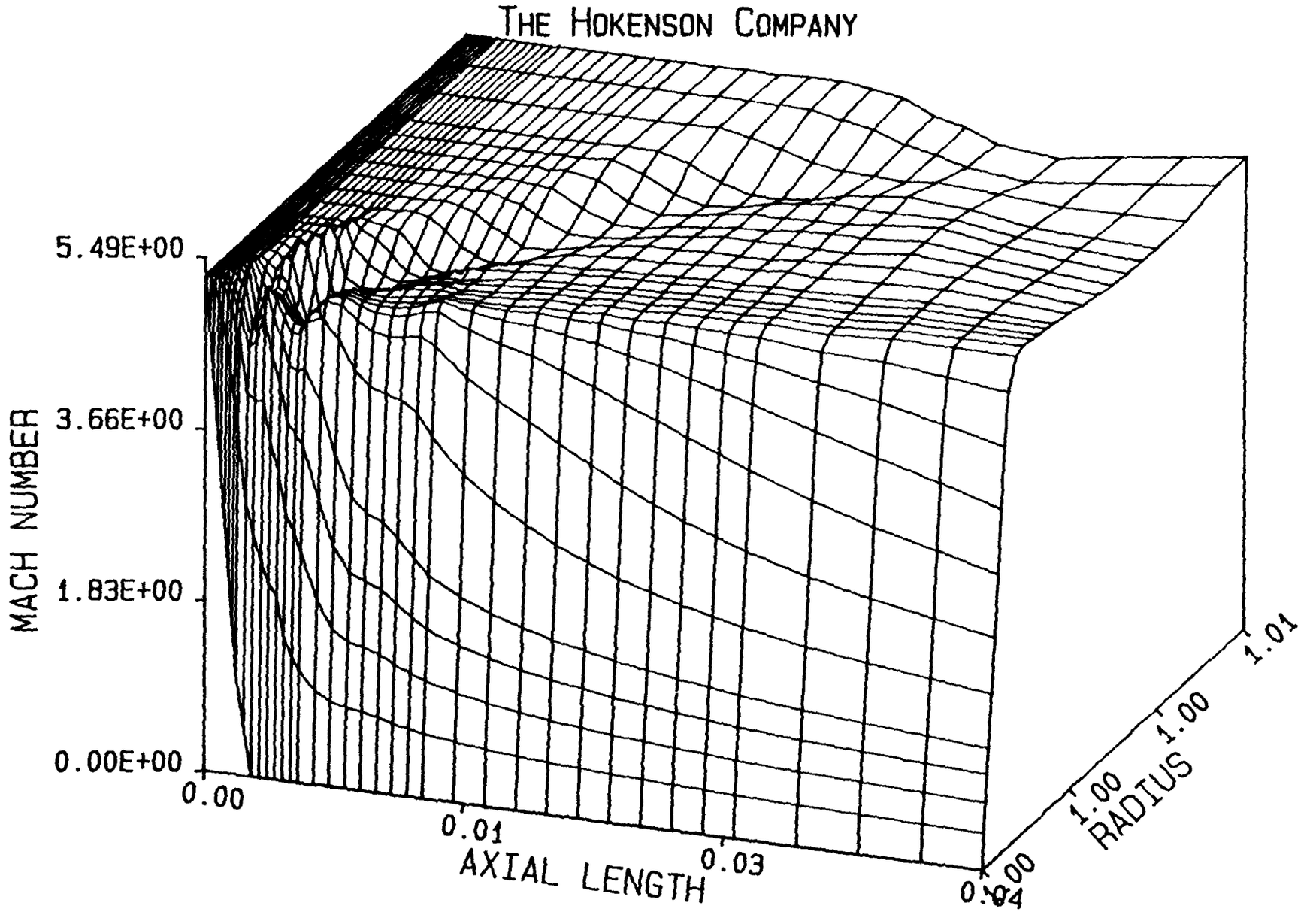
THE HOKENSON COMPANY
5.49E+00
3.66E+00
1.83E+00
0.00E+00
MACH NUMBER
0.00
0.01
0.03
0.04
AXIAL LENGTH
1.00
1.00
1.01
RADIUS

Case II.: M=4.0, Zero Rotation

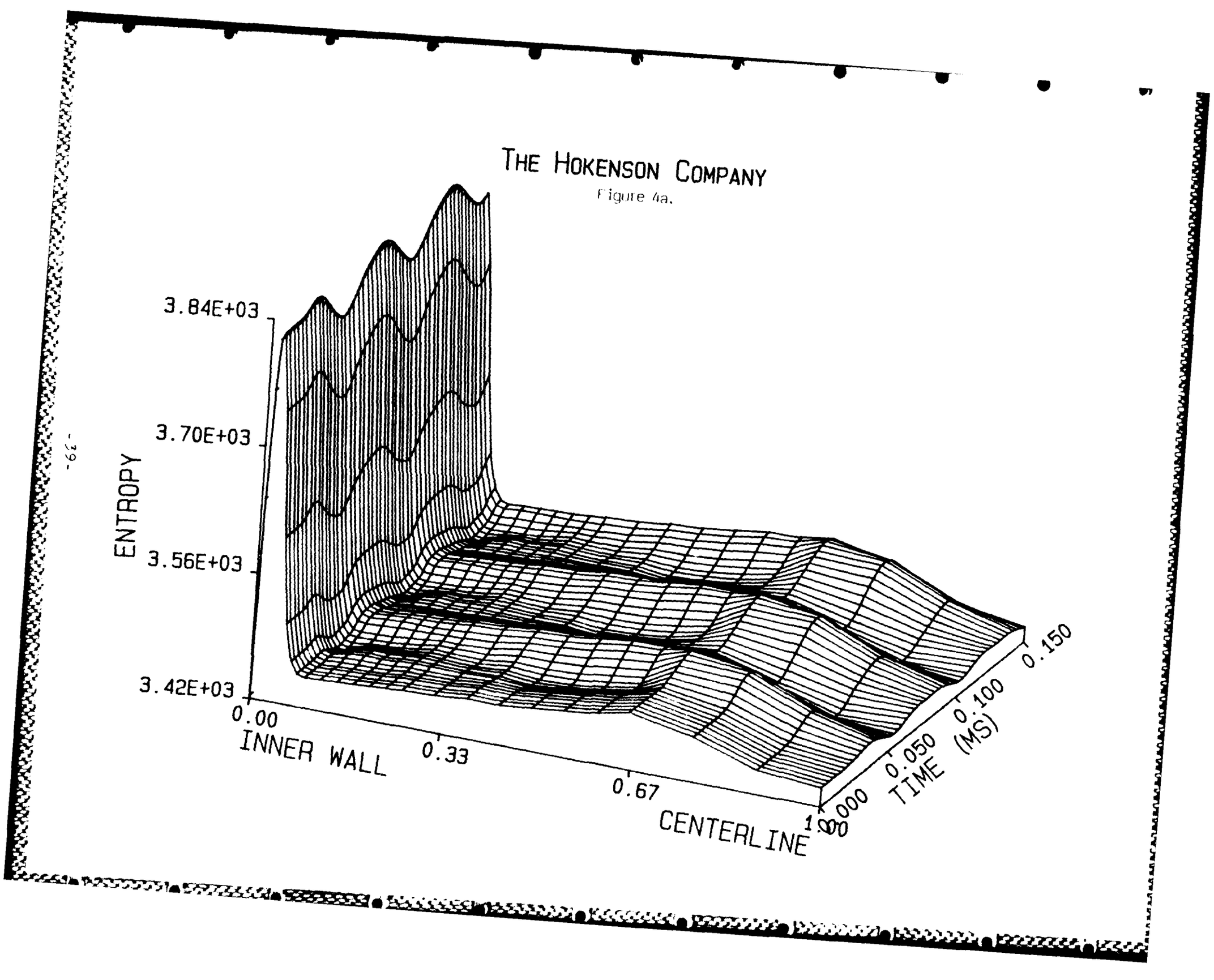
THE HOKENSON COMPANY
Figure 4a.
3.84E+03
3.70E+03
3.56E+03
3.42E+03
ENTROPY
0.00
INNER WALL
0.33
0.67
CENTERLINE
1.000
0.000
0.050
0.100
0.150
TIME (MS)

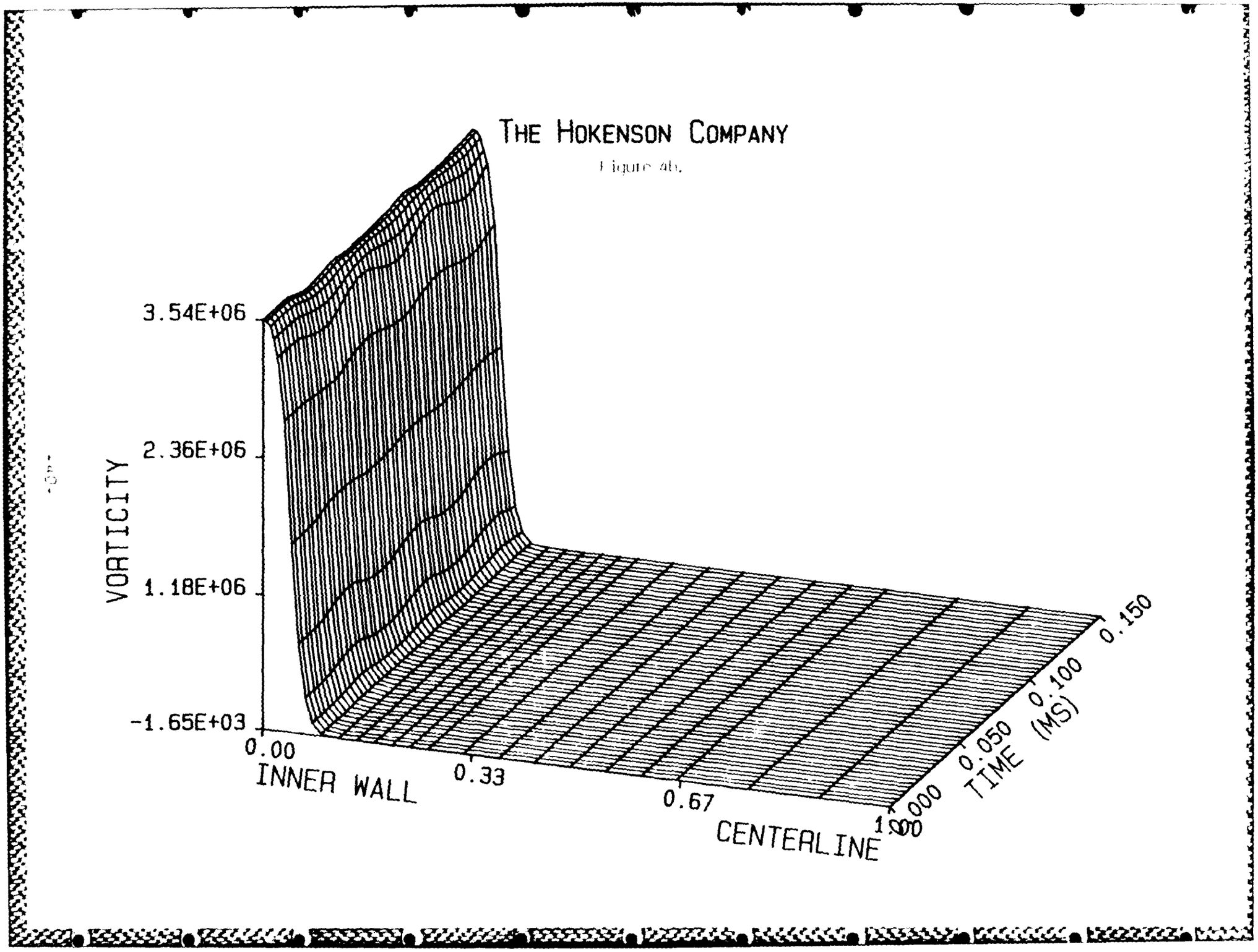
THE HOKENSON COMPANY
VORTICITY
3.54E+06
2.36E+06
1.18E+06
-1.65E+03
0.00
INNER WALL
0.33
0.67
1.00
CENTERLINE
0.000
0.050
0.100
0.150
TIME (MS)

THE HOKENSON COMPANY

Figure 4c.

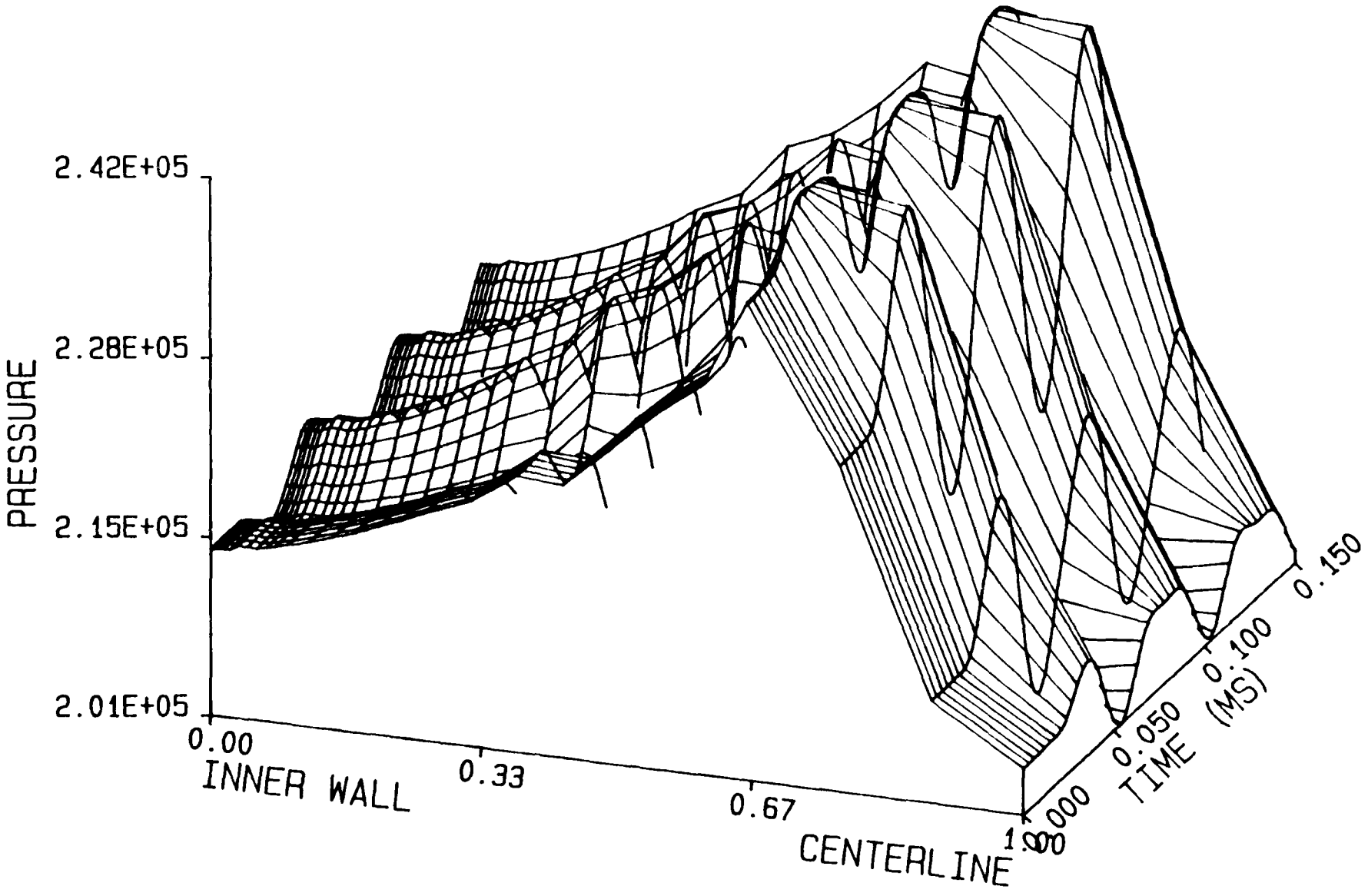

Figure 4d.

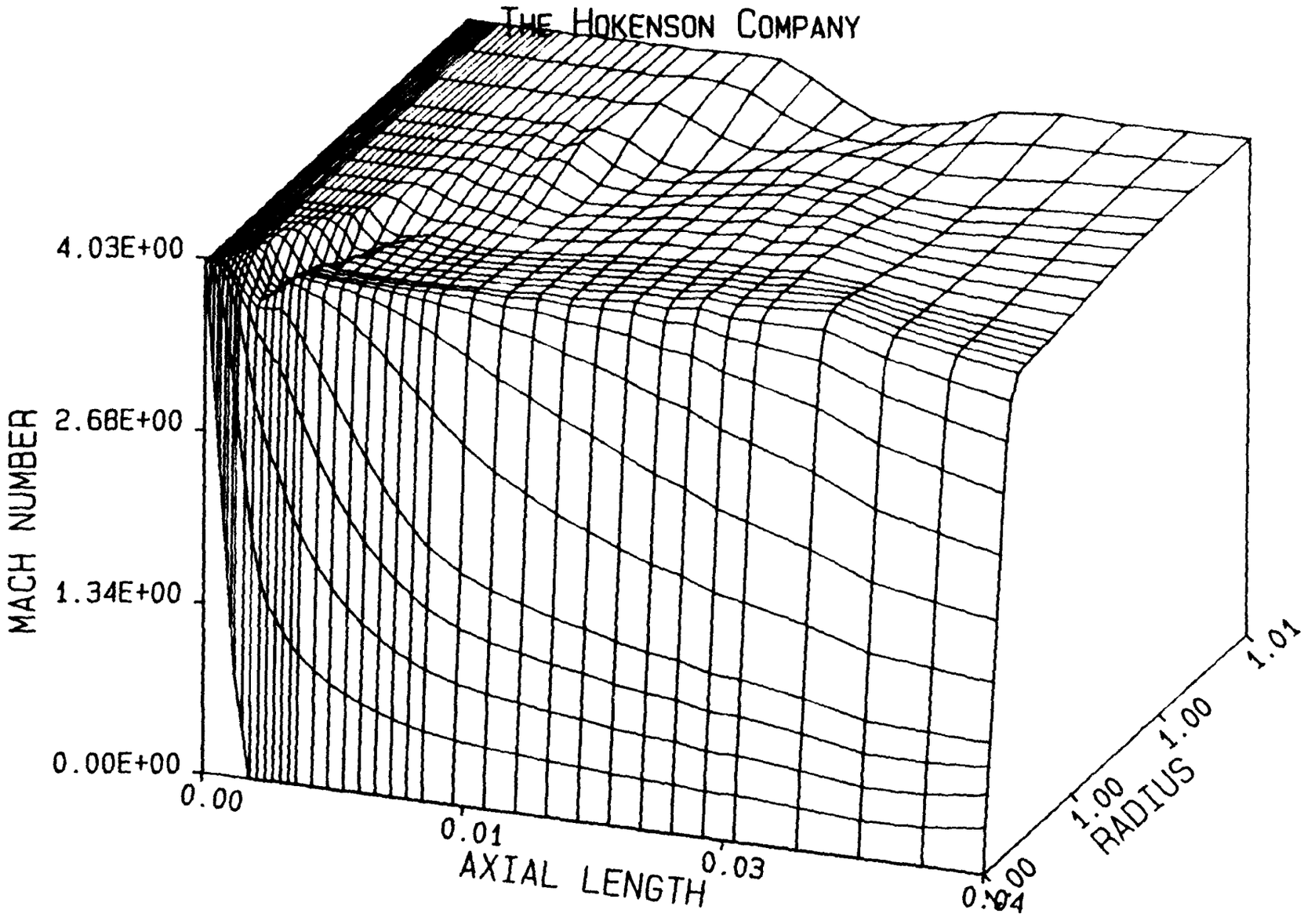
THE HOKENSON COMPANY
MACH NUMBER
4.03E+00
2.68E+00
1.34E+00
0.00E+00
0.00
0.01
0.03
0.04
AXIAL LENGTH
1.00
1.00
1.00
1.01
RADIUS

Case IIIa.; M=3.0, Zero Rotation

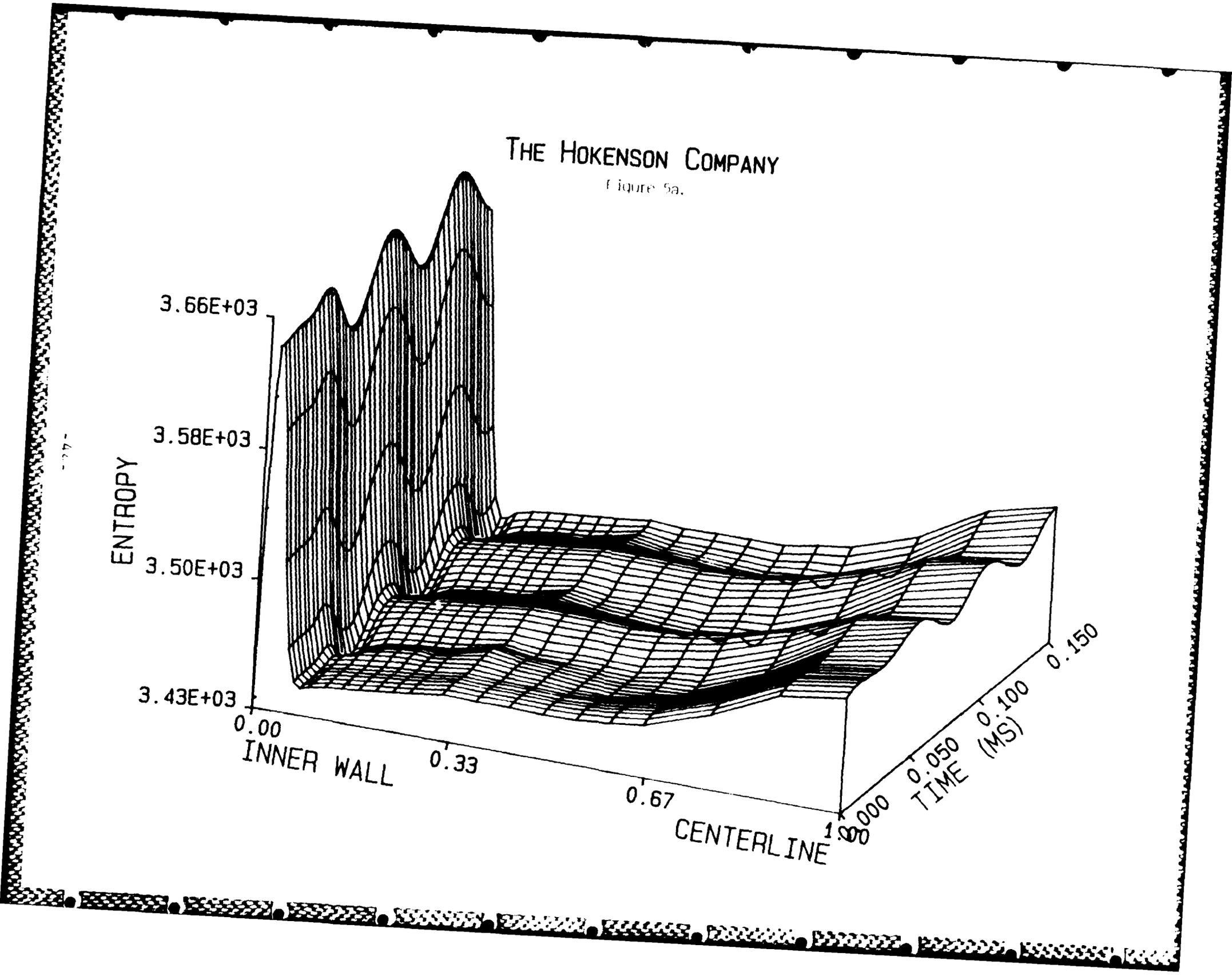
THE HOKENSON COMPANY
Figure 5a.
3.66E+03
3.58E+03
3.50E+03
3.43E+03
ENTROPY
0.00
INNER WALL
0.33
0.67
1.00
CENTERLINE
0.000
0.050
0.100
0.150
TIME (MS)

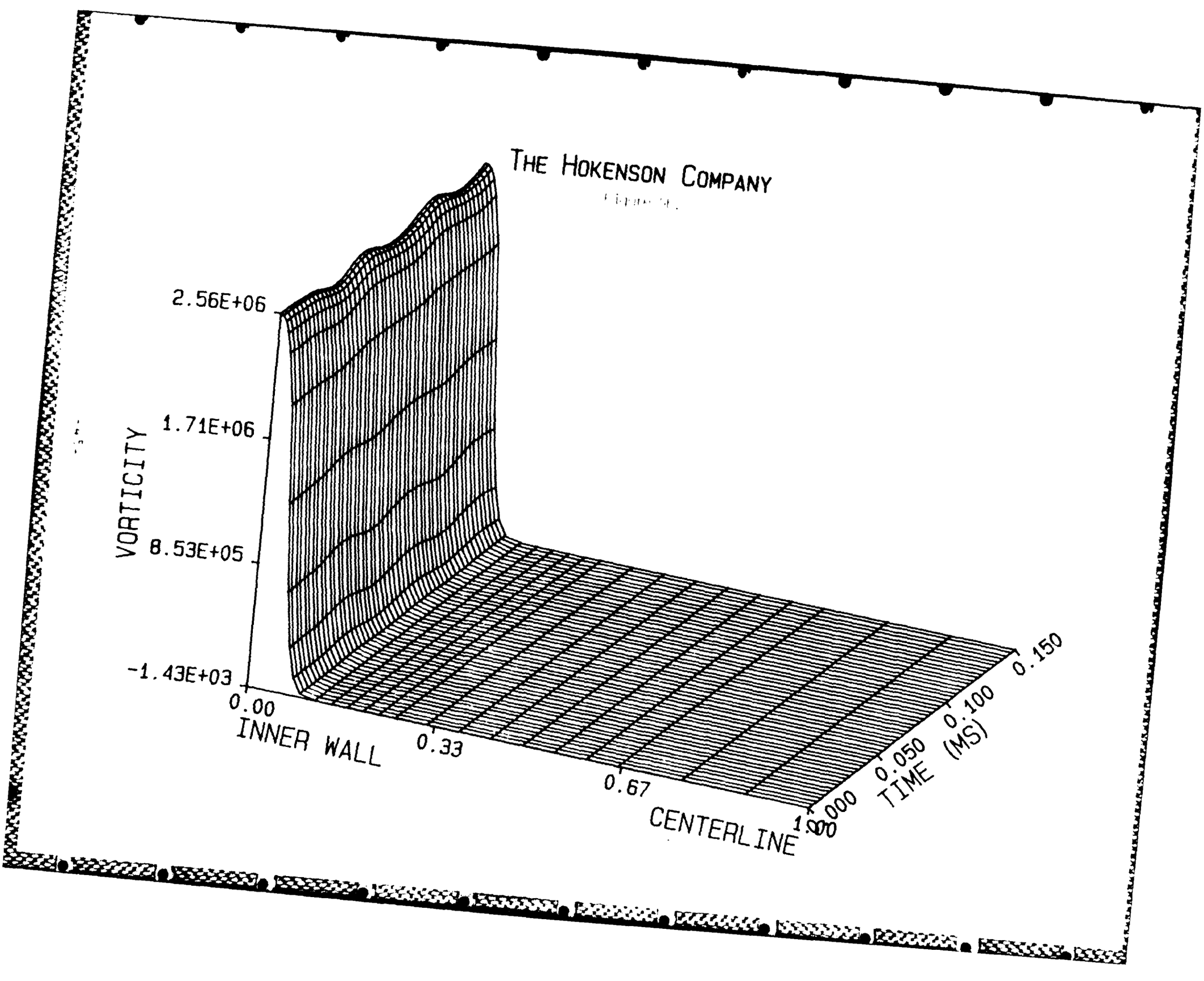
THE HOKENSON COMPANY
2.56E+06
1.71E+06
8.53E+05
-1.43E+03
VORTICITY
0.00
INNER WALL
0.33
0.67
CENTERLINE
1.00
0.000
0.050
0.100
0.150
TIME (MS)

THE HOKENSON COMPANY

Figure 5c.

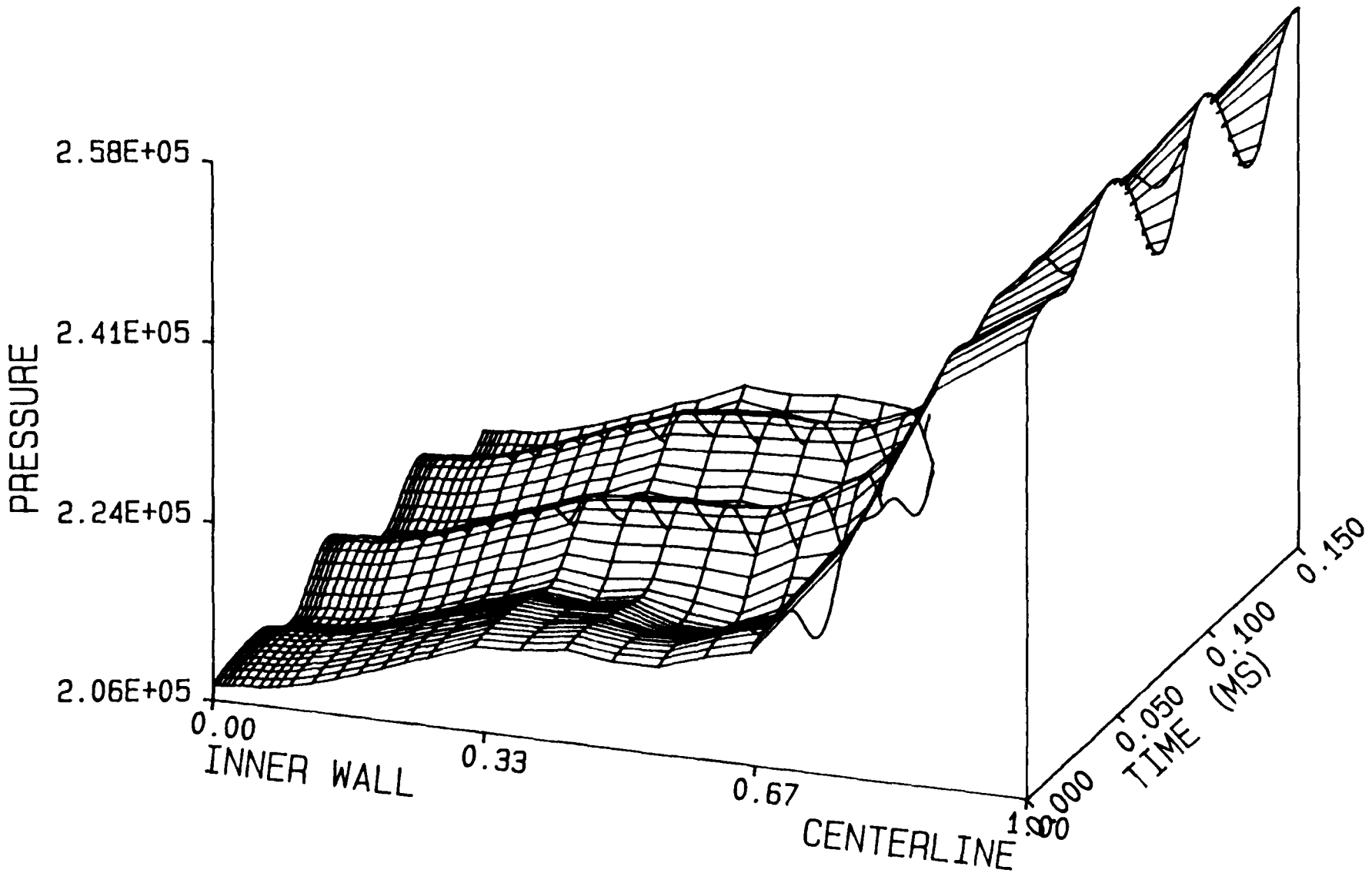

Figure 5d.

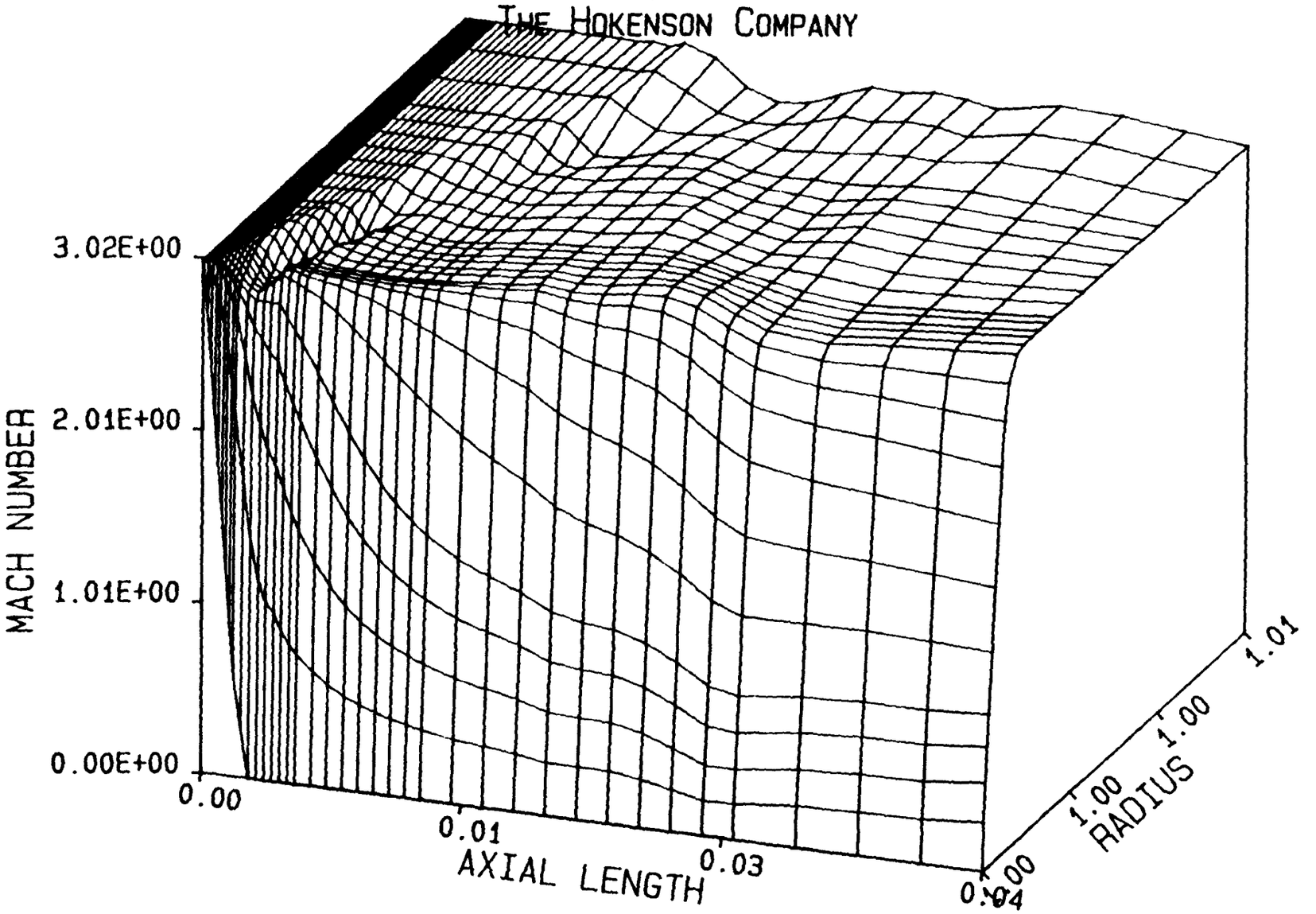
THE HOKENSON COMPANY
3.02E+00
2.01E+00
1.01E+00
0.00E+00
MACH NUMBER
0.00
0.01
0.03
0.04
AXIAL LENGTH
1.00
1.00
1.01
RADIUS

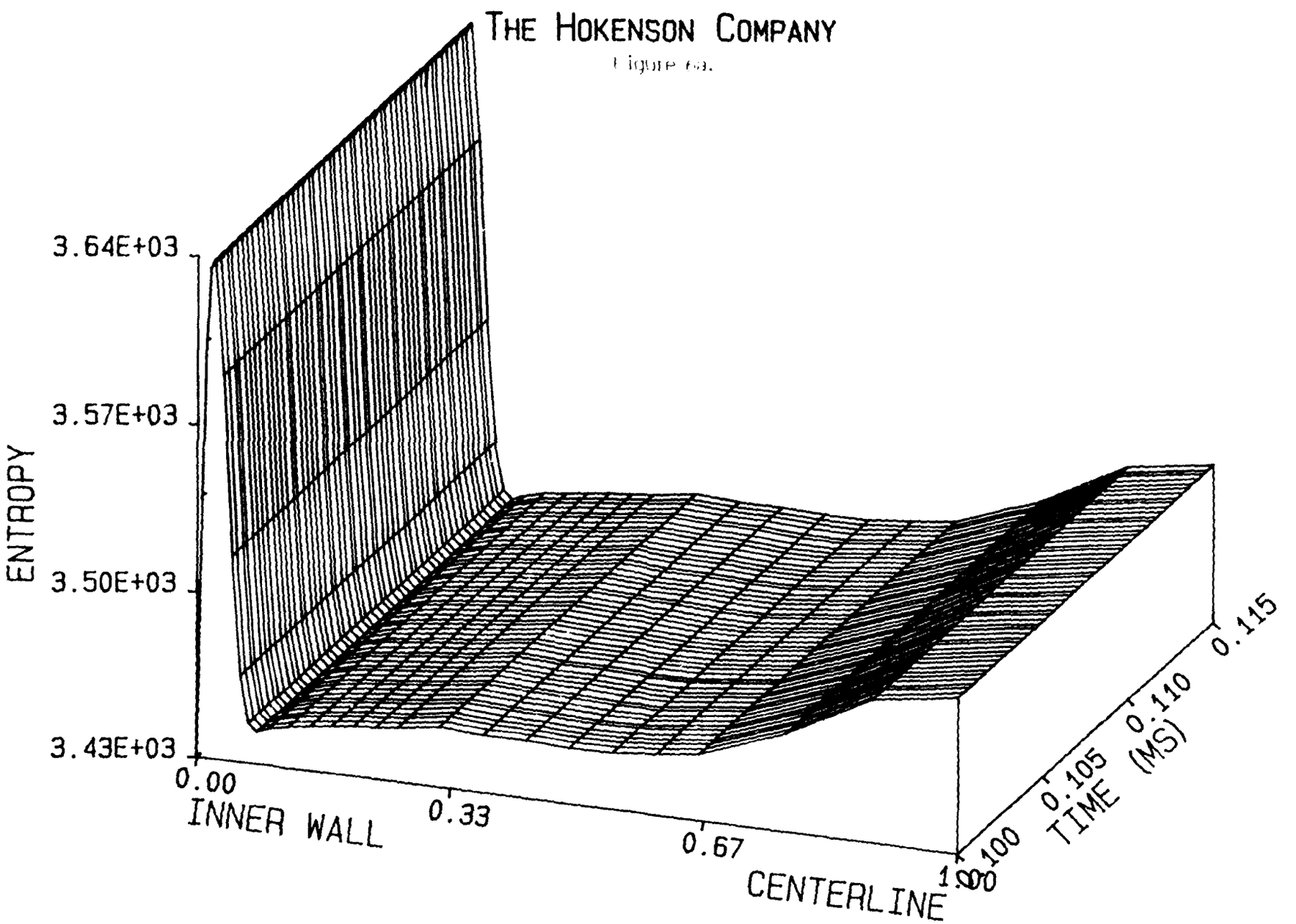
THE HOKENSON COMPANY
3.64E+03
3.57E+03
3.50E+03
3.43E+03
ENTROPY
0.00
INNER WALL
0.33
0.67
CENTERLINE
1.00
0.100
0.105
0.110
0.115
TIME (MS)

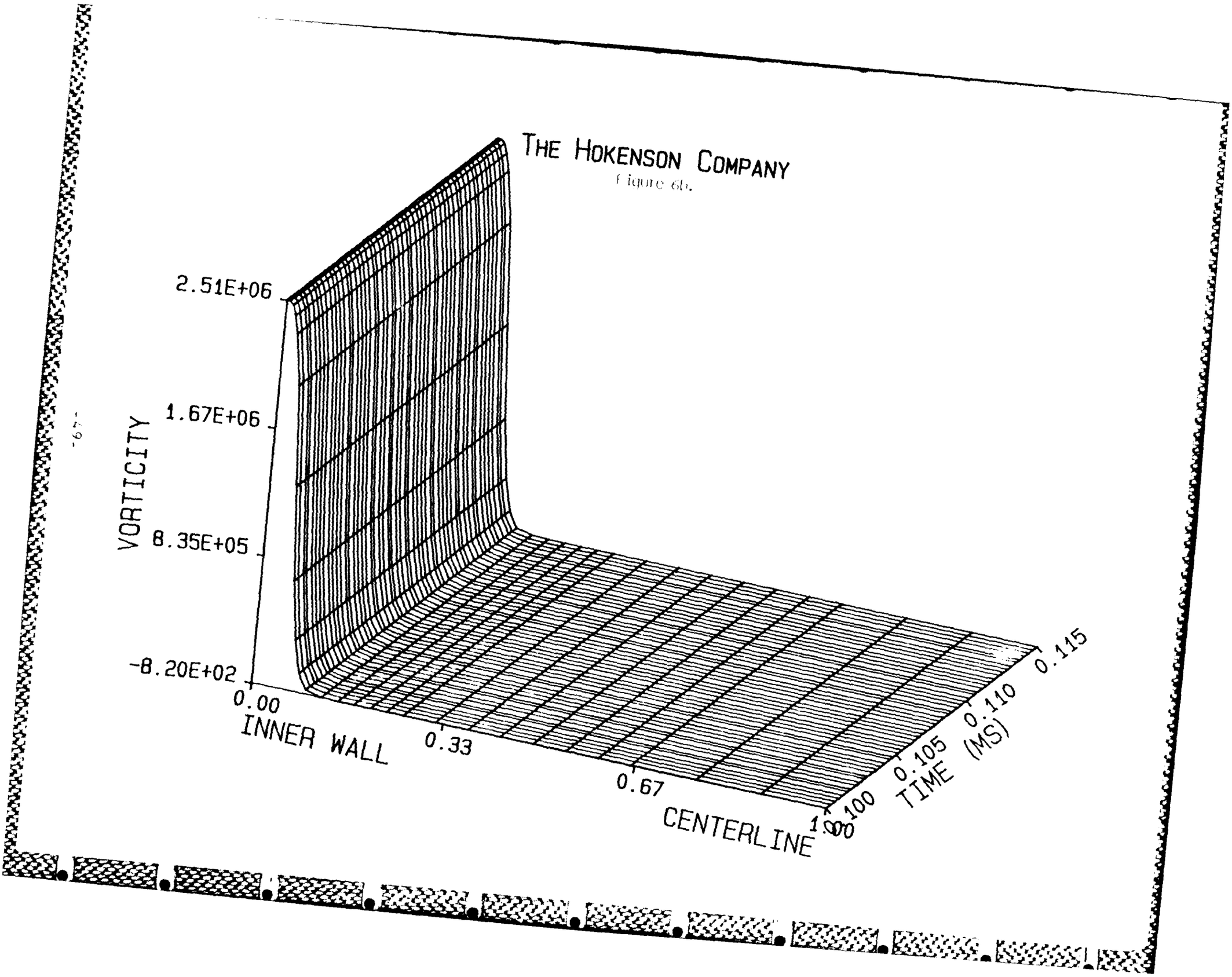
THE HOKENSON COMPANY
2.51E+06
1.67E+06
8.35E+05
-8.20E+02
VORTICITY
0.00
INNER WALL
0.33
0.67
CENTERLINE
1.000
0.100
0.105
0.110
0.115
TIME (MS)

Figure 6b.

THE HOKENSON COMPANY

Figure 6c.

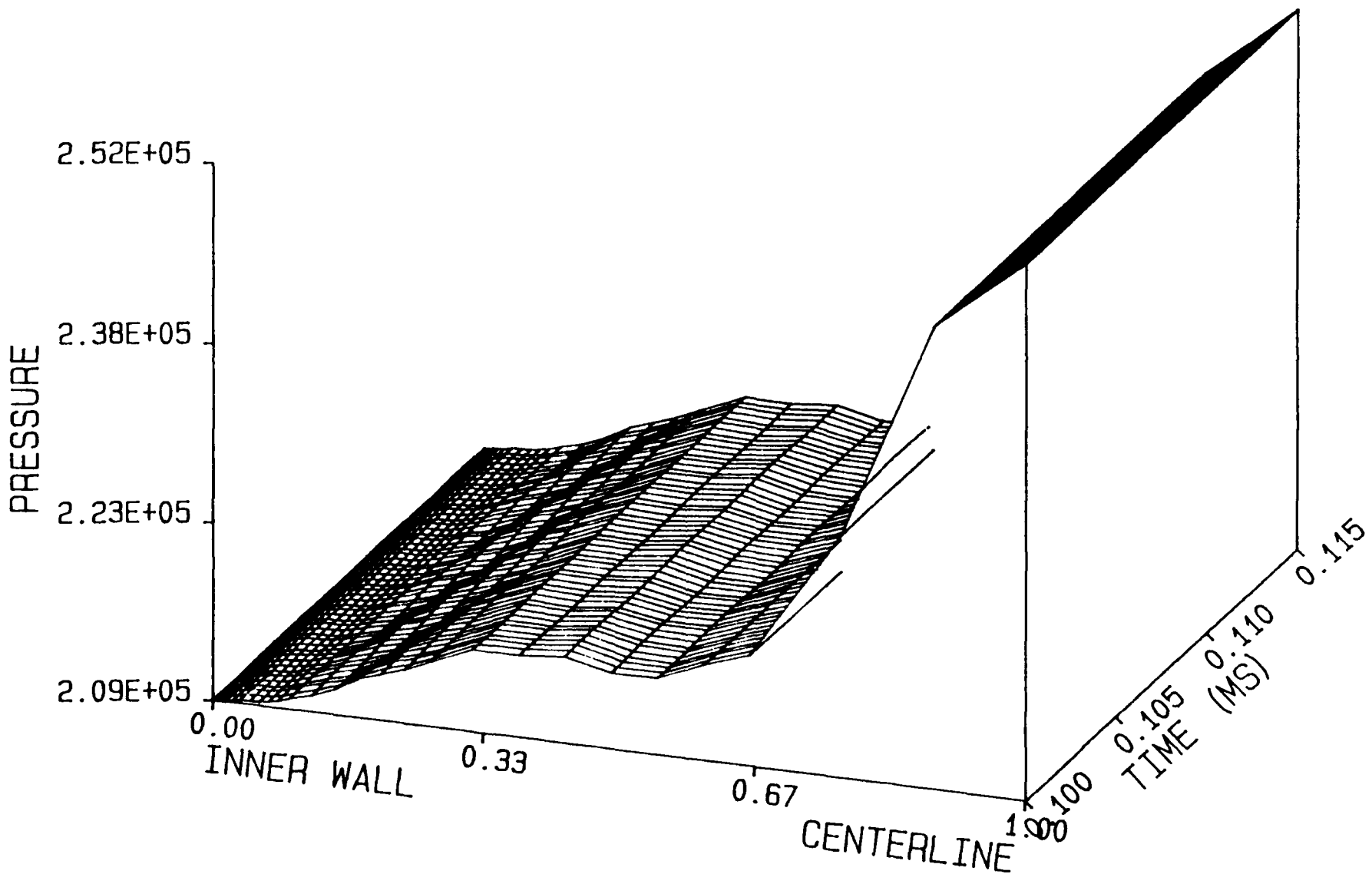

Figure 61.

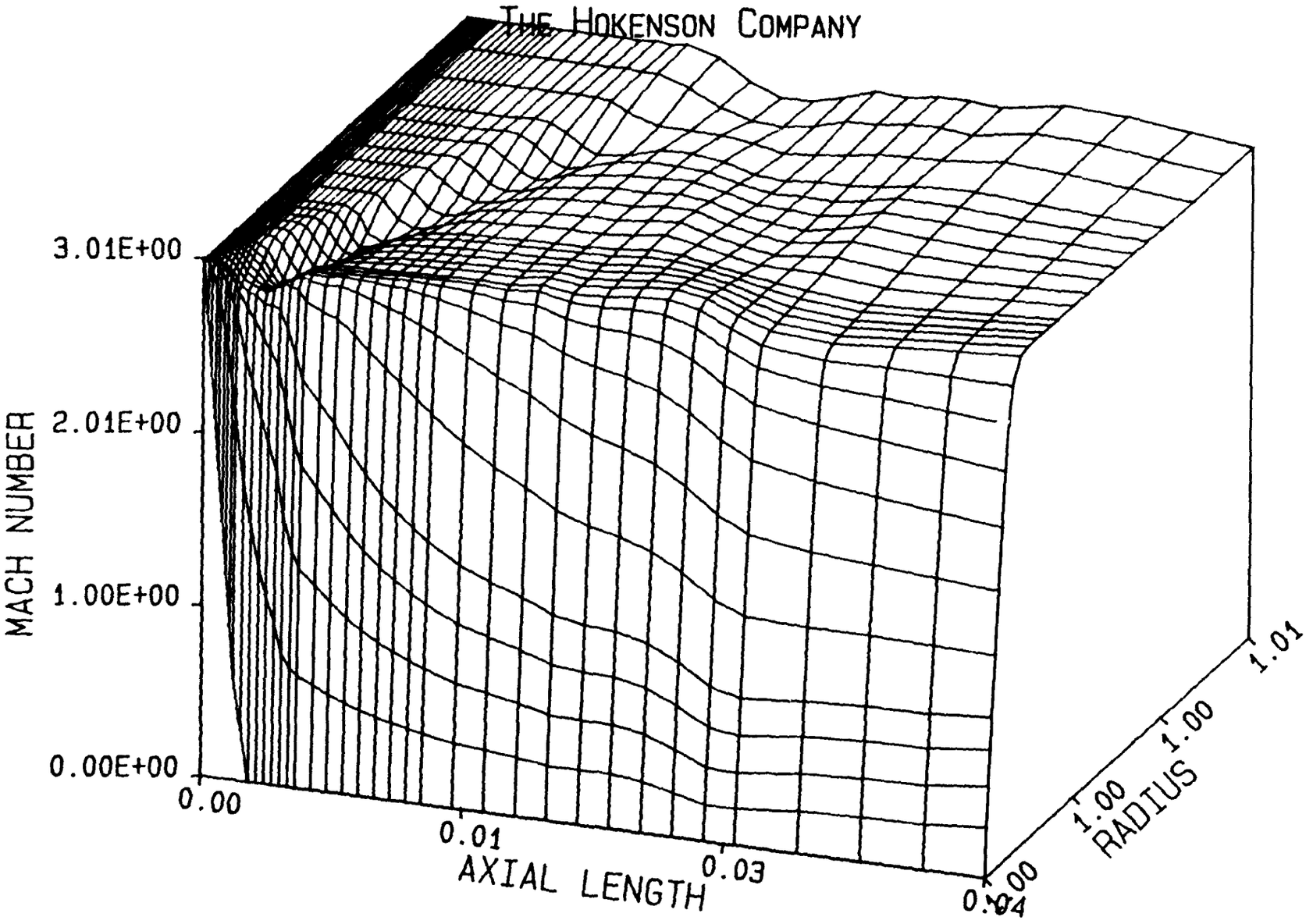
THE HOKENSON COMPANY
MACH NUMBER
3.01E+00
2.01E+00
1.00E+00
0.00E+00
0.00
0.01
0.03
0.04
AXIAL LENGTH
1.00
1.00
1.01
RADIUS

Case IIIb.: M=3.0, Non-Zero Rotation

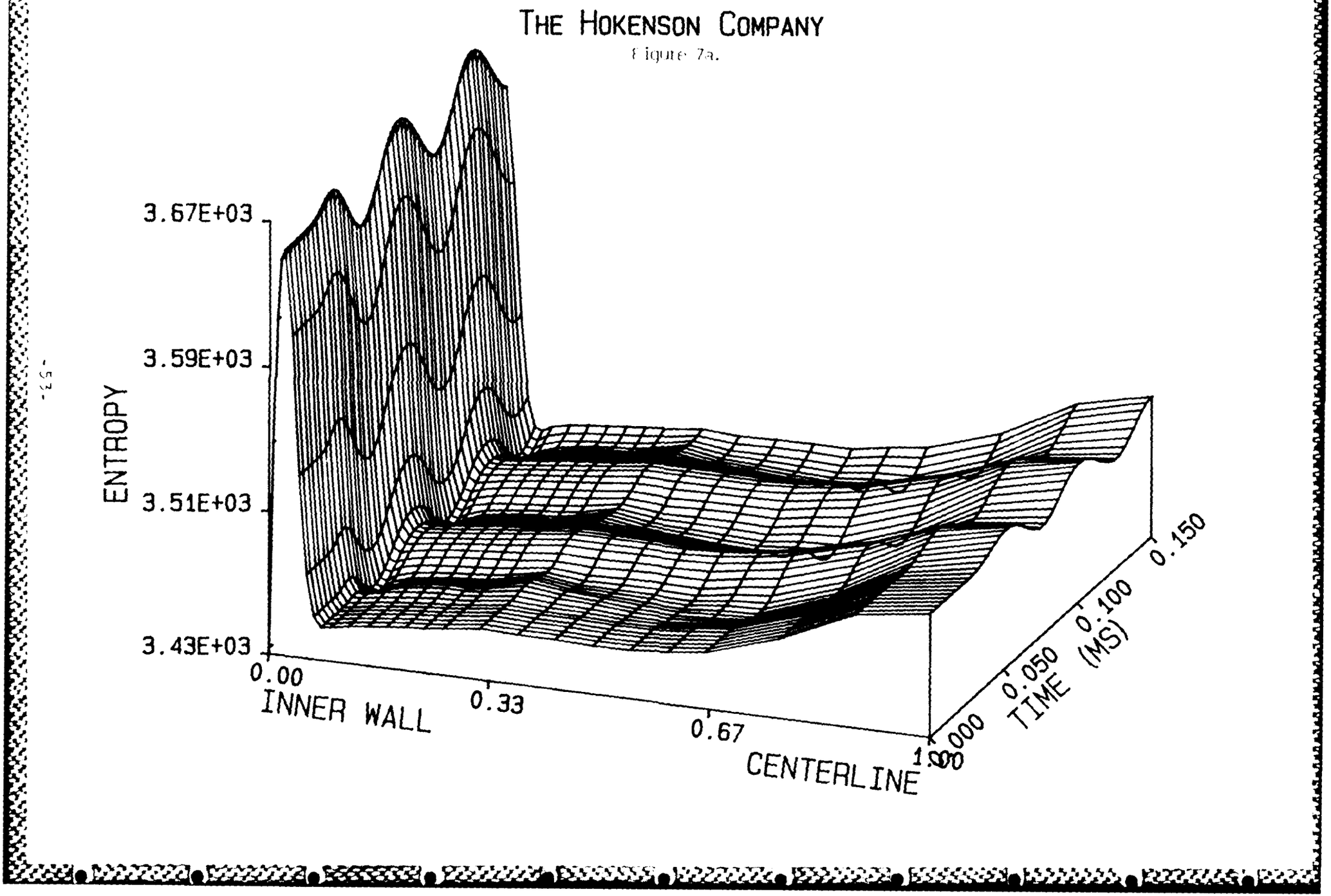
THE HOKENSON COMPANY
Figure 7a.
3.67E+03
3.59E+03
3.51E+03
3.43E+03
ENTROPY
0.00
INNER WALL
0.33
0.67
CENTERLINE
1.000
0.050
0.100
0.150
TIME (MS)

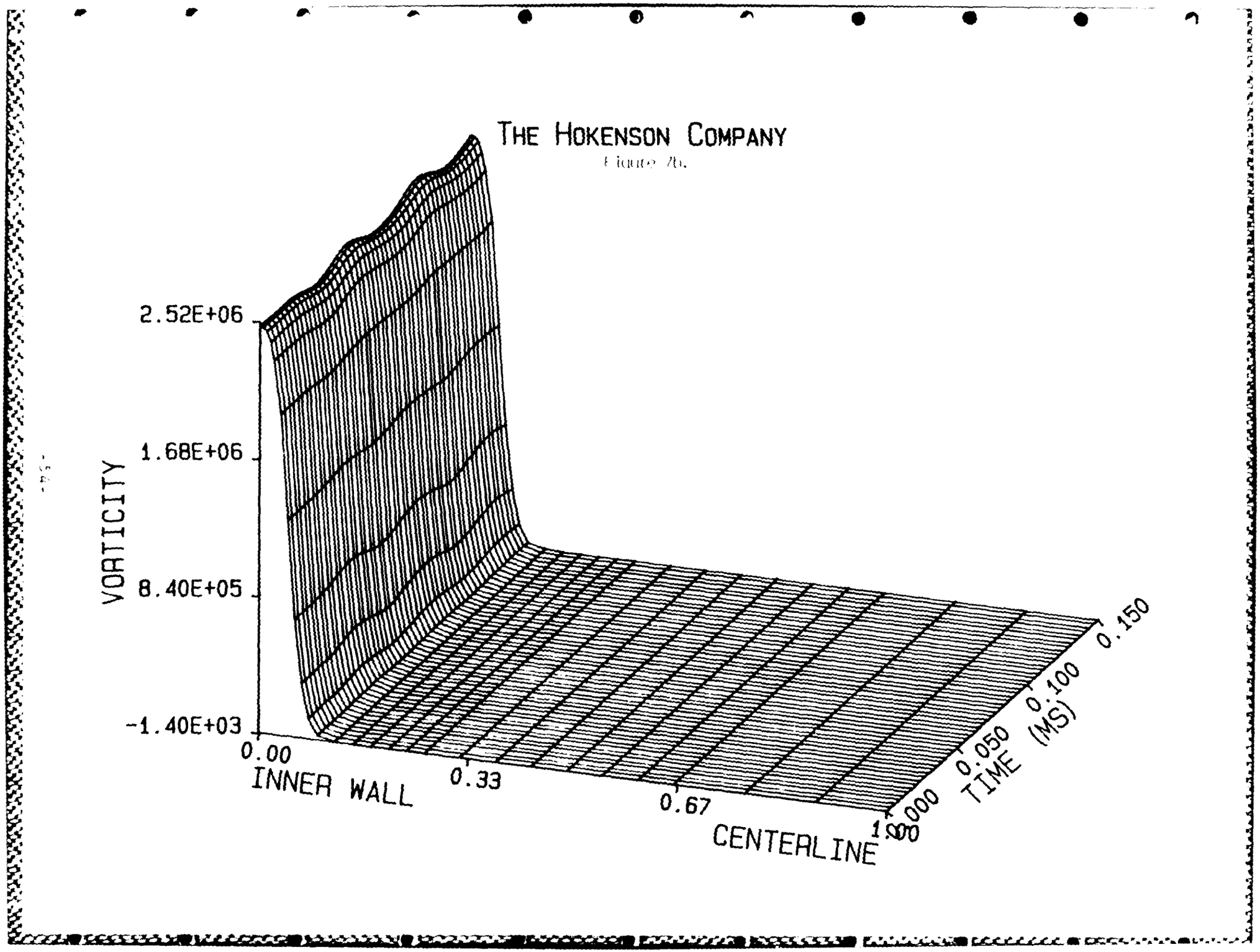
THE HOKENSON COMPANY
2.52E+06
1.68E+06
8.40E+05
-1.40E+03
VORTICITY
0.00
INNER WALL
0.33
0.67
1.00
CENTERLINE
0.000
0.050
0.100
0.150
TIME (MS)

THE HOKENSON COMPANY

Figure 7c.

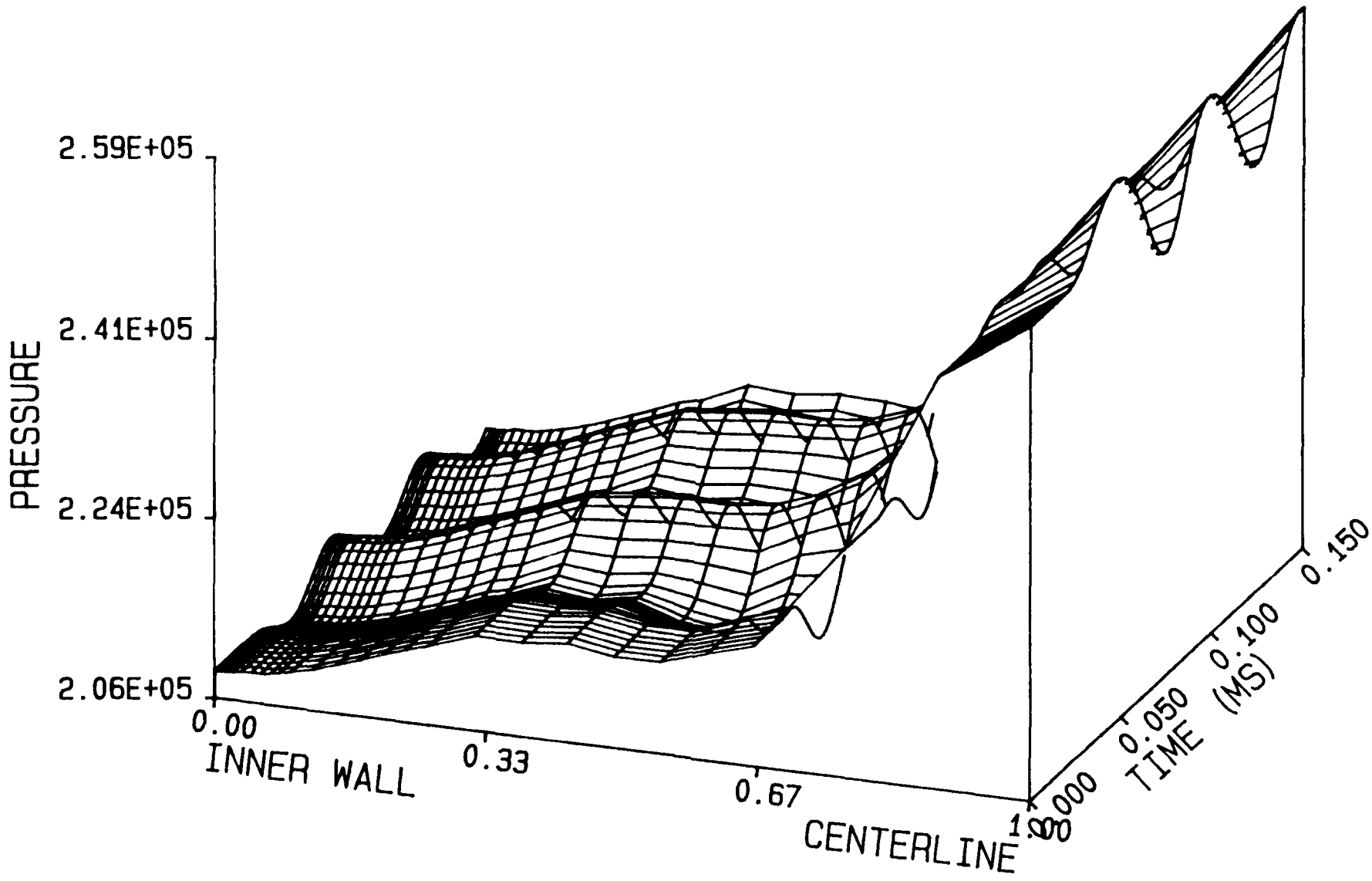

THE HOKENSON COMPANY

Figure 7d.

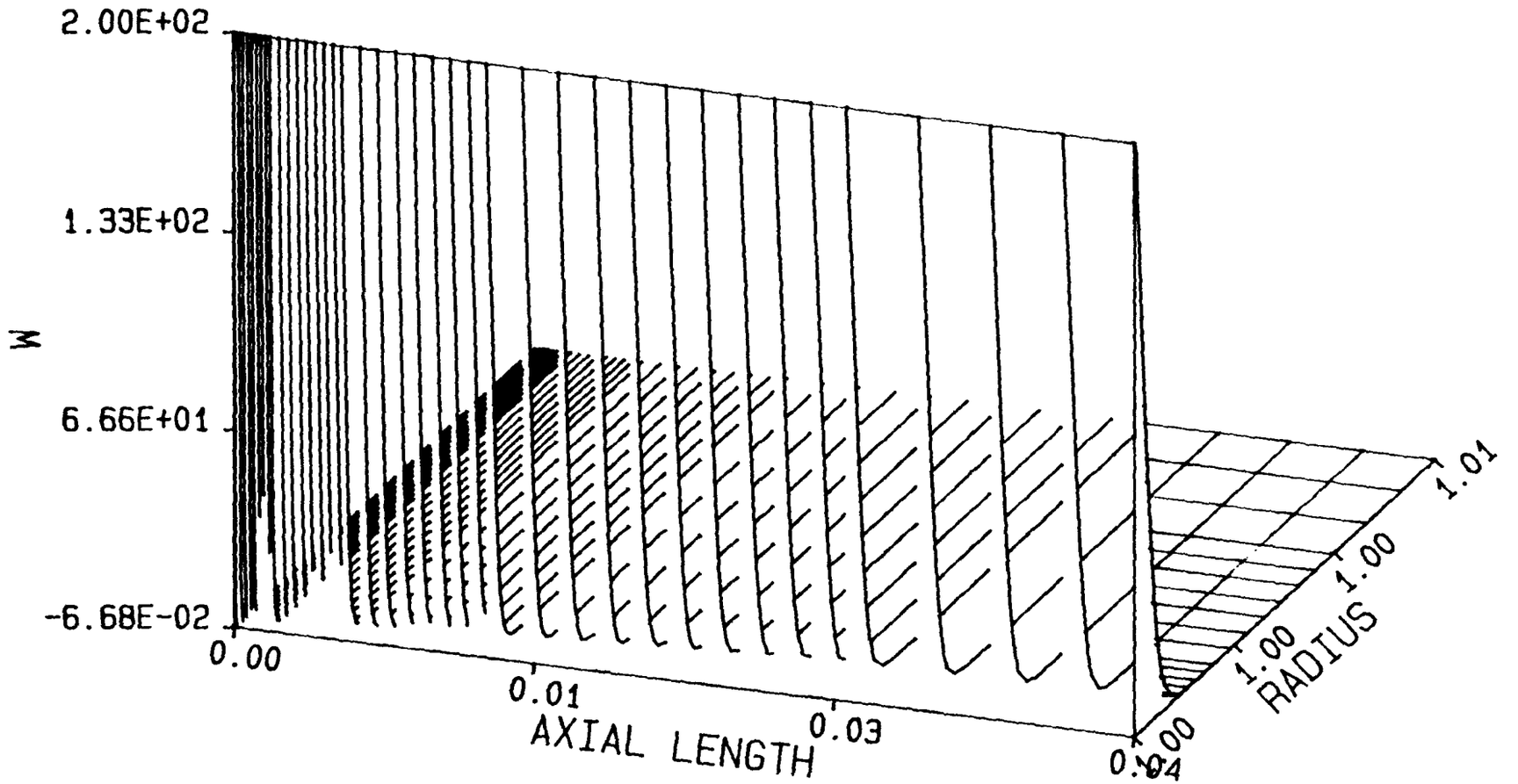

THE HOKENSON COMPANY

Figure 8a.

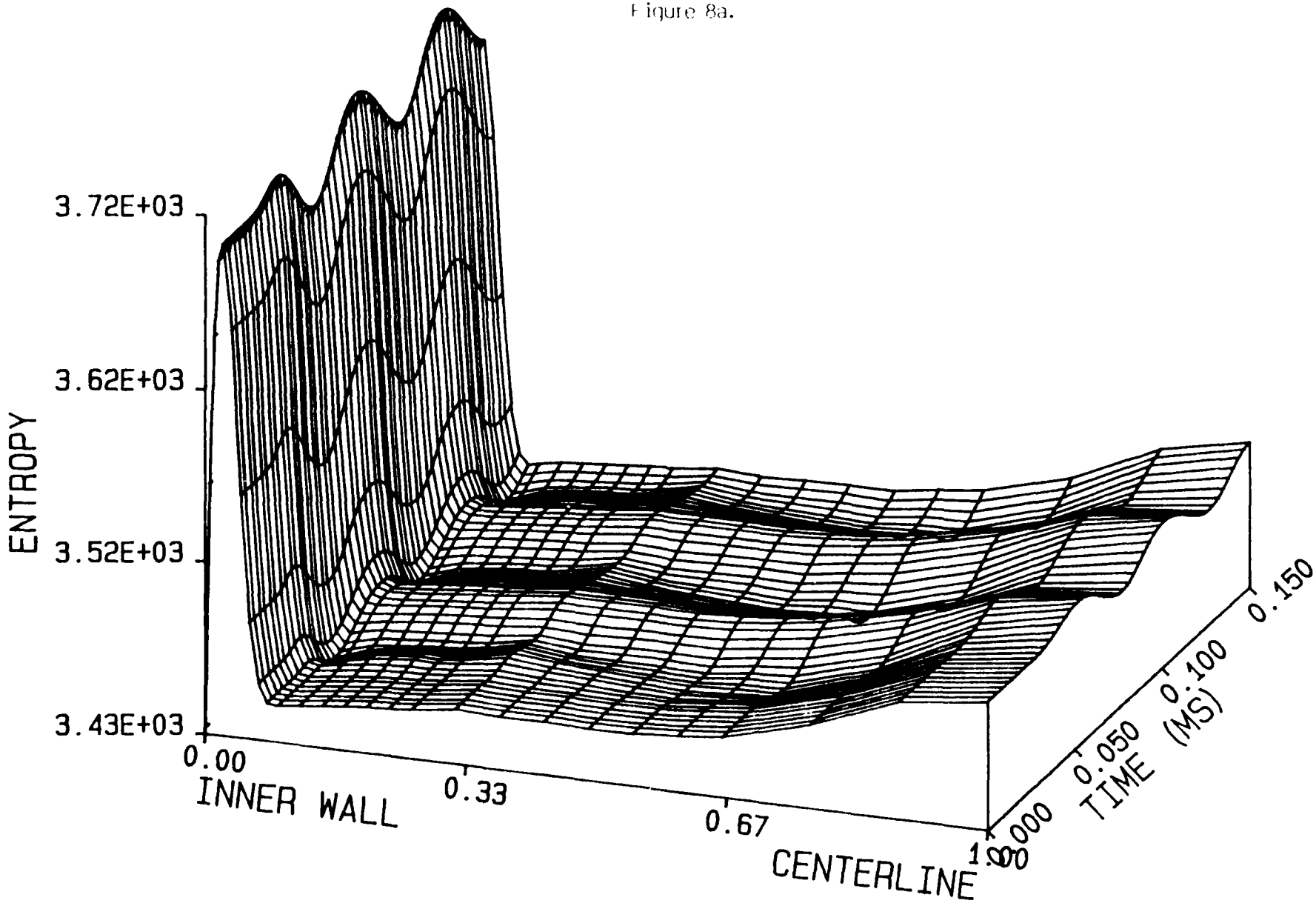

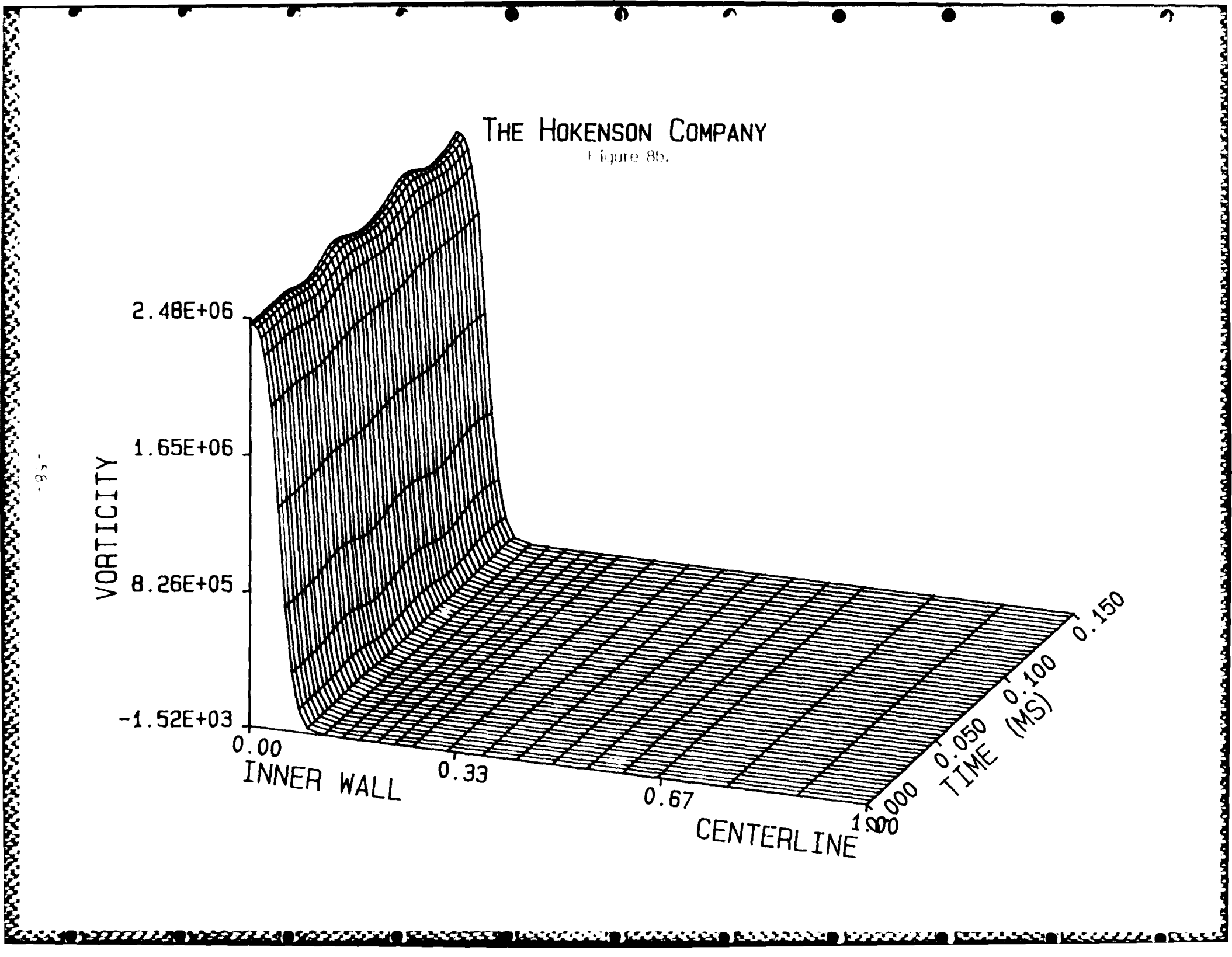
THE HOKENSON COMPANY
Figure 8b.
VORTICITY
2.48E+06
1.65E+06
8.26E+05
-1.52E+03
0.00
INNER WALL
0.33
0.67
CENTERLINE
1.00
0.000
0.050
0.100
0.150
TIME (MS)

THE HOKENSON COMPANY

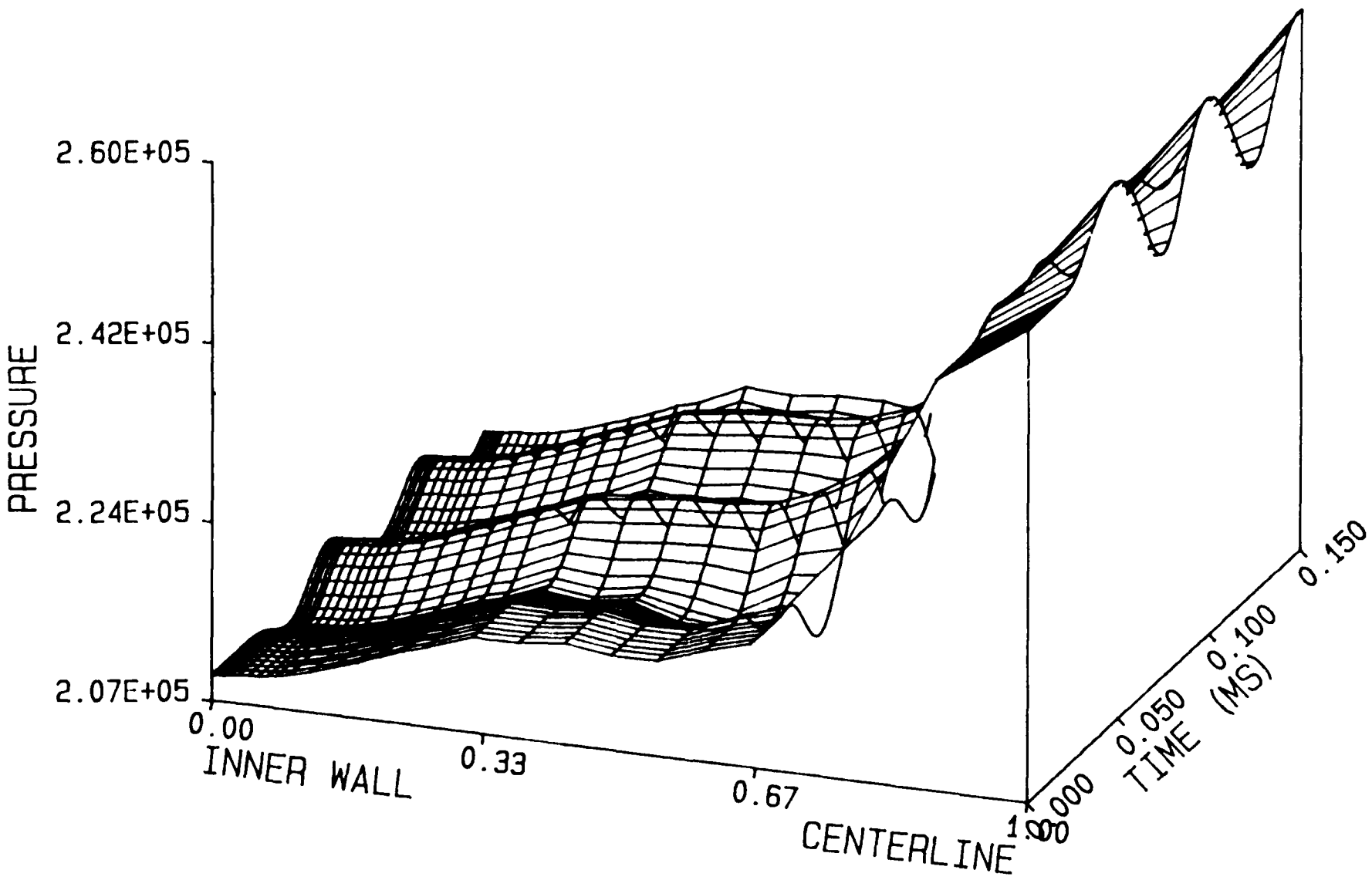

THE HOKENSON COMPANY

Figure 8d.

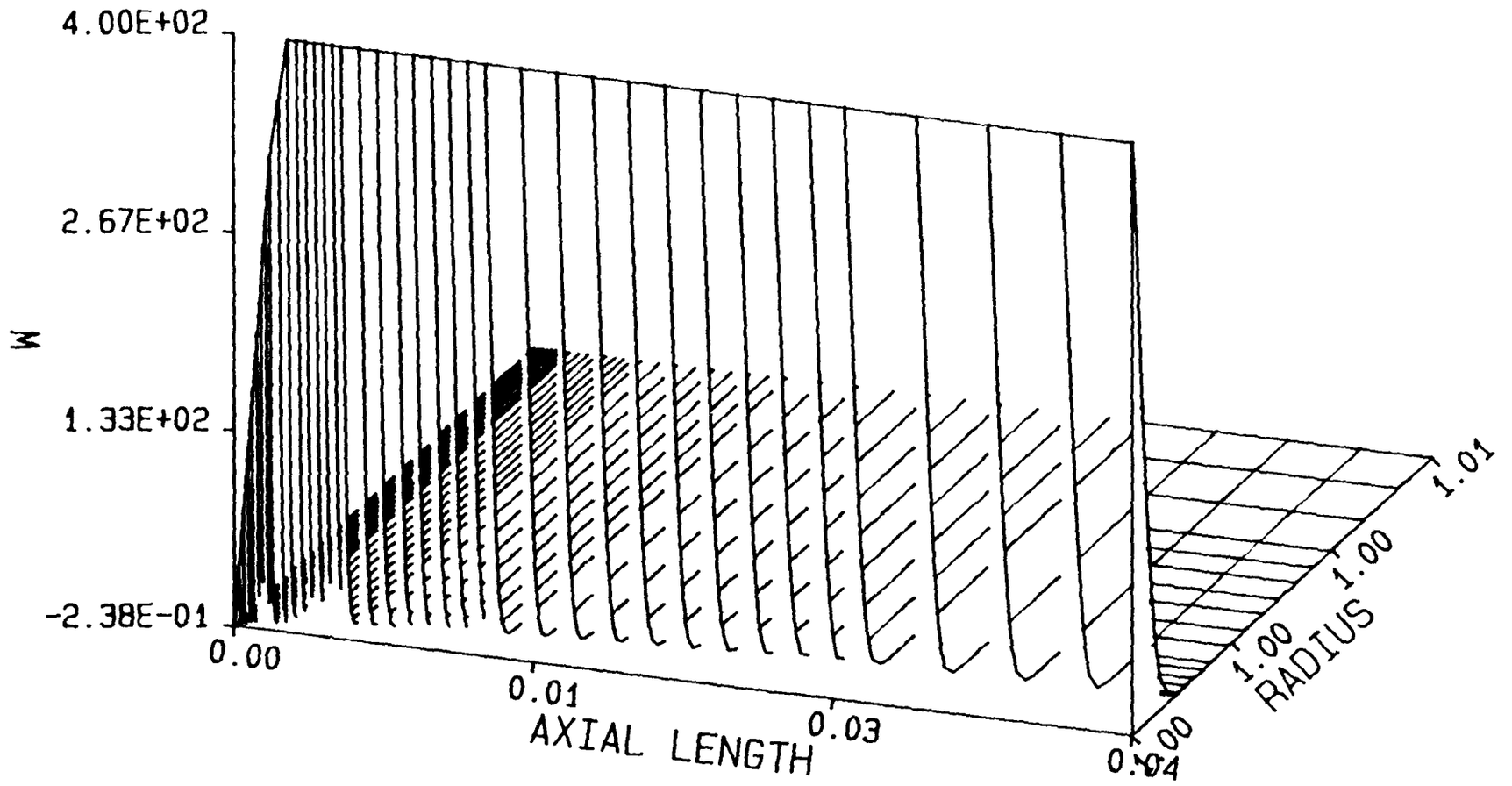

Case IV.: M=2.0, Zero Rotation

THE HOKENSON COMPANY

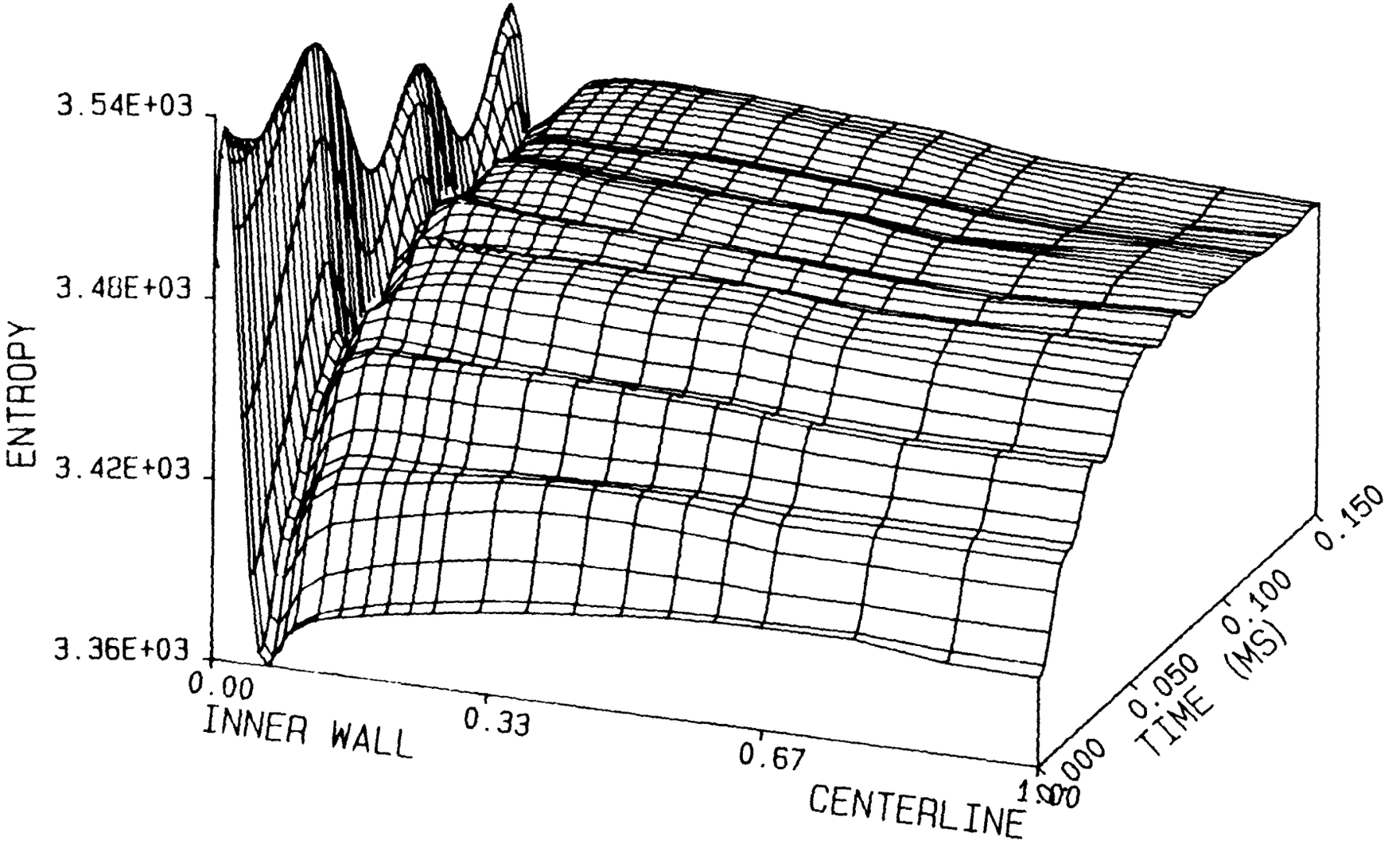

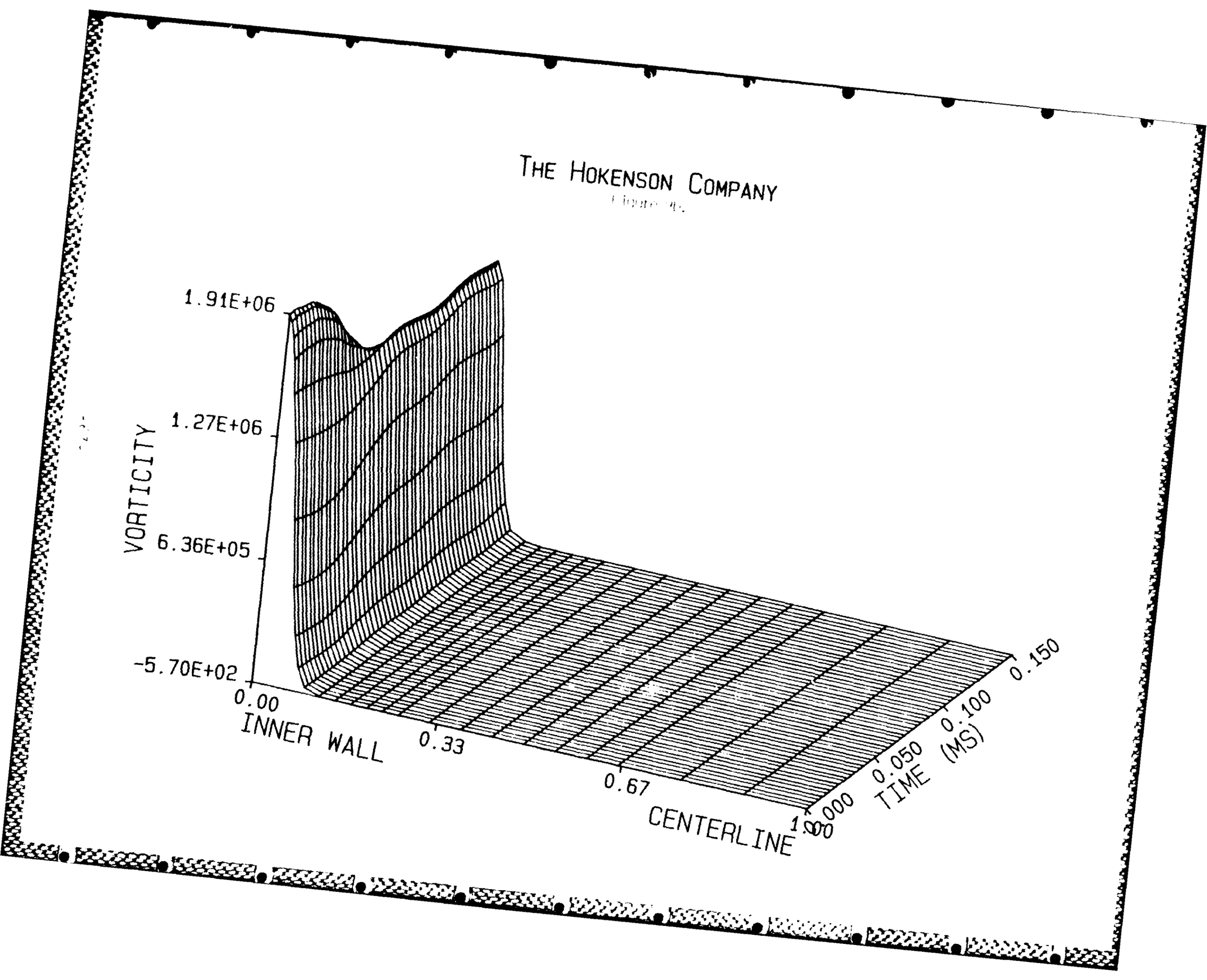
THE HOKENSON COMPANY
1.91E+06
1.27E+06
6.36E+05
-5.70E+02
VORTICITY
0.00
INNER WALL
0.33
0.67
CENTERLINE
1.00
0.000
0.050
0.100
0.150
TIME (MS)

Figure 9c.

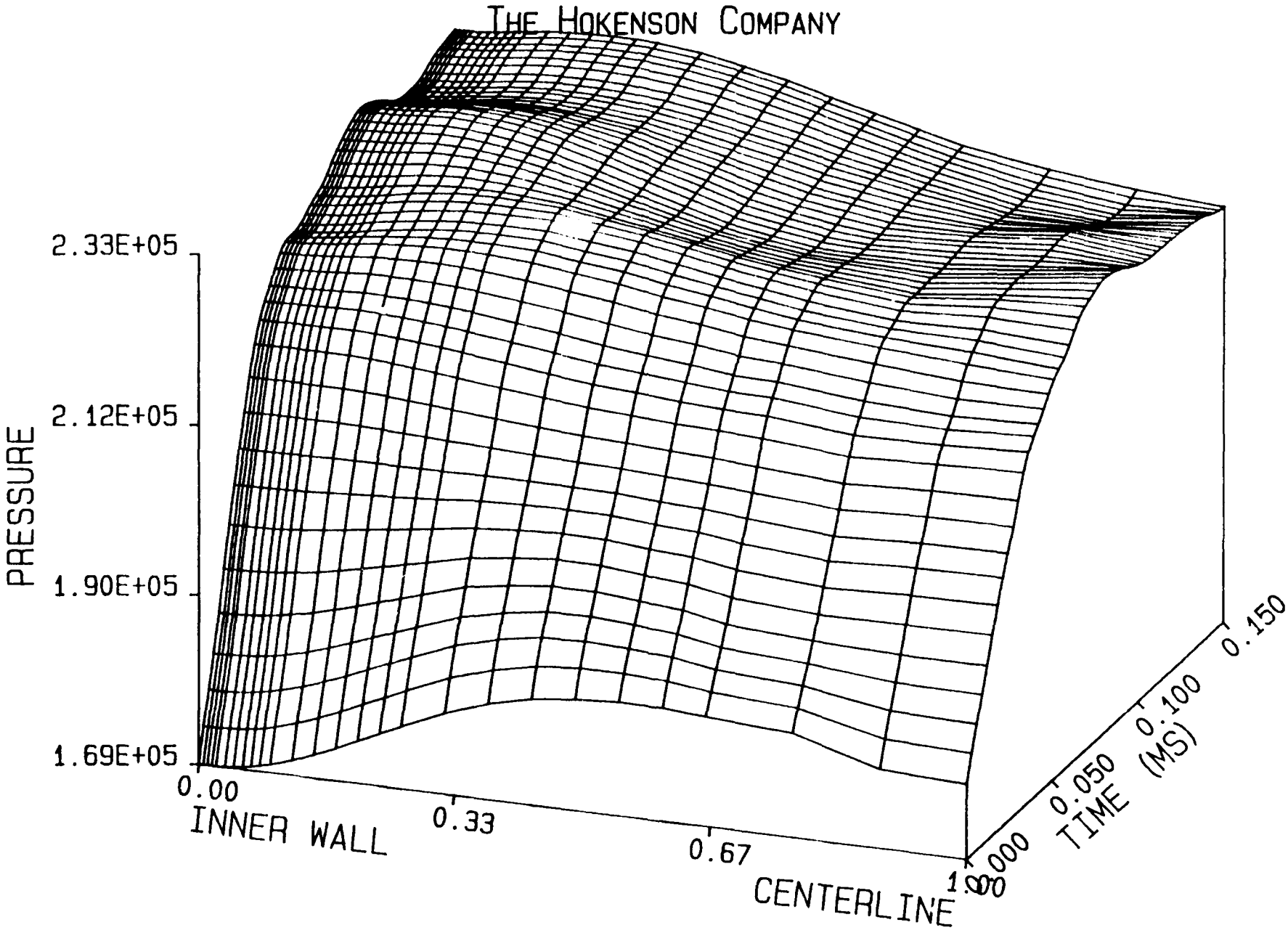
THE HOKENSON COMPANY
PRESSURE
2.33E+05
2.12E+05
1.90E+05
1.69E+05
0.00
INNER WALL
0.33
0.67
1.00
CENTERLINE
0.000
0.050
0.100
0.150
TIME (MS)

Figure 9d.

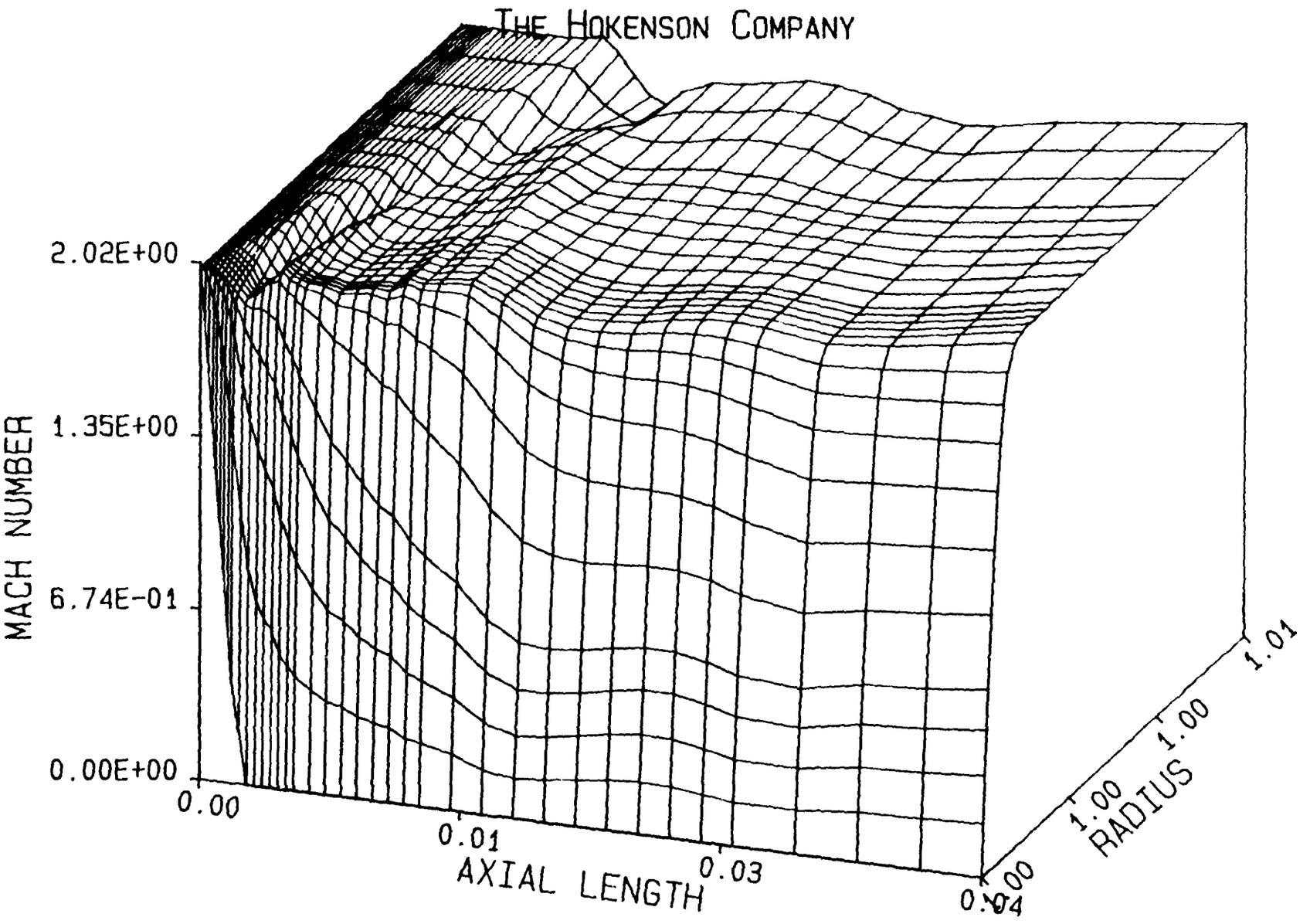
THE HOKENSON COMPANY
2.02E+00
1.35E+00
6.74E-01
0.00E+00
MACH NUMBER
0.00
0.01
0.03
0.04
AXIAL LENGTH
1.00
1.00
1.01
RADIUS

Case V.: M=1.4, Zero Rotation

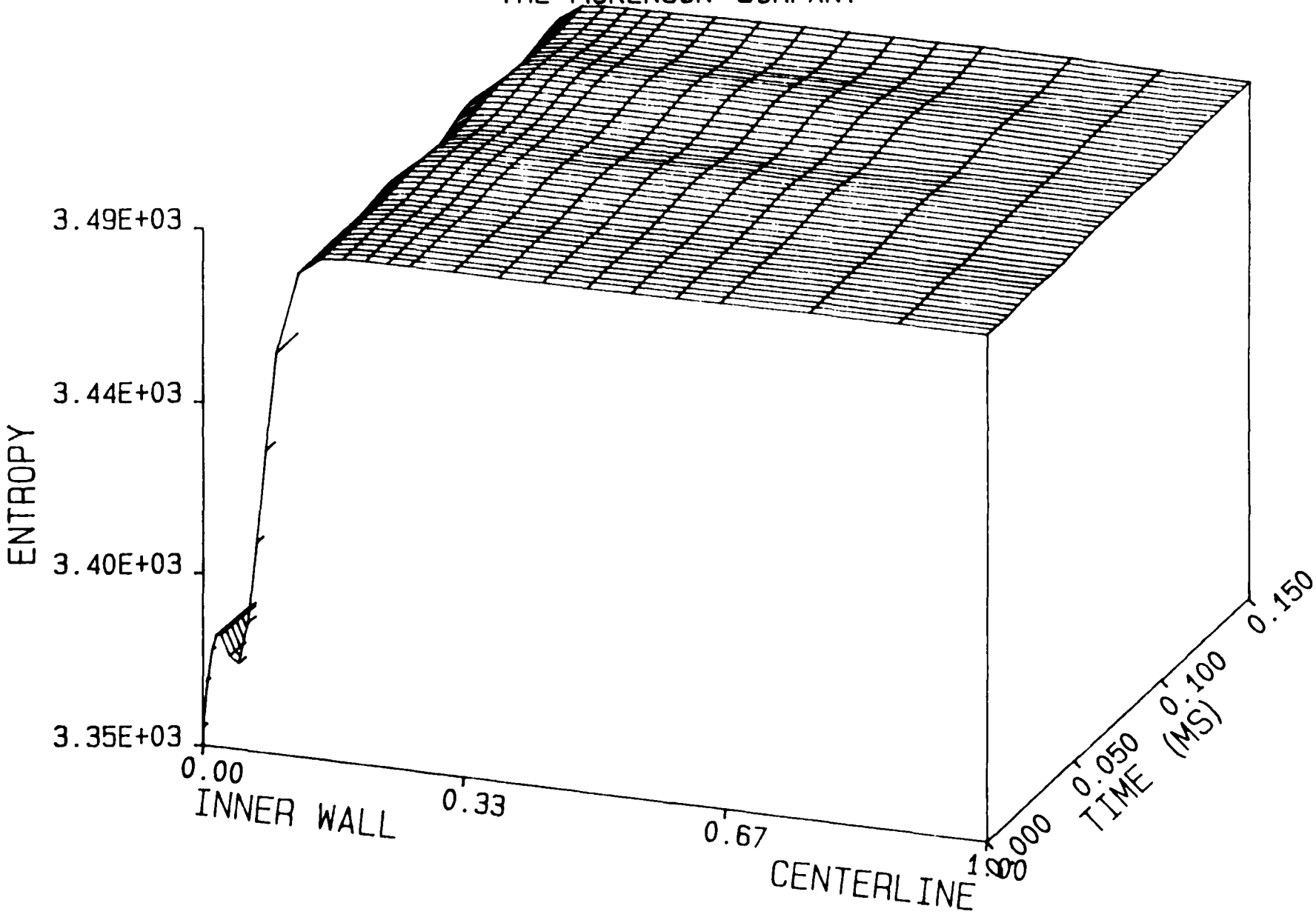
THE HOKENSON COMPANY
3.49E+03
3.44E+03
3.40E+03
3.35E+03
ENTROPY
0.00
INNER WALL
0.33
0.67
1.000
CENTERLINE
0.050
0.100
0.150
TIME (MS)

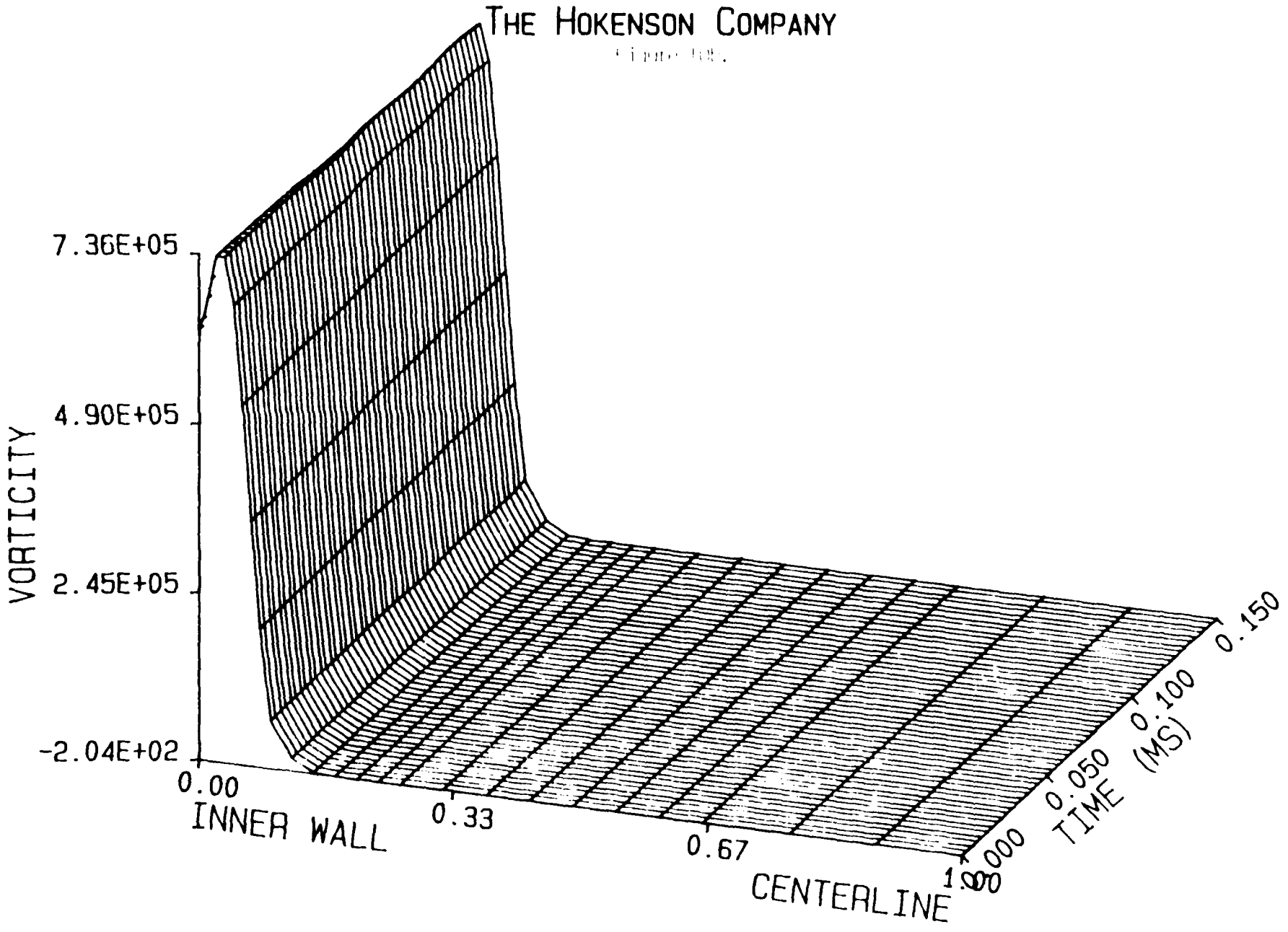
THE HOKENSON COMPANY
7.36E+05
4.90E+05
2.45E+05
-2.04E+02
VORTICITY
0.00
INNER WALL
0.33
0.67
1.000
CENTERLINE
0.050
0.100
0.150
TIME (MS)

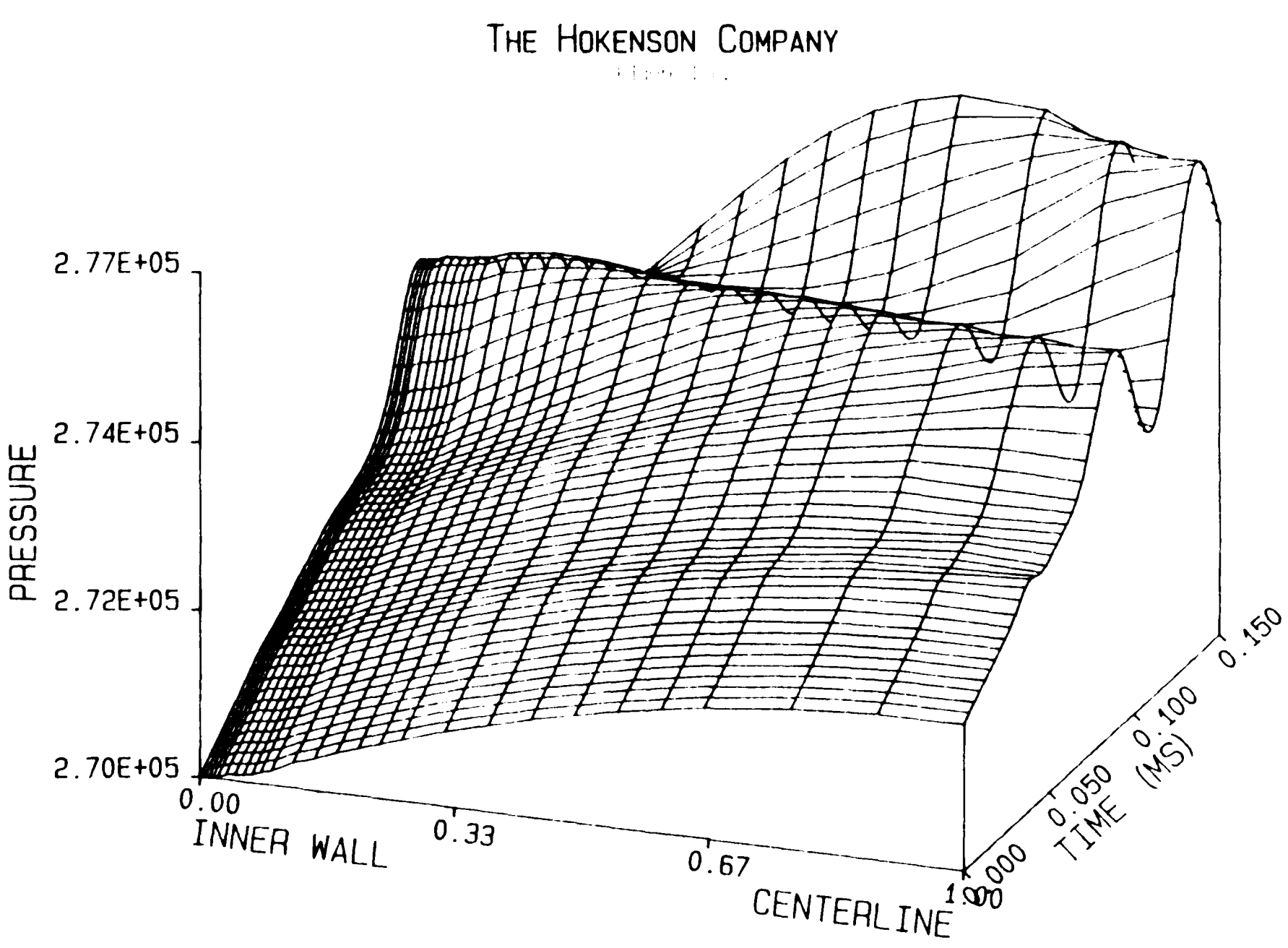
THE HOKENSON COMPANY
2.77E+05
2.74E+05
2.72E+05
2.70E+05
PRESSURE
0.00
INNER WALL
0.33
0.67
1.00
CENTERLINE
0.000
0.050
0.100
0.150
TIME (MS)

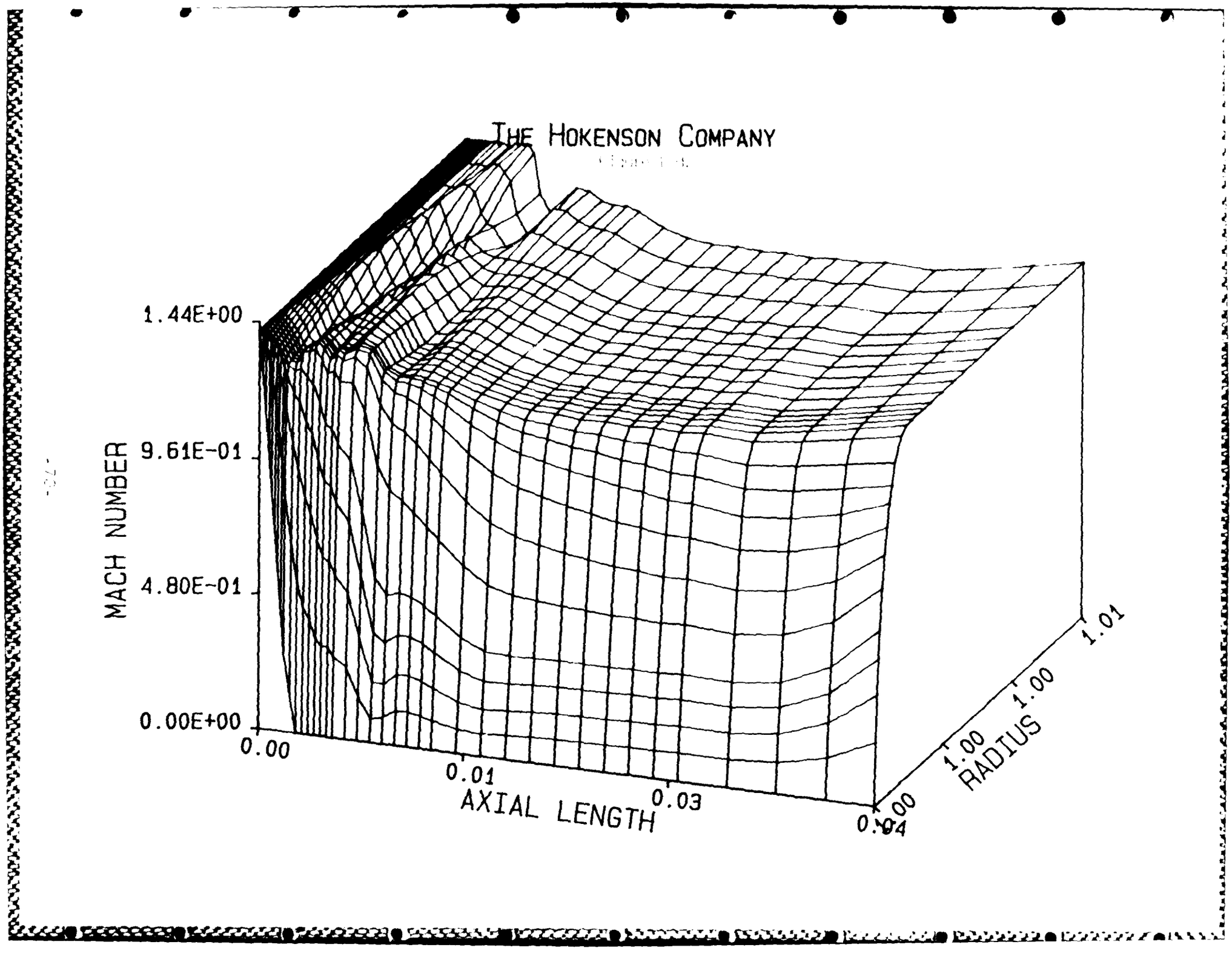
THE HOKENSON COMPANY
1.44E+00
9.61E-01
4.80E-01
0.00E+00
MACH NUMBER
0.00
0.01
0.03
0.04
AXIAL LENGTH
1.00
1.00
1.01
RADIUS

Figure 11a.

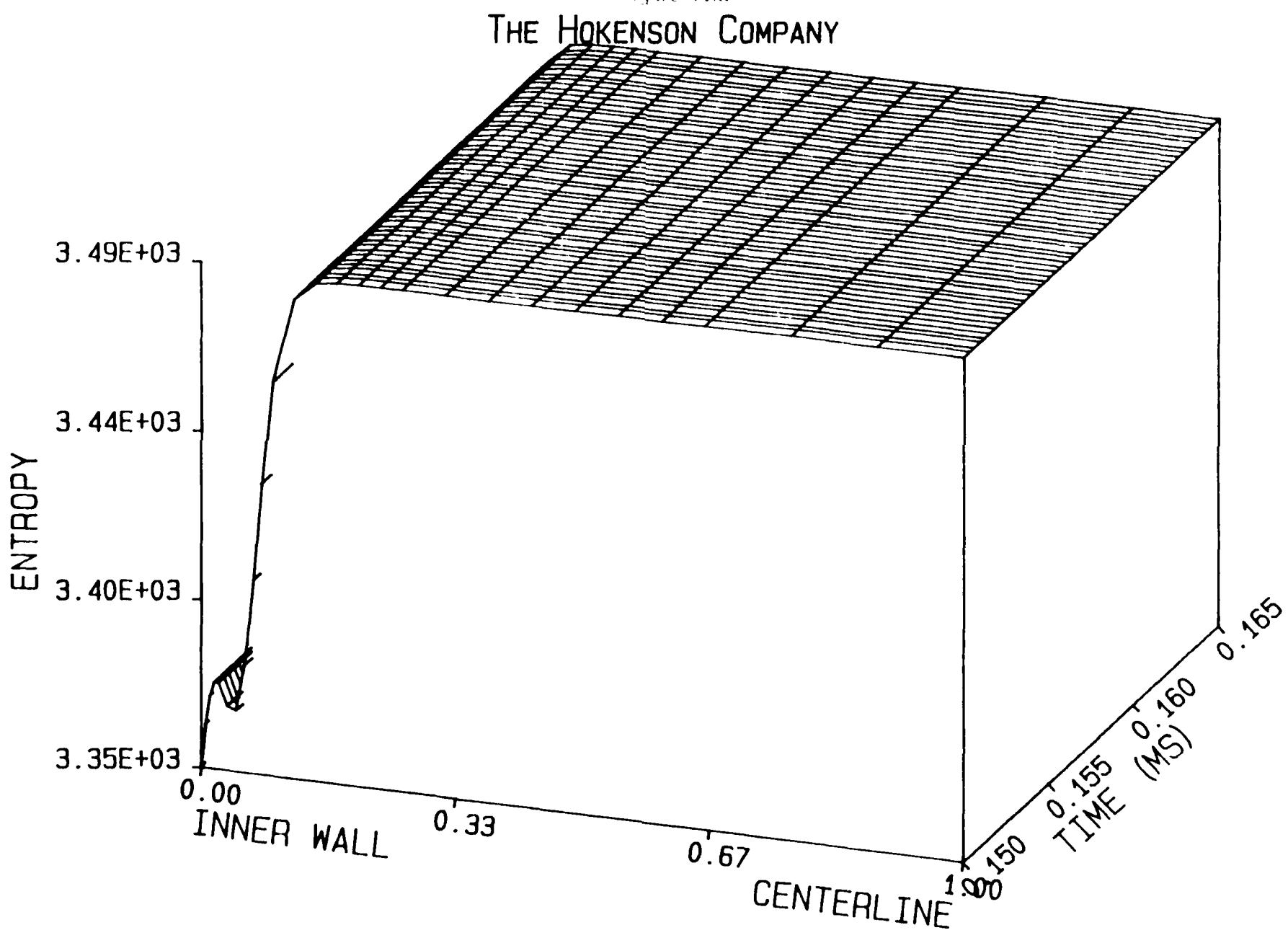
THE HOKENSON COMPANY
3.49E+03
3.44E+03
3.40E+03
3.35E+03
ENTROPY
0.00
INNER WALL
0.33
0.67
1.00
CENTERLINE
0.150
0.155
0.160
0.165
TIME (MS)

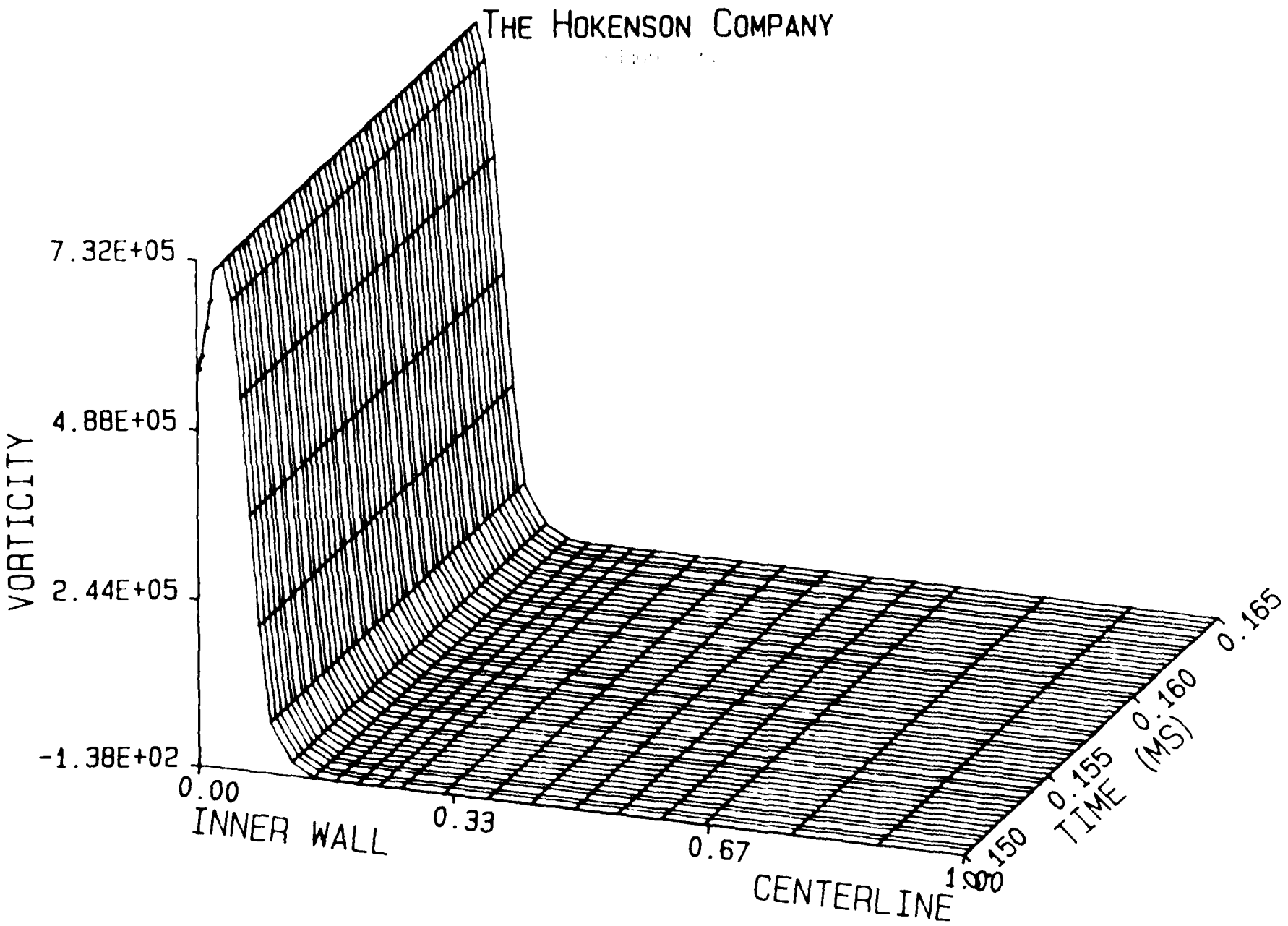
THE HOKENSON COMPANY
7.32E+05
4.88E+05
2.44E+05
-1.38E+02
VORTICITY
0.00
INNER WALL
0.33
0.67
1.00
CENTERLINE
0.150
0.155
0.160
0.165
TIME (MS)

THE HOKENSON COMPANY

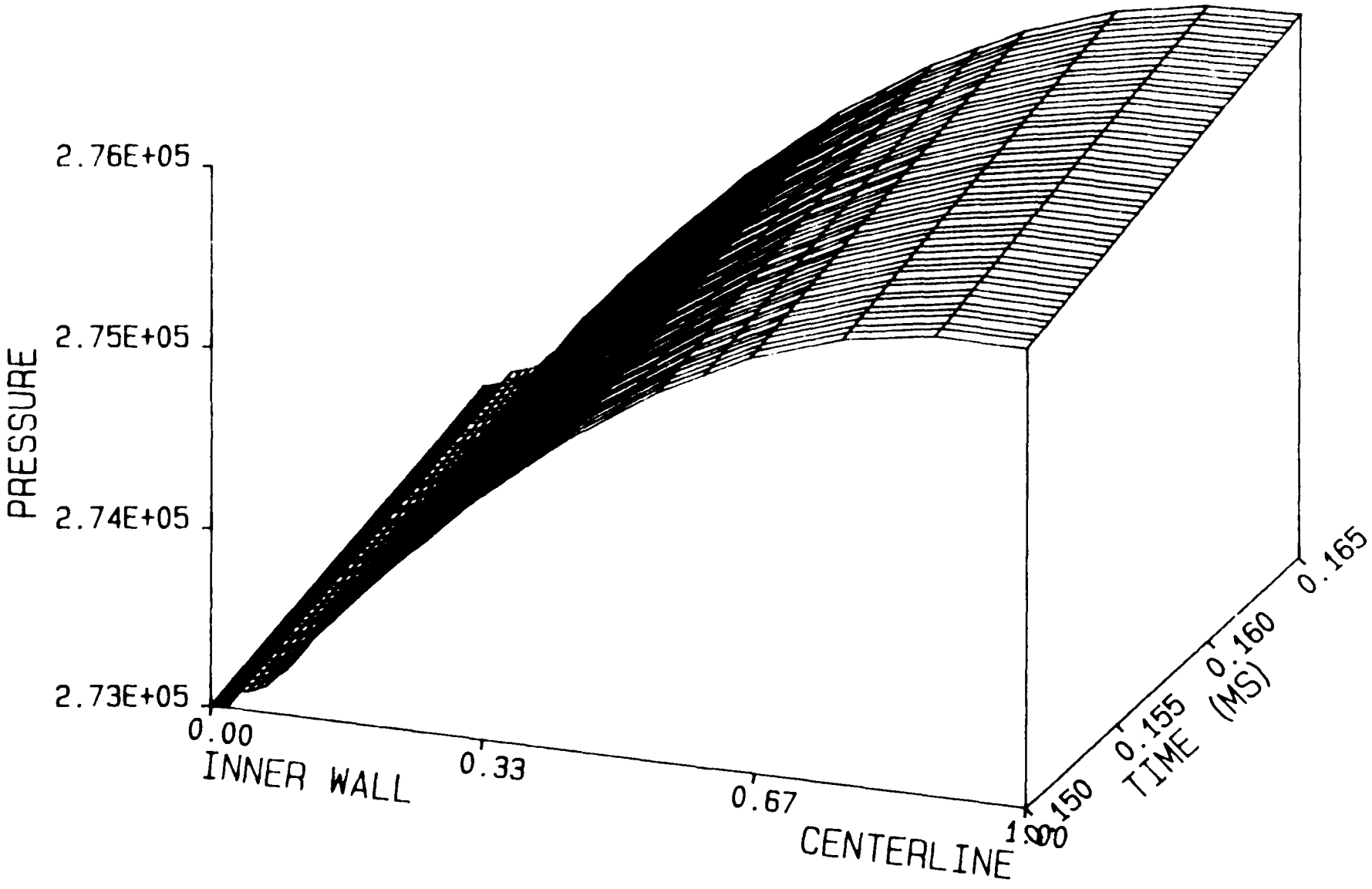

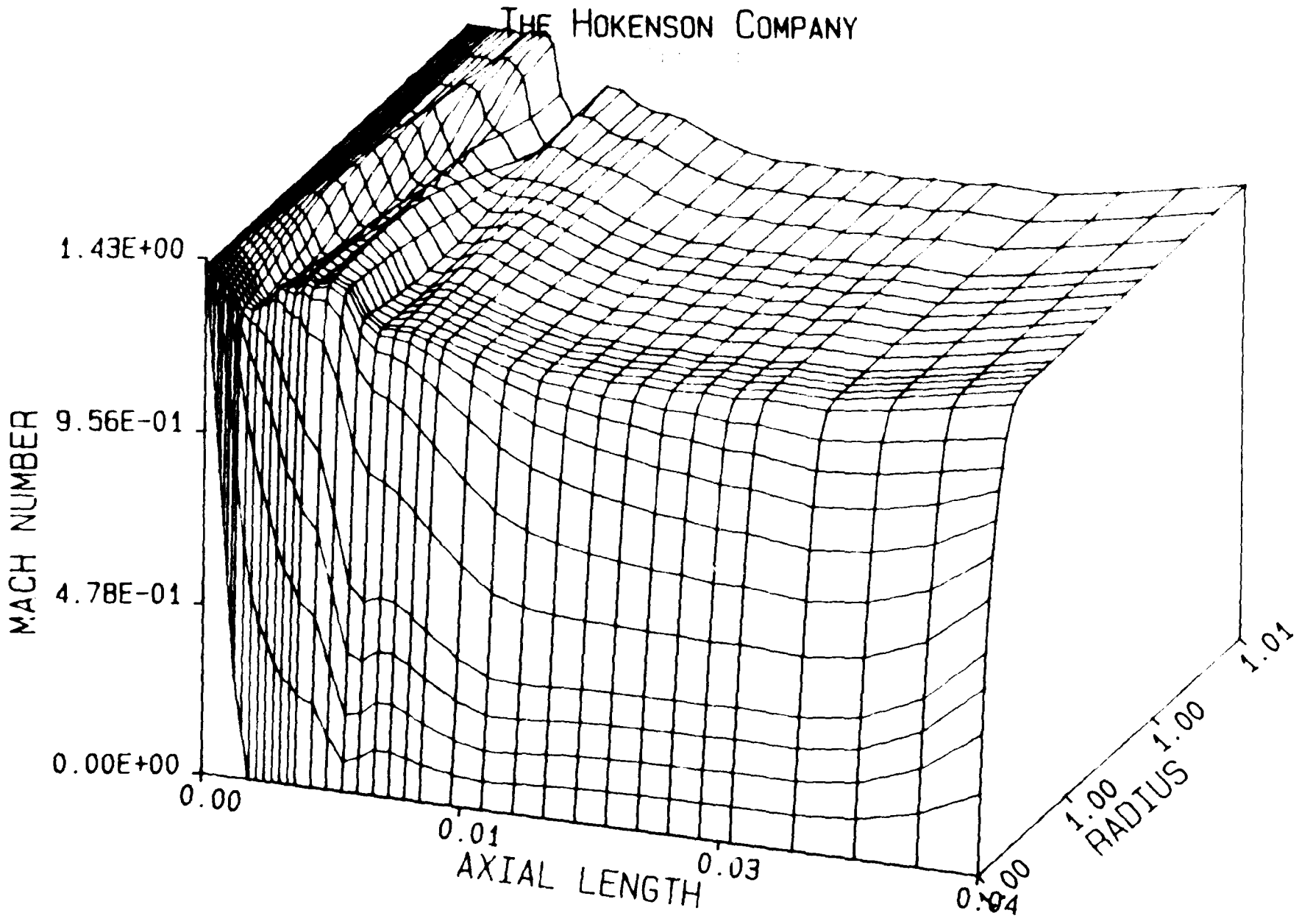
THE HOKENSON COMPANY
1.43E+00
9.56E-01
4.78E-01
0.00E+00
MACH NUMBER
0.00
0.01
0.03
0.04
AXIAL LENGTH
1.00
1.00
1.01
RADIUS

END

12-87

DTIC